8-2013

An Investigation of Energy Migration in Rare Earth Oxyorthosilicate Scintillation Materials

Harold Edward Rothfuss
hrothfus@utk.edu

To the Graduate Council:

I am submitting herewith a dissertation written by Harold Edward Rothfuss entitled "An Investigation of Energy Migration in Rare Earth Oxyorthosilicate Scintillation Materials." I have examined the final electronic copy of this dissertation for form and content and recommend that it be accepted in partial fulfillment of the requirements for the degree of Doctor of Philosophy, with a major in Materials Science and Engineering.

Charles L. Melcher, Major Professor

We have read this dissertation and recommend its acceptance:

Lars A. Eriksson, Mariya Zhuravleva, Jason P. Hayward

Accepted for the Council:

Carolyn R. Hodges

Vice Provost and Dean of the Graduate School

(Original signatures are on file with official student records.)

An Investigation of Energy Migration in Rare Earth Oxyorthosilicate Scintillation Materials

A Dissertation Presented for the

Doctor of Philosophy

Degree

The University of Tennessee

Harold Edward Rothfuss

August 2013

ACKNOWLEDGEMENTS

This process has been a collection of experiences and memories that have been shared with many people. Many of these people have helped me in many ways along the journey and I hope that I can at least acknowledge the invaluable help from them here.

I would first like to thank Dr. Charles (Chuck) Melcher for starting me on this journey. He has been a great mentor and friend along this journey. Even though our trip has been long and sometimes seemingly endless, I would not change a thing. I thank Dr. Lars Eriksson for his patience and guidance through not only through my academic career, but also in my professional life and also being a kind and compassionate friend. I also would like to thank Merry Koschan, who helped in many ways beyond her technical expertise in crystal growth, which would have been far more than enough. From all the pleasant conversations to the advice and contributions to my research, she is a critical member of our research group. I also thank Dr. Mariya Zhuravleva for the many conversations and encouraging words and also many shared great times. It was always fun to see what it would take to make her smile when she was always so serious. To the person I feel I shared most of this academic journey with, I give my thanks to Dr. Kan Yang. From working together on countless projects to sharing many great times, my only regret is that our paths didn't converge to a point where we could continue to work together. Others that I would like to thank

from my time in the Scintillation Material Research Center and the Material Science department are Dr. Jonathan Peak, Paul Cutler, Dr. Mohit Tyagi, Dr. Jason Hayward, Sam Donnald, Dr. George Pharr, Dr. Easo George, Dr. James Morris, Hua Wei, Bonnie Blalock, Fang Meng and all the other current members of the SMRC. These people have contributed to my education in many ways, each in very unique ways. I could write many more pages on how these individuals contributed to my journey.

This journey would have never started without the support of my colleagues and mentors at Siemens (Previously CTI). These influential individuals guided me to continue the pursuit of an advance degree and always have been supportive in the endeavor. The people most responsible for the place I am at now would be Dr. Mike Casey and Dr. Maurizio Conti. If they never gave me the chance initially, I would not be where I am at today. I thank them both for giving me the opportunity to enter this field. A special thanks to Maurizio for guiding me in my early research life and getting me started in independent research. Also a very special thanks to Mike for always presenting an environment that resulted in innovation and new research. He always gives good guidance and encouragement for new ideas and supported me 100% through this journey. There are also many others I have to thank from the physics group at Siemens. Their insight and expertise was always at my disposal and I was always so thankful for. Any time I needed help, everyone in this group would not

hesitate to stop what they were doing to help. All of the people in my group are not only world class scientists, but also great human beings. I'm very privileged to work with such a skilled and kind group of people. This wonderful group is comprised of Dr. Mehmet Aykac, Dr. Harshali Bal, Dr. Bernard Bendriem, Dr. Jim Hamill, Chuck Hayden, Dr. Inki Hong, Dr. Judson Jones, Dr. Christian Michel, Dr. Vladimir Panin, Dr. Stefan Siegel. I also would like to thank members of other groups that helped directly in this work. These other are Dr. Charles Watson, Dr. Mu Chen (former employee), Dr. Josh Schaefferkoetter, John Young, Eric Breeding, Andrew Moor, Bill Jones, Mark Long and Jennifer Seymour. Without all of these people, I could not have made it here.

Lastly there is the support I have received outside of my academic and professional life. First and most significant, is my family. I don't have enough thanks for the patience and support I have received through this whole process. All the love and support was the strength I needed to complete this. I thank every one of my family members and will continue to thank them for years to come for enduring this with me. Lastly I want to thank all of my brothers from my time in the military. These people were a strong influence in my life and shared in many truly hard times. Through these hard times, we carried each other, and at the end, were all better for it.

ABSTRACT

In most scintillator applications, the energy resolution is an important scintillation property and is related to other scintillator properties. In order to observe how these properties relate to the energy resolution, a simulation was created to quantify most of these characteristics for a LSO:Ce scintillator. These results were validated with good agreement to experimental results. From the separable components of the simulation, an understanding of the contributions to the energy resolution broadening was developed. A thought to improve the energy resolution by improving the energy migration was tested by observing and modifying the scintillation kinetics of YSO:Ce. The scintillation kinetics in YSO:Ce are quite different from LSO:Ce even though the materials are similar in crystal lattice structure and the cerium activator dopant. The scintillation kinetics differences are observed when measuring the scintillation decay time with the results varying in decay times and different mathematical decay models. Using thermoluminescence, it was observed that YSO:Ce has more shallow traps with trap lifetimes at ~300K on the same order as the Ce3+ excited state lifetime. Using these same data, it was calculated that these shallow traps have lifetimes ~years when the sample is cooled to 40K. Re-measuring the decay time at 40K yields a decay time of 32ns and shows that the shallow traps in YSO:Ce are the cause of impeded energy migration to the luminescence centers. By using calcium co-doping during crystal growth, most of the trap structure was

significantly suppressed. With these YSO:Ce:Ca samples, the scintillation decay times were decreased nearly to the cerium excited lifetimes. In order to measure any improvement in the non-proportional response, a new measurement technique was developed. The new method used angular based measurements using a PET scanner to calculate the energy of a Compton electron deposited in the sample. The results agreed with published data for NaI:Tl and LSO:Ce scintillators. Finally, it was demonstrated that the non-proportional response of YSO samples were the same with improvement in energy resolution without a large increase in light output. The conclusion was that the homogeneity of our YSO:Ce:Ca samples led to a 3% improvement in energy resolution.

TABLE OF CONTENTS

LIST OF TABLES

LIST OF FIGURES

CHAPTER 1 INTRODUCTION

The Scintillator

The scintillator is a specific type of radiation detection material that encompasses many classes of materials, most states of matter, and a wide variety of applications. It performs a function of transforming incident ionizing radiation into visible light. This resulting visible light can be detected by a photosensor that ultimately results in an electrical signal that is representative of the incident quanta absorbed in the scintillator (Figure 1.1)

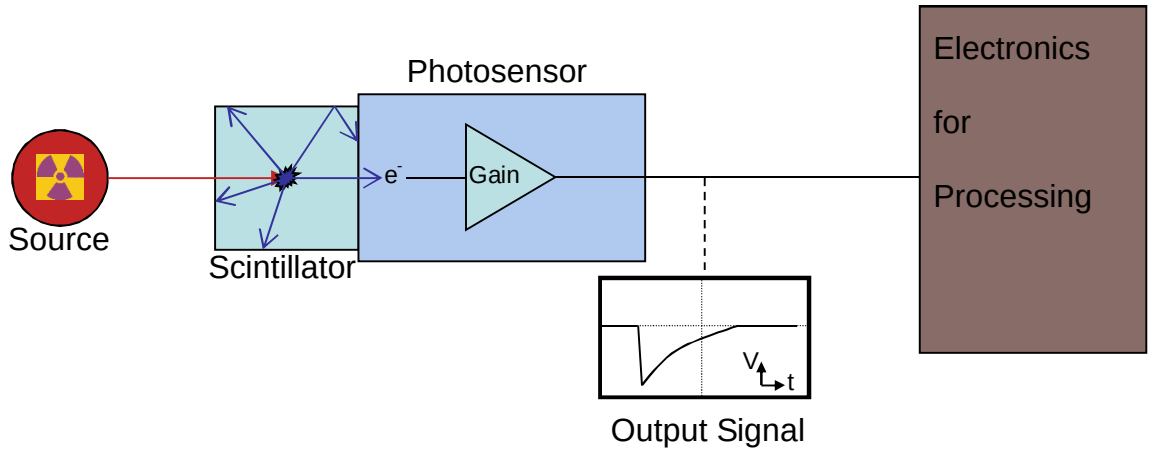

Figure *1.1. Illustration of a simple scintillator setup.*

The different classes of scintillators include organic and inorganic materials, and these two main groups can be further divided into crystals, glasses, gases and liquid scintillators. All these detector types have advantages and disadvantages,

and depending on the particular application, selection from among these classes of materials will depend on specific application criteria.

Single Crystal Inorganic Scintillators

This work will focus on scintillators in the single crystal inorganic family. These can be described as insulating materials with band gaps of the order of few electron volts (eV). Most are grown using a variety of single crystal growth techniques such as the Bridgman or Czochralski methods. The result is generally a single crystal under ideal conditions resulting in minimal defects to increase the scintillation efficiency.

The scintillation mechanism (Rodnyi 1997, Payne, Moses et al. 2011) (Figure 1.2) starts with the initial ionizing radiation interacting with the crystal and liberating a primary electron. In the case where the incident radiation is gamma radiation, this initial ionization is from a Compton scattering event, photoelectric absorption or pair production (appendix A) where the energy is transferred to a primary electron (and positron in the case of pair production). Creation of the primary electron can also result in a hole in which is filled either through electron relaxation resulting in a fluorescence x-ray or by Auger relaxation resulting in the emission in an Auger electron. The primary electron begins to lose its energy by electron-electron inelastic scattering thus creating an avalanche of electrons and holes until the energies of the electrons fall below the threshold necessary to

create ionization. This step of the scintillation process occurs on a time scale of 1-100 fs.

After the generated electrons are unable to ionize other electrons, thermalization of the electrons occurs. During this step the electrons interact with phonons, and the electrons begin to move to the bottom of the conduction band and holes move to the top of the valence band. This step can be seen as the largest loss of energy to non-luminescence tracks as phonon emission can reduce the number of electron-hole pairs created by up to 75%. The thermalization step occurs in a time frame of 1-10 ps in inorganic scintillators. The thermalization typically occurs over a distance of 10-100 of nm for ionic crystals and generally more than 100 nm in semiconductor materials.

The next stage of the scintillation process is the migration of the created electron-hole pairs to luminescence centers. The time scale for the migration of electron-hole pairs to a luminescence center has large variation and is dependent on the distance between luminescence centers and charge trap densities and depth. This step can occur on a scale of 1-10 ns. The luminescence step is a result of recombination of electrons and holes in an activator site. In the case of extrinsic (doped) scintillators, this activator site occurs when a dopant is added to create luminescence centers that give a path of recombination of the electrons and holes within the material's band gap. In intrinsic scintillators, the recombination does not occur at a dopant site, but a

result of a self-trapped exciton emission. This reaction is a result of two anions sharing a hole creating a self-trapped hole. When the self-trapped hole captures a free electron, a self-trapped exciton is formed. When this self-trapped exciton relaxes, a photon can be emitted. For scintillators doped with cerium such as the ones that are studied in this collection of work, the time scale for the cerium transition between the 5d-4f levels the times typically range from 20-70 ns.

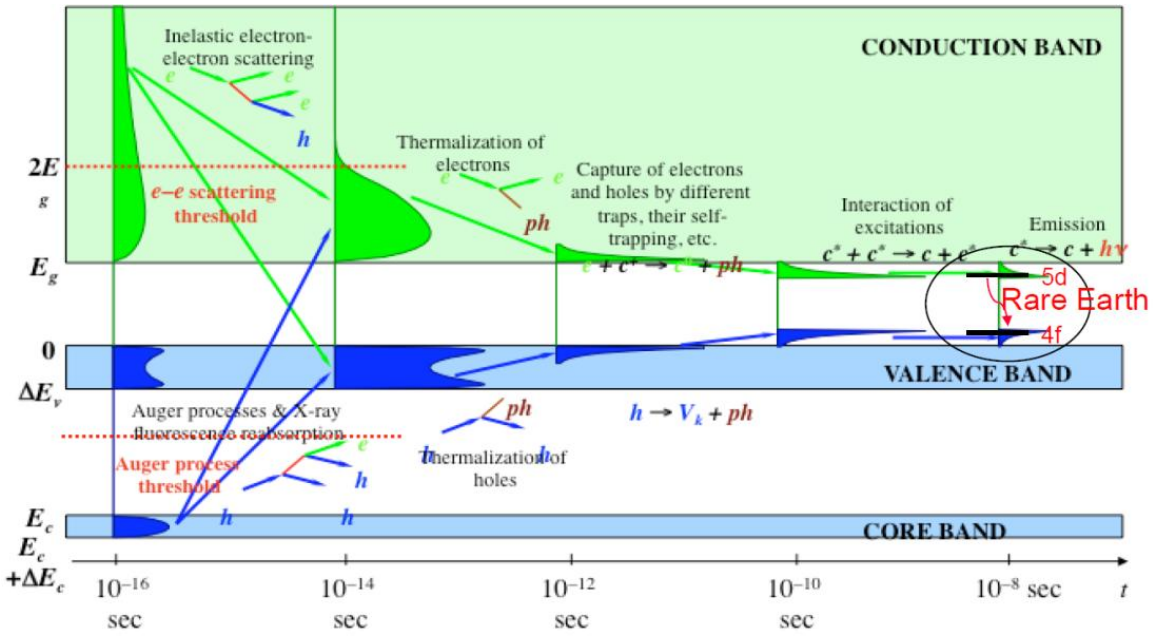

Figure *1.2. Diagram of the scintillation process and the time scales that events occur in. (Lecoq 2011)*

Energy Migration and the Resulting Effects on the Scintillation Mechanism

Energy migration is a step in the scintillation process in which an electron-hole pair migrates to a luminescence center. Sequential capture of first the hole and then the electron produces a metastable excited state of the luminescence center which subsequently de-excites to the ground state via the emission of a photon. From the discussion of the scintillation mechanism above, the major contributors to the scintillation time is the excited state lifetime of the luminescence center and the energy migration step. The migration step is strongly affected by defects in the scintillator which manifest themselves as charge traps. These charge traps capture the electron-hole pairs or individual electrons or holes and are eventually de-trapped, where they can recombine across a luminescence center resulting in a delayed emission. The structure of these charge traps can be measured using thermoluminescence techniques and characterized with analysis of the obtained glow curve (appendix B.4.). A point to be mentioned about this technique is that the characterization of the charge traps is measured by the response resulting from signal generated from a luminescence center. Any charge trap that results in non-radiative relaxation cannot be seen using this technique. By characterizing these trap structures, the trap lifetimes can be calculated for a sample temperature. Knowing this lifetime, one can understand the contribution to the scintillation decay time from charge

traps. This effect can also be observed by measuring the difference of the decay times (appendix B.3) when the material is activated by ionizing radiation or by using optical photons that excite a luminescence centers directly. The decay time measured using optical photons that directly excite the luminescence centers results in a decay time that is representative of the excited state lifetime of the particular luminescence center in a particular host material. Therefore, any variation of the two decay times indicates a difference in the energy migration times that is a function of charge trap depths, densities and lifetimes.

Common Inorganic Scintillators Applications

There are many applications that employ inorganic scintillators. They can range from routine everyday types of applications such as medical imaging that assists a physician in the care and diagnosis of patients to security applications. The latter includes x-ray scanning of baggage and detection of nuclear material that could be used in weapons. There are also more specialized applications of inorganic scintillators that are less common than the previously mentioned applications, such as high energy particle physics experiments, geological surveys, deep well logging, and neutron detection.

One very significant application of inorganic scintillators is medical imaging. Most medical imaging devices based on the detection of gamma/X-ray radiation use scintillators as the detector material. This dependency on scintillators over other types of detectors is due to the maturity of scintillator

technology, the relatively low cost, and its inherent properties such as stability at room temperature and mature pulse processing electronics already established that make scintillators more favorable than the other forms of radiation detection. These modalities include planar x-ray, x-ray CT (computed tomography), SPECT (single photon emission computed tomography) and PET (positron emission tomography). With the exception of the planar x-ray, which may employ a scintillating film, the detection systems used in these modalities are similar to the system shown in Figure 1. The scintillation materials used in these devices will vary from modality to modality as the criteria for detection vary. This results in many different types of inorganic scintillators used in medical imaging. These properties include the radiation stopping power (or attenuation length), luminosity (light output/unit energy deposited), decay time, the spectral emission wavelength, and the energy resolution.

Inorganic scintillators are also widely used in security applications. The detection of nuclear material in the field of security has probably been an application that has advanced scintillator research the most over the past years. To identify nuclear isotopes, the gamma signature of a fissile material has to be measured and compared to a known signature. To do this efficiently, the energy resolution of the scintillator becomes a dominant property in the selection criteria for the scintillator type. Although other radiation detectors such as high purity germanium detectors may have better energy resolutions, inorganic scintillators

offer a selection base that can operate at a larger ambient temperature ranges and also often mature growth processes, resulting in the large volumes of scintillation material needed for screening applications.

Purpose of Work

The work presented in this dissertation is to demonstrate the effects of non-proportionality on a scintillation system, study the energy migration and create a solution to improve it, introduce a new method for studying the non-proportional response of scintillators and report any improvement to the scintillators energy resolution that are a results of the improvement in the energy migration. The collection of works presented in this dissertation is a series of conference presentations which were published as journal articles in Nuclear Instruments and Methods in Physics Research Section A and IEEE Transactions of Nuclear Science. Chapter 5 will be submitted to IEEE TNS.

With Monte Carlo studies of a single crystal inorganic scintillator, the contributions to the energy resolution from a LSO:Ce scintillator's optical transport and non-proportional response can be characterized and understood by individually studying simulated effects. The simulation is only valid if some work is done to validate the simulations with experimental results. Chapter 2 will present a validation of a single crystal simulation and present results of individual contributions to the broadening of the energy resolution.

The energy migration is a major step in the scintillation mechanism and can affect many scintillation properties such as decay times and light output of a scintillator. The energy migration in scintillators is affected by charge trapping. With the knowledge of the trap structure obtained from thermoluminescence measurements and information such as trap depth and trap lifetimes, the temperature can be adjusted to control the contribution of the traps to the energy migration step of scintillation. Chapter 3 shows the results of the measured trap structure of YSO:Ce and measurements of the scintillation decay time measured at room temperature and at cryogenic temperatures. These results demonstrate the traps' contribution to the energy migration within YSO:Ce samples.

A method to improve the energy migration in YSO:Ce scintillators operating at room temperature was discovered and applied to this material. A trend observed in co-doping with calcium studies on oxide scintillators was a suppression of charge traps. From the study in Chapter 3 and the assumption that the energy migration is strongly affected by charge traps, the co-doping of YSO:Ce should result in scintillation decay times that are close to the decay times observed at cryogenic temperatures. Chapter 4 shows the results of the co-doping studies of YSO:Ce with calcium, the resulting trap structure, and the room temperature scintillation decay time results.

It is thought that if the energy migration is improved, the non-proportional response of a scintillator should also improve. In order to demonstrate this, a

new method to measure the non-proportional response of scintillators was developed and tested to more rapidly obtain the non-proportional light yield response of scintillators using resources that were available. This method takes advantage of the fast coincidence electronics and fine angular granularity inherent to a PET scanner. Using these advantages and the Compton scattering relationship of energy deposited versus scattering angle, the non-proportional electron response of scintillators can be obtained more quickly and more accurately than other methods. Chapter 5 will discuss this method and present some data to validate it.

Energy Resolution

A characteristic of an inorganic scintillator that is a requirement of the applications discussed is the energy resolution. Energy resolution can be seen as the energy of the measured energy. The energy resolution of a scintillator is formally defined by (Knoll 1989).

$$E_{Resolution} = \frac{\Delta E}{E} \quad (1.1)$$

Where ΔE is the full width at half maximum (*FWHM)* measured from the spectrum and E is the centroid location of the full energy peak being measured. An example pulse height spectrum is shown in Figure 1.3. The energy resolution

has many contributions to its broadening, including all components of the system such as the scintillation mechanism, optics and electronics. The differences in the spectra with different energy resolutions can be seen in Figure 1.4. This figure shows two different radiation detector systems and a clear illustration of a detector system with good energy resolution (Figure 1.4a) and a system with poorer energy resolution (Figure 1.4b). In Figure 1.4 it is easily seen that the inability to resolve the photopeaks results in the overlapping of these peaks creating spectra that may be hard to resolve in cases where full energy peaks are close to each other.

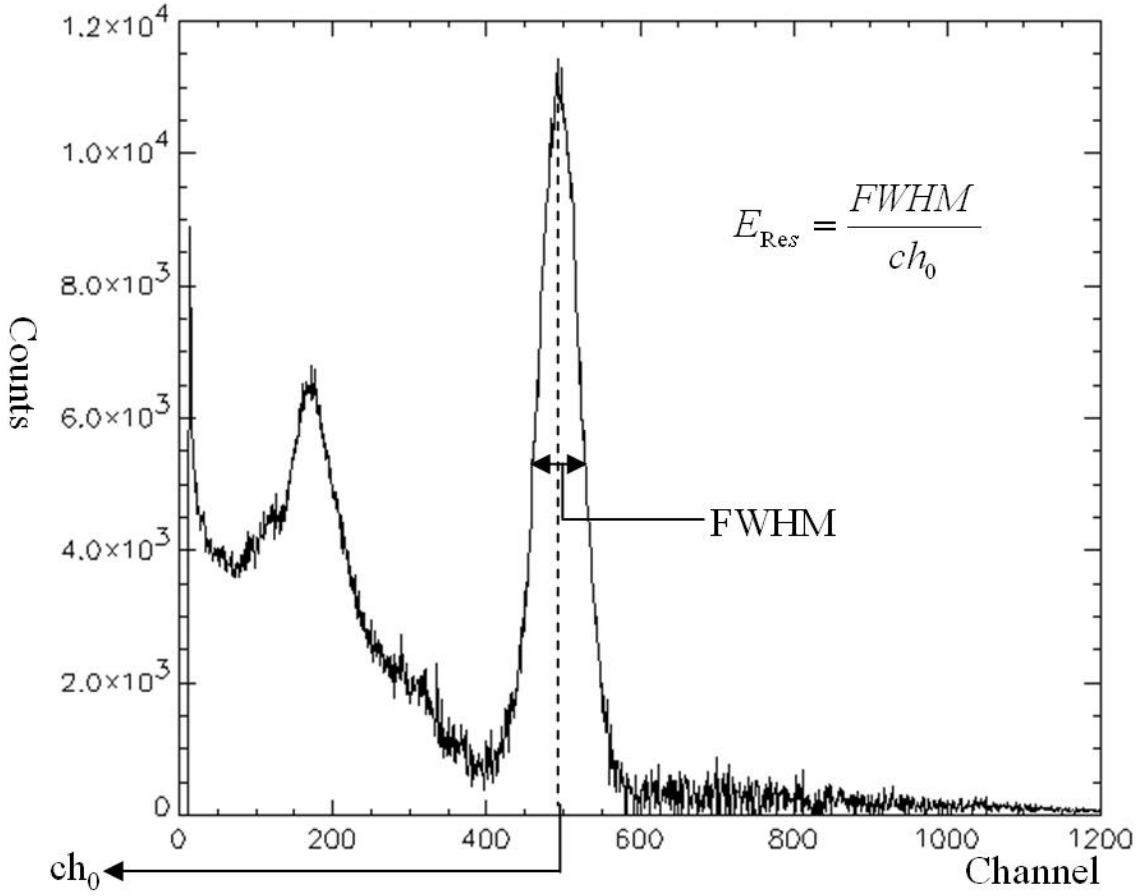

Figure 1.3. Plot of an acquired energy spectra of an LSO:Ce scintillator activated with a Na-22 source. Illustrated is the energy resolution of a 511 keV photopeak. From (Rothfuss, Byars et al. 2007).

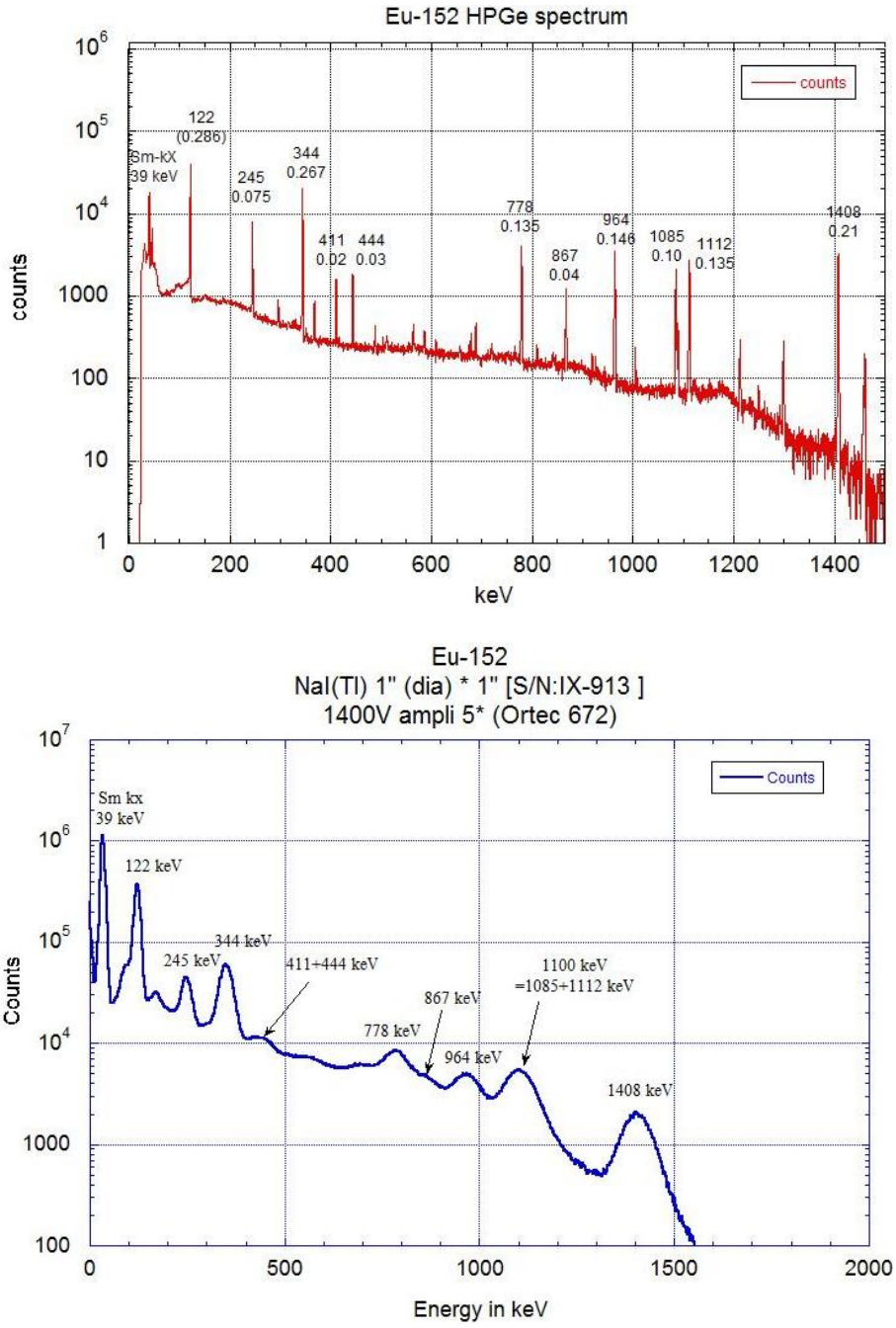

Figure 1.4. Pulse height spectra of a ^{152}Eu source. Top figure (figure 1.4a) is measured using an HPGe detector. The bottom (figure 1.4b) is measured with a NaI:Tl detector.

The energy resolution can be seen as a summation of uncertainties of contributing effects of the entire measurement system. The statistical contribution to the energy resolution is;

$$E_{ResolutionPoissonLimit} = \frac{2.35}{\sqrt{N}} \quad (1.2)$$

where *N* is the number of photoelectrons detected by the scintillation detector system assumed to follow Poisson statistics. This is an ideal case, as most radiation detection systems have more variations than those given by purely Poisson statistics. Additional contributions broaden the energy resolution. Birks (Birks 1967) describes the energy resolution as the quadrature sum of 4 major contributions: (i) emission of photons from the scintillator, (ii) the collecting of these photons at the photocathode of a PMT, (iii) the emission of photoelectrons and the collection of these photoelectrons at the first dynode, (iv) and the electron multiplication process. Dorenbos (Dorenbos, Haas et al. 1995) reduced the number contributions to three, calling them the (i) intrinsic resolution, (ii) the transfer resolution and (iii) the photomultiplier (photosensor) resolution. This relationship is written as;

$$E_{Resolution}{}^2 = E_{Resolution\ Intrinsic}{}^2 + E_{Resolution\ Transfer}{}^2 + E_{Resolution\ Photosensor}{}^2 \quad (1.3)$$

The intrinsic resolution is the resolution that deals with the scintillator at the point where scintillation photons are generated. Dorenbos further separates the intrinsic resolution to two terms:

$$E_{Resolution\ Intrinsic}{}^{2} = E_{Resolution\ Non-Proportionality}{}^{2} + E_{Resolution\ Inhomogeneity}{}^{2} \quad (1.4)$$

The Contribution of Non-Proportionality to the Energy Resolution

The broadening of the energy resolution due to the non-proportionality of the scintillator was first reported in NaI:Tl scintillators by Zerby in 1961 (ZERBY, MEYER et al. 1961). The study looked at data reported for the non-proportionality response of a NaI:Tl scintillator measured using a radioisotope library. The response was then used to extract an electron response by taking out the additional effects that follow the photoelectric effect such as x-ray emission or Auger electron emissions. Taking the electron response of the non-proportional effect, a Monte Carlo simulation was performed, and the results showed a broadening of energy resolution as a result of the non-proportional response across different energies. The result was shown for different sizes of NaI:Tl scintillator crystals and was attributed to the incident Compton scatter event as the first interaction (or first few Compton scatter events) followed by a photoelectric effect resulting in the full absorption of the incident radiation. This

summing of energies resulting in a full energy absorption from partial deposition of energies from a Compton event(s) and a photoelectric absorption creates a resolution broadening by the non-proportional response in scintillators.

The study of energy resolution broadening came back to life in the 1990s when LSO (Melcher and Schweitzer 1991) was introduced as a promising new scintillator with high luminosity, high stopping power and a fast decay time. It was observed that even with the high luminosity, the energy resolution was much worse than expected based on counting statistics. Dorenbos (Dorenbos, Haas et al. 1994) showed that the reason was a high degree of non-proportional response in LSO and the broadening due to intrinsic effects. He reached this conclusion by comparing the non-proportionality data of LSO with NaI:Tl data as found by Zerby. Dorenbos further expanded the theory of the energy resolution broadening found in LSO to other scintillators and found that the intrinsic scintillator energy resolution always plays an important part in energy resolution broadening. Within the same paper, Dorenbos pointed out that the experimental energy resolution can be understood using the methods developed by Zerby based on the electron response and Monte Carlo simulation. It is important to note that in 1995 there was a lack of techniques to obtain the electron non-proportional response. However, there were new promising methods being developed at the time to be discussed later.

A Monte Carlo investigation into the effects that are the causes of energy resolution broadening was performed and presented (Rothfuss, Byars et al. 2007). A study of effects such as the light transportation and the non-proportional effect was performed using Monte Carlo simulation using the GEANT4 package (Agostinelli, Allison et al. 2003). By benchmarking the optical portion of the simulation with experimental data, the optical contribution of the energy resolution was studied. The simulation was further extended by fitting a reported gamma response non-proportional curve (Dorenbos, Haas et al. 1995) and applying the fitted equation to modify the primary electrons energy that is resultant from an electromagnetic interaction within an LSO:Ce sample. The result showed by de-convolving the components that the contributions to the energy resolution were 5.2% from non-proportionality and 9.3% optical processes for a 1x1x1 cm LSO:Ce cube. This further shows that the non-proportional response broadens the energy resolution of scintillators.

Measuring the Non-Proportional Response of Scintillators

There are a few techniques used to measure the non-proportional response of scintillators. These techniques can be divided into two major groups of techniques which differ both by the results obtained and by the principles of the measurements. These techniques are gamma/X-ray response and electron response.

Gamma/X-ray Response

The gamma/x-ray response is probably the simplest method to measure the non-proportional response of scintillators. The most common method used is determining the non-proportional response in the scintillators using sources of known gamma ray energies. This gives the relationship between the gamma ray energy and the measured energy photopeak position (Appendix B). (The photopeak positions give the relationship between the measured peaks relative to the incident energy absorbed by the scintillator.) This ratio of the photopeak position versus the incident energy is generally collected using a radioisotope library and then plotted over a range of energies resulting in the non-proportional response trend of a particular scintillator (Figure 1.5).

Another gamma/x-ray response method that has recently been presented is the excitation of scintillators with the x-ray radiation produced by a synchrotron (Khodyuk, Haas et al. 2010). Using the monochromatic synchrotron x-rays, the non-proportional response can be directly measured from 9 keV to 100 keV with the lowest step size reported as 25 eV steps. This method is extended to lower energies by using the information of the fluorescent x-ray that escapes the measured scintillator, leaving only the energy of the incident x-ray minus the energy of the escaped x-ray. This method is further extended to lower energies using a method called K-dip spectroscopy. This method uses x-ray energies just

above the K-shell edge and assumes that the relaxation sequence from a k-shell photoelectric event is constant. Therefore, by subtracting a

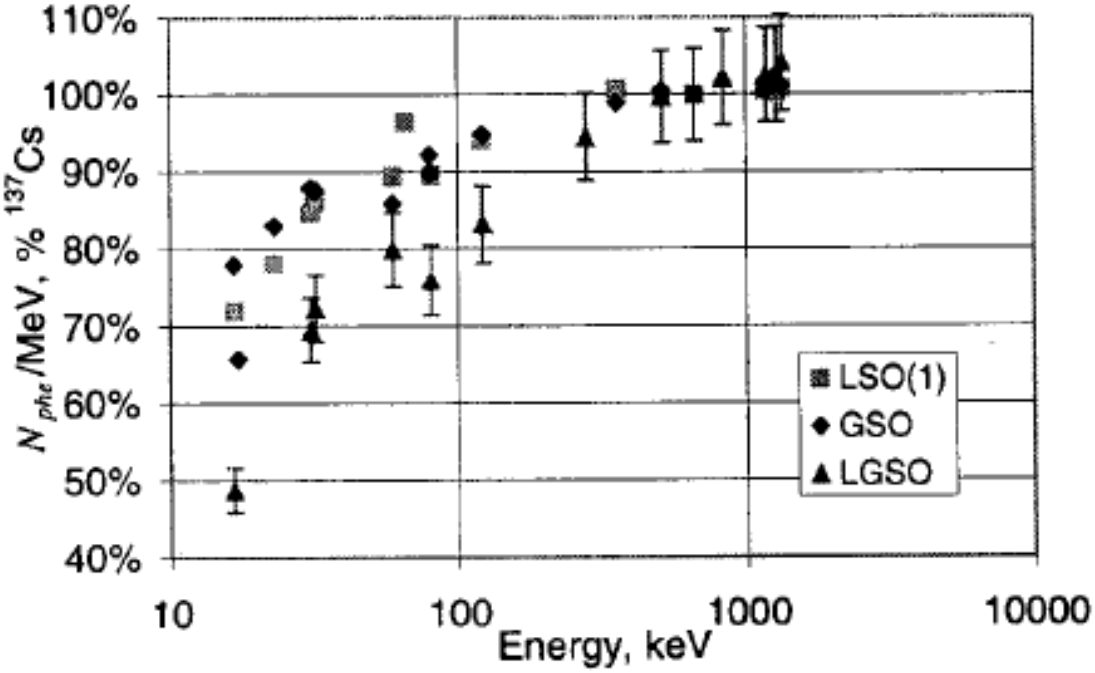

Figure 1.5. The non-proportional gamma radiation response for select oxide scintillators. Plot taken from (Balcerzyk, Moszynski et al. 2000) where the radioisotope library included ^{55}Fe, ^{57}Co, ^{133}Ba, ^{137}Cs, ^{241}Am, ^{170}Tm, ^{203}Hg, ^{22}Na, ^{54}Mn and ^{60}Co.

constant that comes from the photoelectric relaxation from these energies just above the k-shell edge, energies down to 100 eV are reported as measurable.

Electron Response

The electron response is measured by means of measuring a Compton electron in coincidence with the Compton scattered gamma to determine the energy of the electron. This method was first introduced by Valentine et al (Valentine and Rooney 1994). This initial design was described as using an incident monochromatic beam of gamma rays focused onto the scintillator being measured as shown in Figure 1.6.

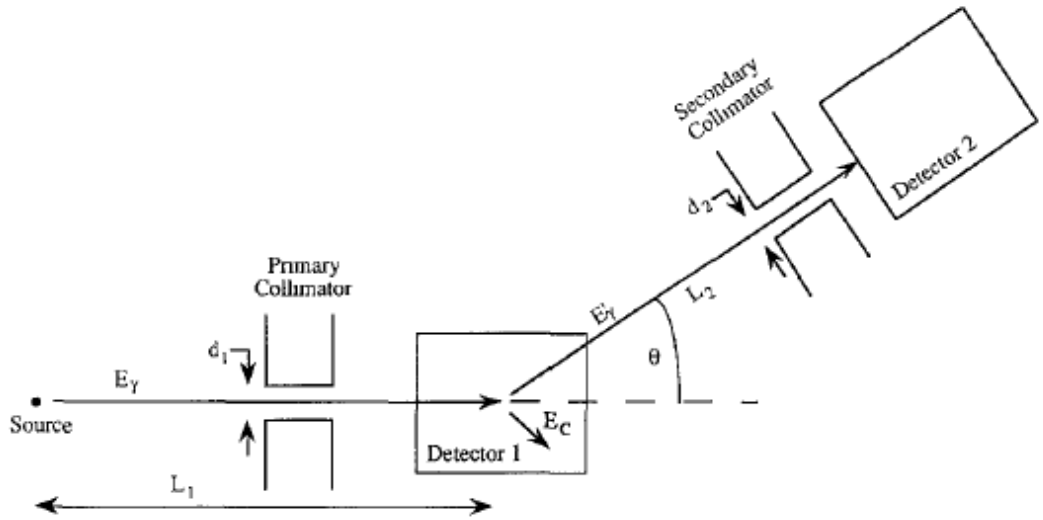

Figure 1.6. Diagram of the first Compton coincidence setup proposed by (Valentine and Rooney 1994)

A second collimator was placed at a known angle from the incident beam and a second detector was placed behind this second collimator to insure that the

scattered Compton gamma was well constrained in angle. When a coincident event was detected (an event that happens within a very short time frame ~ns), the energy was recorded in the measured scintillator. Using the Compton scattering equation (Appendix A) the energy deposited by the Compton electron can be calculated as a function of angle. The method was verified using Monte Carlo analysis and showed that the technique provided a viable solution to the electron response of scintillators.

Two years later the method originally proposed was benchmarked with a series of experiments (Rooney and Valentine 1996). This method used the same method of measuring the Compton electron in coincidence with the absorbed Compton scattered gamma. A modification was performed to measure the scattered Compton gamma with a high purity germanium detector (HPGe) to measure the Compton scattered gamma's energy (Figure 1.7). By using the high energy resolution of the HPGe detector, the Compton electron's energy is now calculated by subtracting the measured Compton scattered gamma from the HPGe from the initial gamma energy. The method used 2 different sources to irradiate the scintillators being characterized. For higher energy non-proportional responses, a ^{137}Ce (662 keV gamma ray) was selected, and a ^{99m}Tc (140 keV gamma ray) source was selected for lower energy studies. The stated major advantage of this method over other methods at the time was that this was a measurement that directly measured the electron response, which is required for

characterization of the contribution of the non-proportional light yield response on energy resolution broadening. The results of the benchmark experiments agreed

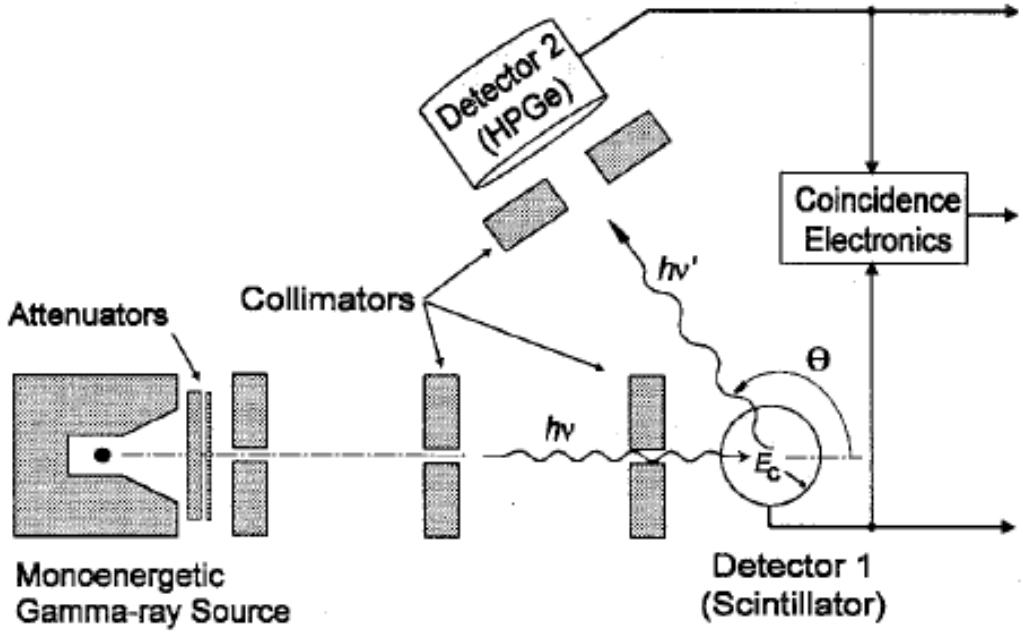

Figure 1.7. Diagram of second Compton coincidence system used to measure the non-proportional light yield response. Figure from (Rooney and Valentine 1996).

well with previously derived and measured experiments stating that the technique was correct and accurate (ZERBY, MEYER et al. 1961, Hill and Collinson 1966, Porter, Freedman et al. 1966). A claim from Rooney and Valentine gave insight to a disadvantage to this measurement technique. As presented, this method

required 12 to 24 hours to measure a single angle (one energy data point) in NaI:Tl. This statement means that to fully characterize one sample, with an energy sampling interval of 10 keV would take 1 to 2 months for a measured range of 10 keV to 660 keV.

This technique was further developed into what is currently known as the scintillator light yield non-proportionality characterization instrument (SLYNCI) (Figure 1.8). The latest iteration on this method was implemented at Lawrence Livermore National Laboratory in collaboration with Lawrence Berkeley National Laboratory and is currently in use to characterize the non-proportional light yield response of scintillators (Choong, Hull et al. 2008, Choong, Vetter et al. 2008). This implementation uses 5 un-collimated HPGe detectors to measure the scattered Compton gamma from the scintillator under test. For the un-collimated design, the method depends on the high energy resolution of the HPGe detector and the energy deposited in the sample being determined from the initial gamma ray energy minus the measured scattered Compton gamma ray detected by the surrounding HPGe detectors. This technique has much higher coverage for the scattered gamma ray and uses a collimated source aimed at the scintillator being measured with a strength of ~1mCi. With these experimental parameters, the acquisition takes about a day per sample to fully characterize the sample being measured.

Another method that gives the benefit of a lower equipment cost was a wide angle Compton coincidence measurement developed by Ugorowski et al (Ugorowski, Harrison et al. 2010). This method uses the same principle as the

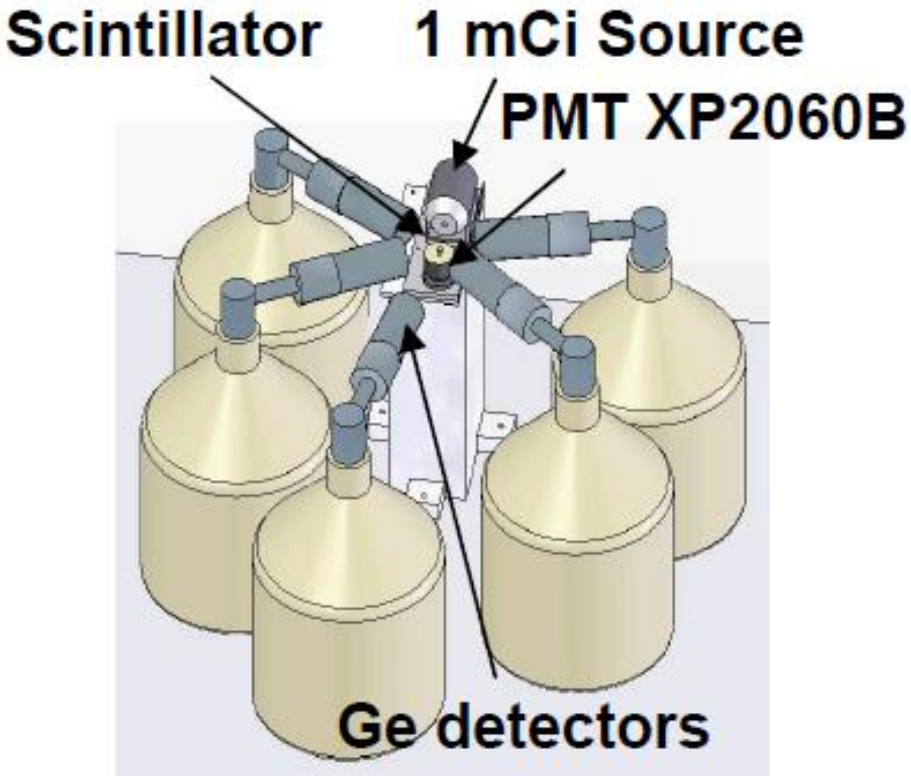

Figure 1.8. Diagram of the SLYNCI currently used at Lawrence Berkeley National Laboratories. From (Hull, Woon-Seng et al. 2009).

SLYNCI, but it requires a source with significantly less strength (µCi strength). The method also puts the second detector that detects the Compton scattered photon much closer to the sample, creating a larger scattering angle coverage

from the second detector (Figure 1.9). The second detector used is an HPGe detector, again selected for its high energy resolution. The non-proportional light yield response is measured by conservation of energy similar to the system from (Rooney and Valentine 1996). Its advantages include using exempt quantity

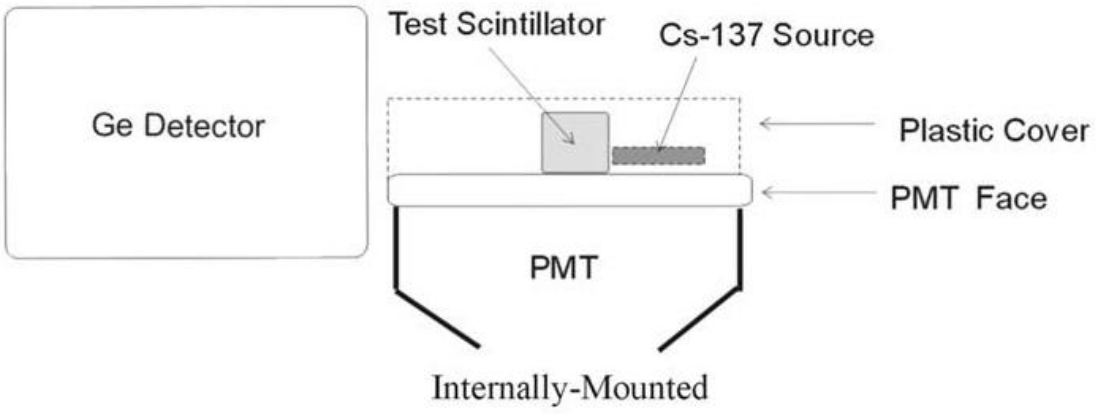

Figure 1.9. Figure showing the configuration for the Compton coincidence setup from (Ugorowski, Harrison et al. 2010). HPGe detector is shown close to the test scintillator with low activity Cs-137 source.

sources, minimal equipment, and inexpensive implementation with respect to other Compton coincidence systems. Its disadvantages are the calibrations necessary for accurate low Compton energy electron measurements based on information from the HPGe and the scintillator-photo-tube system detector corrections for gain drifts and other sources of errors. Another disadvantage is

the acquisition time. It commonly takes days to weeks to acquire the needed statistics in order to have confidence in the response measured.

References for Chapter 1

Balcerzyk, M., et al. (2000). "YSO, LSO, GSO and LGSO. A Study of Energy Resolution and Nonproportionality." IEEE Transactions on Nuclear Science 47(4): 1319-1323.

Birks, J. B. (1967). The Theory and Practice of Scintillation Counting. New York, Pergamon.

Choong, W. S., et al. (2008). "Performance of a facility for measuring scintillator non-proportionality." Nuclear Science, IEEE Transactions on 55(3): 1073-1078.

Choong, W. S., et al. (2008). "Design of a facility for measuring scintillator non-proportionality." Nuclear Science, IEEE Transactions on 55(3): 1753-1758.

Dorenbos, P., et al. (1995). "Non-Proportionality in the Scintillation Response and the Energy Resolution Obtainable with Scintillation Crystals." IEEE Transactions on Nuclear Science 42(6): 2190-2202.

Dorenbos, P., et al. (1994). "Non-linear response in the scintillation yield of Lu2SiOs:Ce3+." IEEE Transactions on Nuclear Science 41(4): 735-737.

Hill, R. and A. Collinson (1966). The Effects on theScintillation Efficiency of NaI (Tl) of Changes in the Thallium Concentration and Strain. I. Experimental, Borough Polytechnic, London.

Hull, G., et al. (2009). "Measurements of NaI(Tl) Electron Response: Comparison of Different Samples." Nuclear Science, IEEE Transactions on 56(1): 331-336.

Khodyuk, I. V., et al. (2010). "Nonproportional Response Between 0.1–100 keV Energy by Means of Highly Monochromatic Synchrotron X-Rays." IEEE Transactions on Nuclear Science 57(3): 1175-1181.

Knoll, G. F. (1989). Radiation Detection and Measurements, Wiley.

Lecoq, P. (2011). "New Approaches to Improve TIming Resolution in Scintillators." SCINT 2011 Giessen Germany Presentation.

Melcher, C. and J. Schweitzer (1991). Cerium-doped lutetium oxyorthosilicate: a fast, efficient new scintillator. Nuclear Science Symposium and Medical Imaging Conference, 1991., Conference Record of the 1991 IEEE, IEEE.

Moszyński, M. (2010). "Energy resolution and non-proportionality of scintillation detectors – new observations." Radiation Measurements 45(3-6): 372-376.

Murray, R. and A. Meyer (1961). "Scintillation Response of Activated Inorganic Crystals to Various Charged Particles." Physical Review 122(3): 815-826.

Porter, F., et al. (1966). "Response of NaI, anthracene and plastic scintillators to electrons and the problems of detecting low energy electrons with scintillation counters." Nuclear Instruments and Methods 39(1): 35-44.

Rodnyi, P. A. (1997). Physical processes in inorganic scintillators, CRC.

Rooney, B. D. and J. D. Valentine (1996). "Benchmarking the Compton coincidence technique for measuring electron response nonproportionality in inorganic scintillators." Nuclear Science, IEEE Transactions on 43(3): 1271-1276.

Rothfuss, H., et al. (2007). "Energy resolution and absolute detection efficiency for LSO crystals: A comparison between Monte Carlo simulation and experimental data." Nuclear Instruments and Methods in Physics Research Section A: Accelerators, Spectrometers, Detectors and Associated Equipment 580(2): 1087-1092.

Ugorowski, P. B., et al. (2010). "Design and performance of a Compton-coincidence system for measuring non-proportionality of new scintillators." Nuclear Instruments and Methods in Physics Research Section A: Accelerators, Spectrometers, Detectors and Associated Equipment 615(2): 182-187.

Valentine, J. D. and B. D. Rooney (1994). "Design of a Compton spectrometer experiment for studying scintillator non-linearity and intrinsic energy resolution." Nuclear Instruments and Methods in Physics Research Section A: Accelerators, Spectrometers, Detectors and Associated Equipment 353: 37-40.

Zerby, C. D., et al. (1961). "Intrinsic Line Broadening in NaI(Tl) Gamma Ray Spectrometers." Nuclear Instruments and Methods 12: 115-123.

CHAPTER 2 ENERGY RESOLUTION AND ABSOLUTE DETECTION EFFICIENCY FOR LSO CRYSTALS: A COMPARISON BETWEEN MONTE CARLO SIMULATION AND EXPERIMENTAL DATA

A version of this chapter by H. Rothfuss was submitted and accepted as, *Energy Resolution and Absolute Detection Efficiency for LSO Crystals: A Comparison Between Monte Carlo Simulation and Experimental Data, Nuclear Instruments and Methods in Physics Research Section A: Accelerators, Spectrometers, Detectors and Associated Equipment 580, (1087-1092)*

This chapter is the reformatted version of the original work submitted to the referenced journal. No additional changes to the content of the original article were done other than formatting to conform to the thesis format and placement of figures to retain the flow of information that aids the reader. The references to sections were also changed to a format of 2.x.x to be consistent with the chapter numbering of this work.

Abstract

Non-proportionality between energy deposition and scintillation light production in a scintillator and transport of scintillation photons in the detector have been introduced in a Geant4-based simulation code. Simulation and experimental results were compared for samples of LSO detectors: absolute detector efficiency and energy resolution obtained from simulation are consistent with the experimental data. We also studied the average path length of scintillation photons in the detector and its contribution to the time resolution.

Introduction

When investigating new scintillating materials and/or new detector systems, Monte Carlo simulation can play an important role if it is able to properly describe the complexity of the whole radiation detection process (i.e energy deposition, scintillation light production and optical photons transport and their detection). While interaction mechanisms for charged particles, X-rays or gamma-rays interaction in matter are generally well described in most Monte Carlo simulation system codes, scintillation light production, transport and detection are generally parameterized globally. On the other hand, these phenomena play a major role in determining performance parameters such as energy resolution and detector efficiency.

In particular, in an inorganic scintillator such as Lu_2SiO_5 (LSO)(Melcher and Schweitzer 1991), one should consider: (i) non-proportionality of the scintillator response which causes deviation from linearity (with energy deposition) of the light output, (ii) inhomogeneities in the crystal responsible for local variations of light output, (iii) the transport of scintillation photons in the crystal, the reflection or transmission of scintillation photons at the surfaces, the role of light guides, (iv) the Quantum Efficiency (QE) of the associated PhotoMultiplier Tube (PMT) and all other effects relative to the PMT.

Other authors have tried to theoretically and experimentally characterize the different processes involved in the scintillation in inorganic materials, in

particular the non-proportionality between energy deposition and scintillation light production (Dorenbos, Haas et al. 1995), (Balcerzyk, Moszynski et al. 2000), (Kapusta, Szupryczynski et al. 2005). The purpose of this work is to introduce some of the phenomena of above in a coherent Monte Carlo simulation, in order to provide a reliable tool for detector design. We restricted this work to a specific material (LSO) and to photons in the 10keV-1MeV energy range, but the methodology could be applied to other scintillators and also extended to a larger energy range.

In this paper we assumed a nominal absolute light output of the scintillator and a nominal QE of the PMT, neglected the effects of crystal inhomogeneity, and focused our attention on the the optical transport of scintillation photons (in the bulk material and on the surfaces) and on the non-proportionality effect. In order to reduce the variables in play, simple geometries such as a single detector directly coupled to a PMT were used.

The simulation, based on Geant4 (Agostinelli, Allison et al. 2003), (Thompson, Camborde et al. 2005), ("http://geant4.web.cern.ch/geant4") was benchmarked with experiments, and the fundamental parameters of absolute detector efficiency and energy resolution were used to evaluate the correctness of the simulation.

It is well known that, if only the electromagnetic interaction of the incident photon in the scintillator is described in the simulation, unrealistic energy spectra

are obtained. A typical solution to this problem is to convolve the simulated spectrum with a Gaussian function with a Full Width Half Maximum (FWHM) extracted from a measured energy resolution. This phenomenological approach is presented in section 2.5.1. The next natural step in complexity is to introduce the effect of both non-proportionality and light transport in the simulation. The former effect uses a model based on experimental data (Kapusta, Szupryczynski et al. 2005). The latter uses the Geant4 intrinsic capability to track light scintillation photons. These results are presented in section 2.5.2.

Section 2.5.4 concerns time resolution, another important performance parameter for a scintillator, especially when involved in complex detection systems. Time resolution is not only driven by intrinsic material properties, such as the scintillation decay time, but also to some extend by the path length of the scintillation photons in the crystal which depends on the crystal geometry and its surface state. In that section we modeled a system with two detectors in coincidence and evaluated the contribution of scintillation photon transit time to the time resolution.

Experimental Set-up

Pointlike calibrated sources (alternatively ^{137}Cs, ^{68}Ge,^{57}Co) were mounted on a positioning system able to move in 3D, in order to have the best possible alignment between the source and the central axis of the detector crystal.

The LSO crystals were coupled to a Photonics XP 2020Q PMT, biased by a high voltage power supply ORTEC Model 556, with a negative voltage of 2000 V. The signal of the PMT was sent to preamplifier ORTEC Model 113, with a 200 pF input capacitance. The Preamplifier's signal was sent to an amplifier with a gain of 15. The amplified signal is fed into a MultiCahnnel Analyzer (MCA) emulator (MAESTRO-32, ORTEC).

LSO crystals were attached to the PMTs using an optical couplant grease (Dow Corning Q2-3067) to reduce the mismatch of indexes of refractions. The remaining five sides of the crystal were covered by several Teflon sheets acting as reflector. Detector and PMT were wrapped in a light tight enclosure.

The LSO crystals used in different experiments were saw-cut with no polishing or etching. The following dimensions were used: 10x10x10 mm^3, 4x4x20 mm^3, 10x10x20 mm^3. The source was placed at 20 cm from the 10x10x10 mm^3 LSO. In the case of the 4x4x20 mm^3 crystal, the 4x4mm^2 face was coupled with the PMT, the gain of the amplifier was increased to 25, and the source was placed at 10 cm from the detector to reduce acquisition time.

For each acquisition, an LSO background spectrum (from ^{176}Lu) was acquired in the same conditions without external source and the background was subtracted.

A different set-up was used for the time resolution measurement. Two LSO crystals were coupled to two PMTs, and the fast anode signals were sent to

a Constant Fraction Discriminator (CFD) and to the start and stop inputs of a Time Analog Converter (TAC). The TAC analog output was sent to the MCA to produce a time difference histogram. The dynode signals of the PMTs were amplified, thresholded, and put in coincidence: the time coincidence of two energy qualified events was used as a gate for the MCA. In this experiment we used a pair of identical LSO crystals, either 10x10x10 mm^3 or 10x10x20 mm^3, and a ^{68}Ge source was placed the detectors.

Monte Carlo Simulation

GEANT 4.7 was used to develop the simulation code. This package has the capability to model the electromagnetic interaction and the optical transportation. The electromagnetic interaction simulation included the following physical processes: photoelectric effect, Compton scattering and Rayleigh scattering. The cross sections of these effects were taken from the GEANT4 Low Energy libraries.

The experimental set-up was simulated in its fundamental parts (source and detector), no mechanical support (mainly made of plastic material) or other laboratory equipment from the environment was considered in the simulation. The LSO composition was Lu_2SiO_5 with a density of 7.4 g/cc.

The parallel code (Parallel Geant4, Top-C) ran on a 7-node Linux Cluster, where each node comprised of two Xeon, 3.06 GHz processors with 2 Gb of

RAM per node. The event processing rate was about 11.5 detected-primary-photons/sec, when full transportation of optical photons was included.

Phenomenological model

The phenomenological approach for reconciliation between measured and simulated energy resolution convolves the energy spectrum with a Gaussian function whose standard deviation fits the experimental full-energy peak. In this case, all effects after energy deposition of the primary and secondary particles are not modeled but are included in the experimentally-based broadening. The standard deviation of the Gaussian depends on the deposited energy *E*, as shown in eq. (2.1), where $Eres_0$ is the energy resolution (*FWHM/E*) measured at energy E_0, in this work E_0 being 662 keV.

$$\sigma = \left[\frac{\sigma}{E}\right]_0 \sqrt{E_0} * \sqrt{E} = \left[\frac{Eres_0}{2.35}\right] \sqrt{E_0} * \sqrt{E} \qquad (2.1)$$

Scintillation light generation and transport

In a second phase, the simulation was extended to include processes following the energy deposition: the conversion of energy into optical photons and their transport until the photocathode of the PMT. We can estimate the mean number of detected scintillation light photons as:

$$\overline{N} = N_{MeV} * E_{dep} * \varepsilon_{LightTransport} * QE_{PMT} \qquad (2)$$

Where, N_{MeV} is the average number of photons per MeV, E_{dep} the deposited energy, QE_{PMT} the quantum efficiency of the PMT, $\varepsilon_{LightTransport}$ the efficiency of optical photons transport from the point of emission to the surface of the PMT. Instead of approximating $\varepsilon_{LightTransport}$, a better approach is an actual simulation of the optical processes, now possible in Geant4, even though at the cost of long computing time. We observed in this work that the efficiency of the light transportation was usually 50%-60%, which is a consistent reduction of the scintillation light: this loss of scintillation photons in the bulk and at the surfaces of the crystal seems to be the major contributor to the widening of the energy spectrum.

It was assumed that in LSO a mean value of N_{MeV}=30000 scintillation photons per MeV were emitted. This being a mean value, for each deposited energy E_{dep} a Gaussian distribution of mean $N_{MeV} * E_{dep}$ was sampled to obtain an actual number of scintillation photons N. The next phase is the transport of each of the N photons in the detector bulk. Some of the optical properties of the LSO material were found in the literature or heuristically estimated. At the peak emission wavelength of 420 nm, the index of refraction is 1.8. The bulk material mean free path was assumed very large when compared to the crystal

dimensions, so in the simulation a nominal values of 3 m was used. The window between the detector and the photosensitive area of the PMT was modeled as a piece of glass, with thickness of 1 mm and an index of refraction of 1.5. The PMT was assumed to have a quantum efficiency of 25%. The surfaces of the crystal were described as a ground surface with a reflectivity of 0.99, and the reflection was assumed to be a 40% specular spike and a 60% specular lobe (Geant4 terminology is used here to identify the features and the processes). The surface of the crystal facing the PMT was modeled differently, since no reflector was present and optical grease was used to facilitate coupling and transmission of light to the PMT: it was modeled as a ground surface with a reflection coefficient of 0.8 with a specular spike contribution of 20% and a specular lobe contribution of 80%.

Non-Proportionality

It has been observed that for some scintillators such as LSO at low energies (below 200-300 keV), the number of scintillation photons is not anymore proportional to the deposited energy. This was introduced in the simulation by modeling the experimental LSO non-proportionality and fitting the experimental data [4] with the following model:

$$E_{depNP} = E_{dep}(1 - e^{(-2.13E_{dep} - 0.625)}) \quad (2.3)$$

Where E_{depNP} is the deposited energy corrected for non-proportionality and E_{dep} is the deposited energy in MeV. The deposited energy used was the kinetic energy of the electron created by a Compton scatter or photoelectric absorption. Using the equation (2.3) the energy deposited is corrected on the fly prior to the production of scintillation photons. The light transport described in section 2.3.2 is subsequentely applied to the scintillation photons.

Methods

In order to estimate the absolute detection efficiency of the LSO detector, a calibrated source was used: the ^{137}Cs had an activity of 0.404 MBq with an uncertainty of 3.1%. A 0.851 branching ratio was applied to obtain the 662 keV photon emission rate. For each acquisition the acquisition time was corrected for dead time of the Multichannel Analyzer (MCA). We defined the absolute detection efficiency as the integral of counts measured or simulated in the Full Energy Peak (FEP), in the energy window 540-775 keV, divided by the number of 662 keV photons emitted in the set acquisition time. An LSO background subtraction was performed for all experimental spectra. A similar method was used to compute the simulated detection efficiency: the number of photons detected within the energy window divided the emitted photons.

The experimental and simulated energy resolution was measured by fitting the photopeak with a Gaussian function. From the Gaussian fit, the mean deposited energy (*E*) and sigma (σ) were extracted and used to calculate the energy resolution, defined as the Full Width Half Maximum (FWHM) of the gaussian divided by the energy, $E_{res} = 2.35 \cdot \sigma / E$.

Experiments and simulation were repeated 5 times: the reported values are the average values over the series of measurements and simulations, and the reported error is the standard deviation.

The non-proportionality of the LSO detector was tested overlapping the energy spectra obtained by exposing the detector sequentially to the individual gamma sources (^{137}Cs, ^{68}Ge, ^{57}Co). Each Full Energy peak was identified and fitted with a Gaussian, providing mean deposited energy and standard deviation for the corresponding photon energy.

The coincidence simulation and measurement produced time histograms, whose FWHM provided the time resolution of the system. We did not simulate the scintillation decay time, and considered only the difference in transit time between the scintillation photons. When both 511 keV photons from the ^{68}Ge source were detected, the track lengths of all scintillation photons in each detector were converted into transit time (using the value of the speed of light divided by 1.8, the index of refraction of LSO) and were stored in two separate histograms. The time difference recorded for this event was defined as the

difference of the maxima (close to the mean values) of the two histograms. Finally, time differences of all coincidence events were histogramed, and the FWHM of this distribution was estimated.

Results and discussion

Phenomenological Model

Using the set-up described in Section 2, a 10x10x10 mm^3 LSO crystal with saw-cut surfaces and a ^{137}Cs source, we measured an energy resolution of 10.5% for 662 keV peak. The simulated spectrum is convolved with a Gaussian of corresponding FWHM. In Figure 2.1 the simulated and experimental energy spectra are compared. The absolute detector efficiency in the energy window 540keV-775keV is (4.36 **±** 0.13) 10^{-5} for the experimental measurement and (4.57 ± 0.09) 10^{-5} for the simulation. The comparison of simulation results against the experimental data show good agreement in the absolute detection efficiency. This comparison was performed with the polished 1 cm^3 crystal with reflector on all sides as described in Section 2. This result was confirmed by additional experiments and simulations using different reflector configurations, which were performed to understand if partial light loss could affect the detection efficiency. In those experiments, we observed that the FEP shifted towards lower energies when less efficient reflector configurations were used, but that there was no significant change in the number of counts under the FEP.

It is also observed that simulated and experimental spectra (in Figure 2.1 and following figures) show good agreement in the FEP and in the vicinity of the Compton edge. The broad peak observed experimentally at low energy is due to

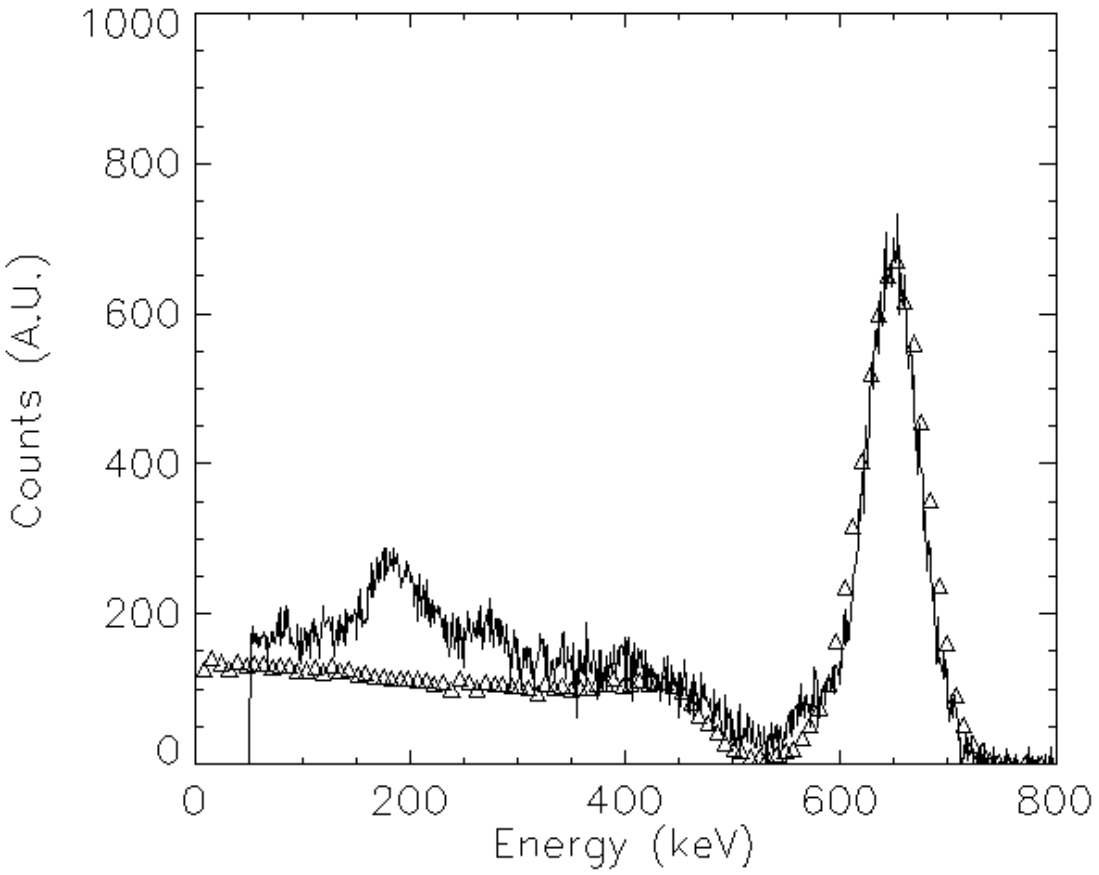

Figure 2.1. Deposited energy spectra, experimental (line) and simulated (triangle), for 662 keV photons from ^{137}Cs. The phenomenological model is used for the simulated spectrum. The detector is a 10x10x10 mm^3 LSO crystal.

backscatter from the environment and was not simulated. This was confirmed by additional experiments with collimated sources.

Modeling Light Transport and Non-Proportionality

Following the model described in Section 3, a mechanism of non-proportionality in the production of scintillation photons was introduced in the simulation, and the resulting scintillation photons were transported in the detector material. Simulation and experiment were performed with two different crystal samples: a 10x10x10 mm^3 and a 4x4x20 mm^3 LSO crystal, both with saw-cut surfaces. As can be seen in Figure 2.2 and 2.3, these two components alone explain the experimentally observed broadening of the FEP and reproduce closely the experimental energy resolution. In table 2.1, the measured and simulated energy resolutions at 662 keV are reported for the two samples, together with their absolute detection efficiencies.

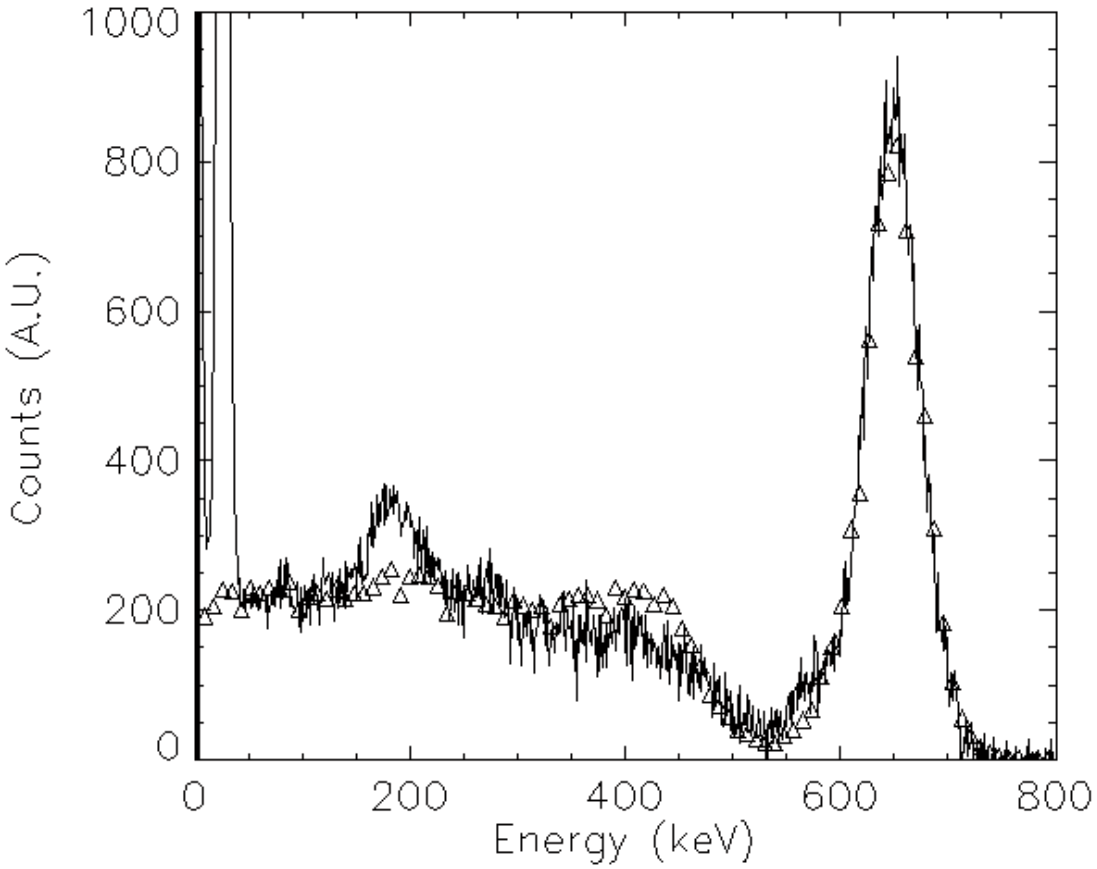

Figure 2.2. Deposited energy spectra, experimental (line) and simulated (triangle), for 662 keV photons from ^{137}Cs. Non-proportionality and transport of scintillation photons are included in the simulation. The detector is a 10x10x10 mm^3 LSO crystal

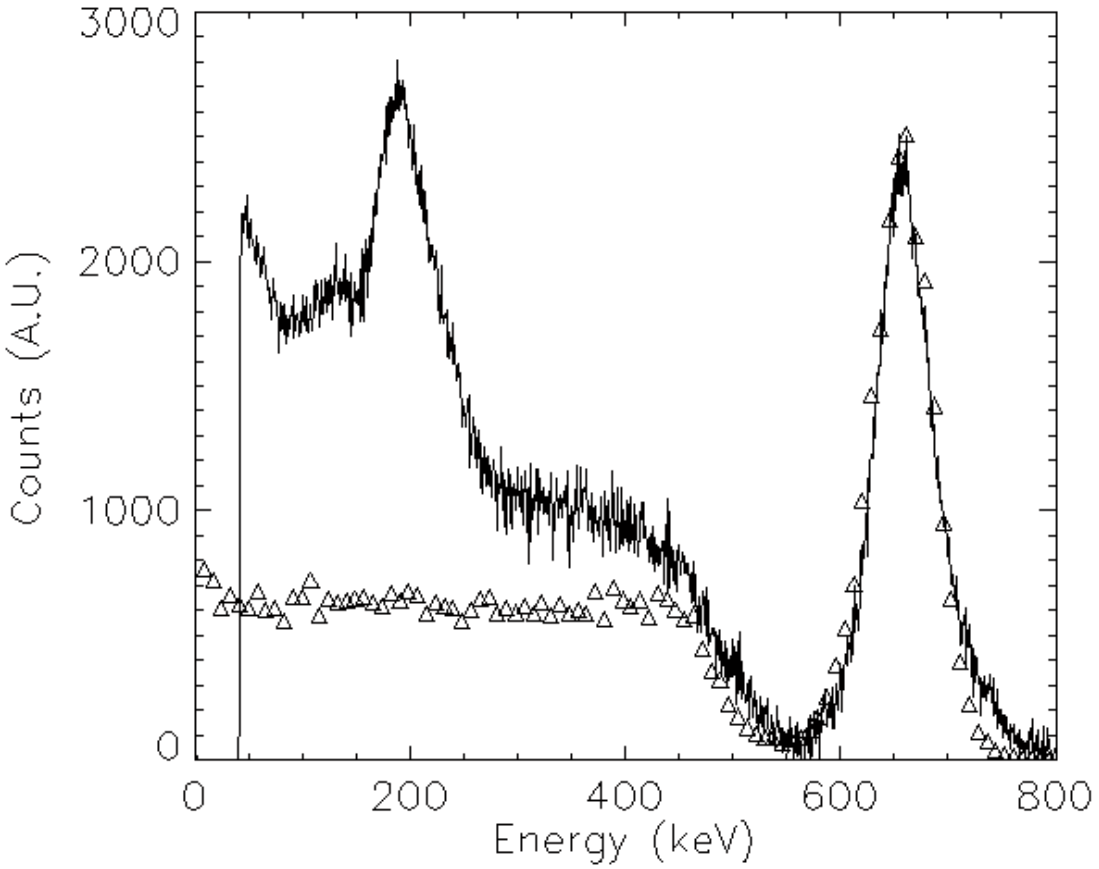

Figure 2.3. Deposited energy spectra, experimental (line) and simulated (triangle), for 662 keV photons from ^{137}Cs. Non-proportionality and transport of scintillation photons are included in the simulation. The detector is a 4x4x20 mm^3 LSO crystal

Table 2.1: Energy resolution and absolute detector efficiency, experimental and simulated, for two LSO samples. Source is 137Cs (662 keV photons), placed at 20 cm from sample 1 (10x10x10 mm3) and at 10 cm from sample 2 (4x4x20 mm3)

Sample		Experiment	Simulation
1 cm^3 LSO	Energy Resolution	(10.48 ± 0.04)%	(10.2 ± 0.4)%
1 cm^3 LSO	Efficiency	(4.36 ± 0.13) 10^{-5}	(4.39 ± 0.05) 10^{-5}
4x4x20 mm^3 LSO	Energy Resolution	(10.5 ± 0.1) %	(10.4 ± 0.4)%
4x4x20 mm^3 LSO	Efficiency	(3.68 ± 0.19) 10^{-5}	(3.54 ± 0.09) 10^{-5}

In order to evaluate the separate contribution of non-proportionality and optical processes to the final energy resolution, the simulation was run without non-proportionality effect. The contribution of non-proportionality can be estimated using :

$$E_{resNP} = \sqrt{E_{resTOT}^2 - E_{resOP}^2} \qquad (2.4)$$

Where E_{resNP} is the contribution of the non-proportionality effect to the energy resolution, E_{resOP} is the contribution of the counting statistics, the optical properties and transportation, and the Q.E. of the photosensitive area, E_{resTOT} is the energy resolution with both effects. The result of the simulation showed that the contribution of the non-proportionality to the energy resolution was 5.2%, while the combined contribution of the remaining processes (mainly optical) was

9.3%. Non uniformity of the crystal and the photosensitive area where not included in the simulation.

Non-Proportionality study

The effect of non-proportionality has been observed by exposing the $1cm^3$ LSO crystal to a set of γ sources of different energy, and in Figure 2.4 the resulting spectrum is shown, together with the corresponding simulated spectrum. Each FEP has been fitted with a Gaussian, and position of the centroid and standard deviation were determined, and energy resolution computed. These data are reported in table 2.2.

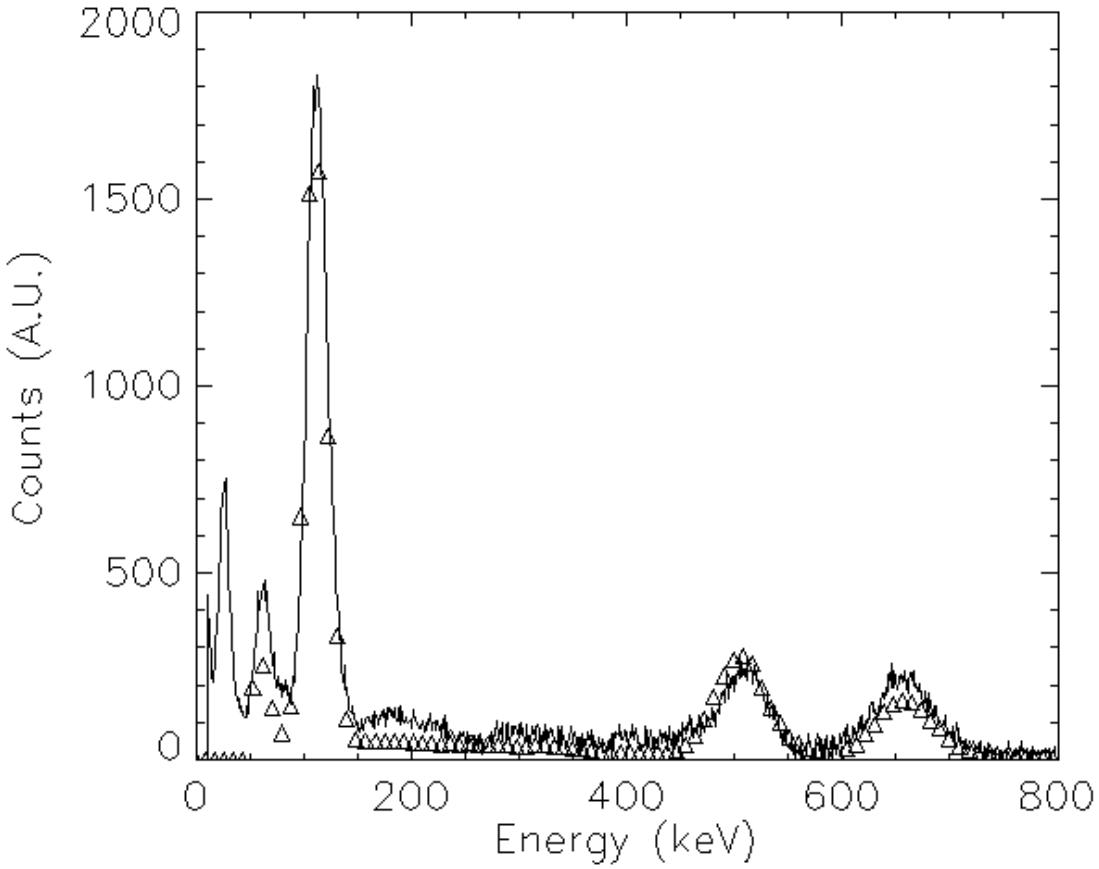

Figure 2.4. Deposited energy spectra, experimental (line) and simulated (triangle), for a 10x10x10 mm^3 LSO crystal exposed to 662 keV photons from ^{137}Cs, 511 keV photons from ^{68}Ge, 122 keV photons from ^{57}Co.

Table 2.2: Energy resolution and photoelectric peak position, experimental and simulated, obtained with a 1 cm3 LSO detector, for three photon sources.

Source	Energy		Experiment	Simulation
^{137}Cs	662 keV	Photopeak centroid (a.u)	656	654
		Standard deviation (a.u.)	28	29
		Energy Resolution (%)	10.0	10.4
^{68}Ge	511 keV	Photopeak centroid (a.u)	509	503
		Standard deviation (a.u.)	27	25
		Energy Resolution (%)	12.3	11.8
^{57}Co	122 keV	Photopeak centroid (a.u)	112	113
		Standard deviation (a.u.)	27	25
		Energy Resolution (%)	11.0	10.2

Figure 2.5 shows, as a function of the photon energy, the proportionality of the light output as a fraction of the light yield per MeV at 662 keV, where the non-proportionality effect is know to be negligible: the position of the FEP is divided by the incident photon energy, and normalized to the value at 662 keV. If non-proportionality effect were negligible, the centroid of the FEP would be

proportional to the incident photon energy, and their ratio should be constant. Instead, one can notice a clear deviation from the unit value at 122 keV. Again,

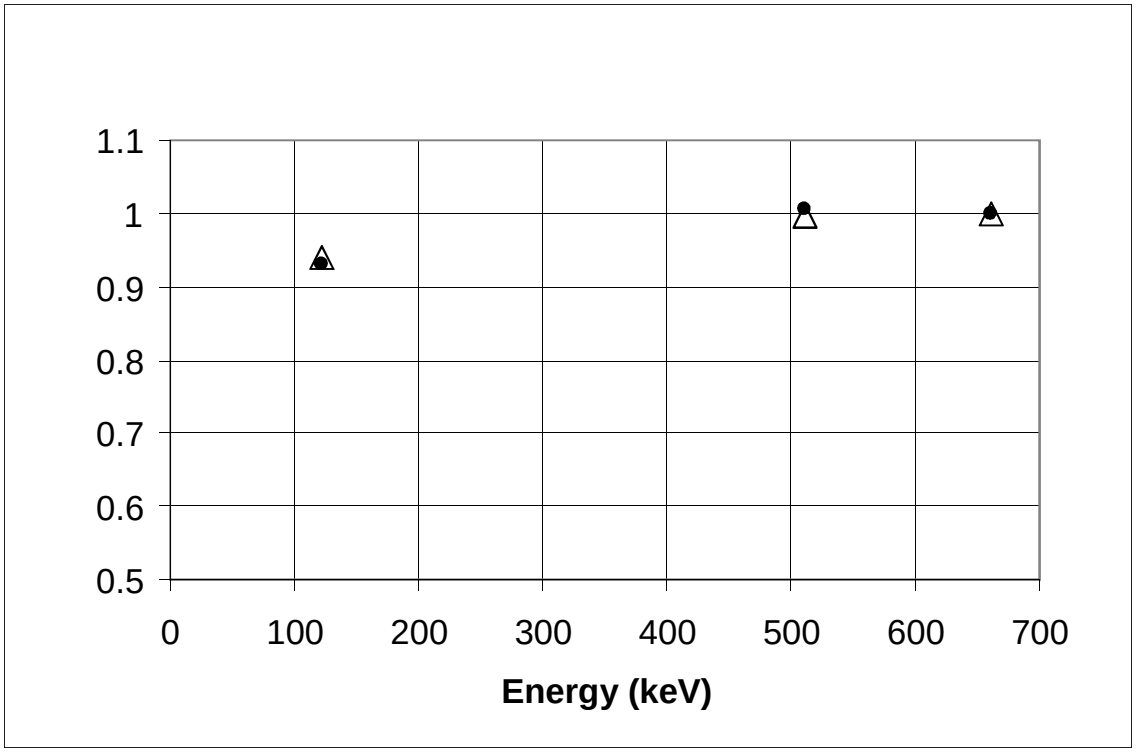

Figure 2.5. Proportionality of the light output as a fraction of the light yield per MeV at 662 keV vs. incident photon energy: experimental data (solid circle) and simulation data (triangle). Values smaller than one show a deviation from proportionality.

the simulation is in good agreement with the experimental data. A deviation from proportionality causes also a degradation of energy resolution reported in Table

II: one could also verify that the low energy (122 keV) energy resolution does not follow the expected $\approx 1/\sqrt{E}$ behavior. One should note that although the non-linearity behavior is important only at low energy, it does contribute to the shape of the FEP for multiple interaction events.

Timing properties

As explained in Section 2.4, we did not simulate the scintillation decay, but considered only the difference in average transit time of the scintillation photons in two detectors. We expect the scintillation decay time to be the major contributor to the time resolution, and this is clearly visible in the results of the simulation shown in Table 2.3: for two 10x10x10 mm^3 crystals, the measured time resolution is about 250 ps, while the simulated contribution of the path length is only 50 ps. It is interesting to note that when using a longer crystal (10x10x20 mm^3), the simulated transit time increases linearly with the crystal length. However, when subtracting (quadratically) the simulated (light transport) time resolution from the experimental time resolution, we do not obtain, as would be expected, a constant value depending only from the intrinsic properties of the scintillating material. This problem likely deserves further attention.

Table 2.3: Time resolution of a system of two detectors in coincidence, experimental and simulated. Source is 68Ge (511 keV photons). The simulated values include only the contribution of transit time of the scintillation photons in the two detectors.

Sample	Experiment	Simulation
10x10x10 mm^3 LSO	254 ± 12 ps	52 ± 7 ps
10x10x20 mm^3 LSO	296 ± 7 ps	108 ± 4 ps

Conclusions

In order to predict basic detector crystal properties such as absolute efficiency and energy resolution in the energy range 100-1000 keV, we developed a Monte Carlo simulation code based on Geant 4.7 to take advantage of its capability to transport optical photons. We introduced an experimental model for the non-proportionality between energy deposition and scintillation light production in LSO. Simulation results for energy resolution and absolute efficiency did compared favorably to experiment using single LSO crystals of 10x10x10 mm^3 and 4x4x20 mm^3 (coupled with PMT), confirming the validity of the model parameters (non-proportionality model, crystal surface description, bulk material properties). In a coincidence set-up between two 1 cm3 LSO crystals, the simulation showed that the main contribution to the time resolution

(250 ps FWHM) was not the jitter in the photon path length (50 ps FWHM) but the scintillation time of LSO itself

This code has the potential to be a reliable tool to estimate key performance parameters for novel detector architectures based on inorganic scintillators (proportional or not), provided the bulk material properties and surface treatment are known.

Acknowledgements

The authors would like to thank Eric Arnsdorff for his help with building the 3d translation stage and all of the materials to do so. We would also like to thank Chuck Melcher, Piotr Szupryczynski and Merry Spurrier for their discussions on LSO and also for providing us with all of the samples that we needed for this research.

References for Chapter 2

Agostinelli, S., J. Allison, et al. (2003). "GEANT4—a simulation toolkit." Nuclear Instruments and Methods in Physics Research Section A: Accelerators, Spectrometers, Detectors and Associated Equipment 506(3): 250-303.

Allison, J., K. Amako, et al. (2006). "Geant4 developments and applications." Nuclear Science, IEEE Transactions on 53(1): 270-278.

Balcerzyk, M., M. Moszynski, et al. (2000). "YSO, LSO, GSO and LGSO. A Study of Energy Resolution and Nonproportionality." IEEE Transactions on Nuclear Science 47(4): 1319-1323.

Dorenbos, P., J. T. M. d. Haas, et al. (1995). "Non-Proportionality in the Scintillation Response and the Energy Resolution Obtainable with Scintillation Crystals." IEEE Transactions on Nuclear Science 42(6): 2190-2202.

GEANT4 website “http://geant4.web.cern.ch/geant4/

Kapusta, M., P. Szupryczynski, et al. (2005). " Non-Proportionality and Thermoluminescence of LSO:Ce " IEEE Transactions on Nuclear Science 52(4): 1098-1104.

Melcher, C. and J. Schweitzer (1991). Cerium-doped lutetium oxyorthosilicate: a fast, efficient new scintillator. Nuclear Science Symposium and Medical Imaging Conference, 1991., Conference Record of the 1991 IEEE.

CHAPTER 3 SCINTILLATION KINETICS OF YSO:CE

A version of this chapter was submitted by Harold Rothfuss as, *Scintillation Kinetics of YSO:Ce*, *Nuclear Science Symposium Conference Record, 2007. NSS '07. IEEE (1401-1403)*

This chapter is the reformatted version of the original work submitted to the referenced journal. No additional changes to the content of the original article were done other than formatting to conform to the thesis format and placement of figures to retain the flow of information that aids the reader.

Abstract

Compared to the fast rise and exponential decay of Lu_2SiO_5:Ce, Y_2SiO_5:Ce has a slower rise time and a non-exponential decay. In an effort to understand this difference, the scintillation kinetics of YSO:Ce were investigated as a function of x-ray and gamma-ray energy as well as under alpha particle excitation. Although some influence of excitation energy and energy density on the kinetics was observed, in no case did the behavior match LSO:Ce. Therefore, a further investigation using thermoluminescence techniques probed the effect of electron traps on the rise and decay times. TL glow curves revealed several large trap populations, particularly near 100K. The participation of the traps in the scintillation process was eliminated by making scintillation decay time measurements at 40K, and a time profile similar to LSO:Ce was observed, possibly because the traps do not release electrons at this low temperature and

only direct energy transfer to Ce luminescence centers contributes to the observed scintillation time profile.

Introduction

This investigation of the scintillation kinetics of Y_2SiO_5 doped with Ce (YSO:Ce) is motivated by an interest in YSO:Ce as a member of the rare earth oxyorthosilicates that also includes the well-known lutetium and gadolinium analogues, Lu_2SiO_5:Ce (LSO:Ce) and Gd_2SiO_5:Ce (GSO:Ce). Also, YSO:Ce itself is potentially useful as a detector of relatively low energy X-rays or gamma rays. Although the scintillation emission of cerium-doped scintillators generally arises from de-excitation of the lowest 5d level of Ce^{3+} to the 4f ground state, the rise time, decay time, and emission wavelength can be influenced by the surrounding crystal field sometimes resulting in significantly different scintillation properties, depending on the host matrix.

Experimental Procedures

A single sample with dimension of 4 x 4 x 10 mm was used for all measurements performed. The decay time measurement was initially measured at room temperature using different radioisotopes for varying excitation energies and different incident particles. In order to measure the decay time of the sample of YSO, the Bollinger and Thomas (Moses and Thompson 2006) method was used.

When further characterization of this sample was needed a thermoluminescence measurement was performed. This was performed on the same crystal that was used in the initial room temperature decay time measurement. The sample was glued to a cold finger and cooled to ~ 40K. The sample was then irradiated with an xray tube for 15 minutes and allowed to stabilize. The sample was heated to 500K at a rate of 9K per minute.

From the thermoluminescence spectrum, it was seen that it might be beneficial to make a low temperature decay time measurement. The sample was again glued to the cold finger and cooled to 40k again. In this setup the excitation source was a Cs-137 source placed close to the sample. The decay time spectrum was acquired using the same technique that was used when acquiring the room temperature decay time spectrum.

Results

Energy Dependent Decay Time

Figure 3.1 shows the difference in decay time between different excitation energy and excitation resulting from a gamma or alpha particle.It can be seen that the decay time is not dependent on the incident gamma excitation energy. There is, however, a dependence on particle type, likely due to the large difference in ionization density. The alpha particle shows a longer decay time than the gamma excitation. This can arise from the difference in ionization

density and penetration effects associated with the difference of incident particle.

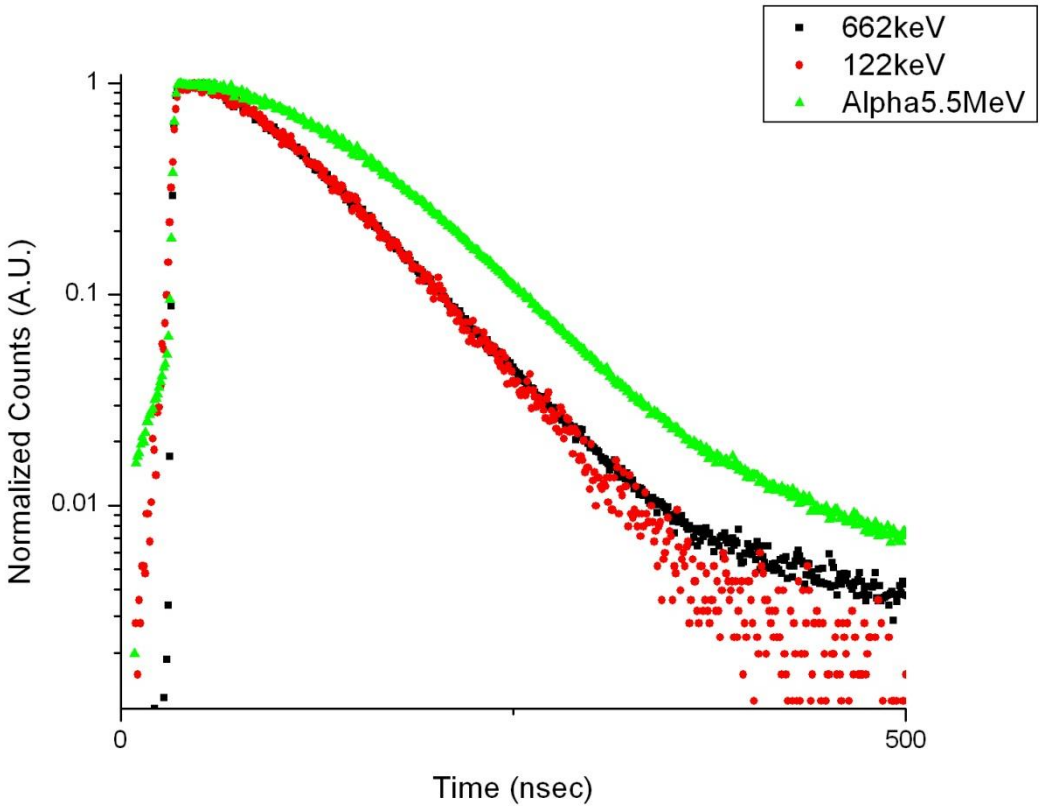

Figure 3.1. Scintillation decay of YSO:Ce under excitation from various source strength and particle types.

It was initially thought that the decay schemes of YSO and LSO could be fairly similar because the luminescence centers were the same. The greatest difference between the two crystals is rare earth element. Figure 3.2 shows that the decay times and decay schemes are different. The decay scheme of LSO is

easily described with a one component exponential decay, whereas the decay scheme of YSO is more complex then LSO. It is seen in all of the decay schemes of YSO that there seems to be an additional component in the decay after the rising has completed and the decay begins. In order to find the origin of this additional component, a thermoluminescence measurement was performed in order to further understand the mechanisms of YSO decay.

Thermoluminescence of YSO:Ce

Figure 3.3 shows the thermoluminescence spectrum of YSO and LSO and how they relate to each other over a temperature range of ~ 40K to ~ 450K. The results show that there is a large difference between LSO and YSO glow curves. They are different in the intensity of the traps at different temperature ranges. The YSO has a higher number of traps with higher intensity than LSO in the temperatures below room temperature. Particularly in the range of 40 K to 200 K. LSO has the higher intensity traps in the region above room temperature in the range of 290 K to 450 K. This difference in trap location and intensity may explain some of the difference in decay time mechanisms between the two samples.

Temperature Dependent Decay Time

From the thermoluminescence experiment, it was assumed that the decay time is dependent on the temperature. In Figure 3.4 it can be seen that the low

temperature decay time experiment behaved closer to the decay scheme of LSO. The decay could be modeled with a one component exponential decay function.

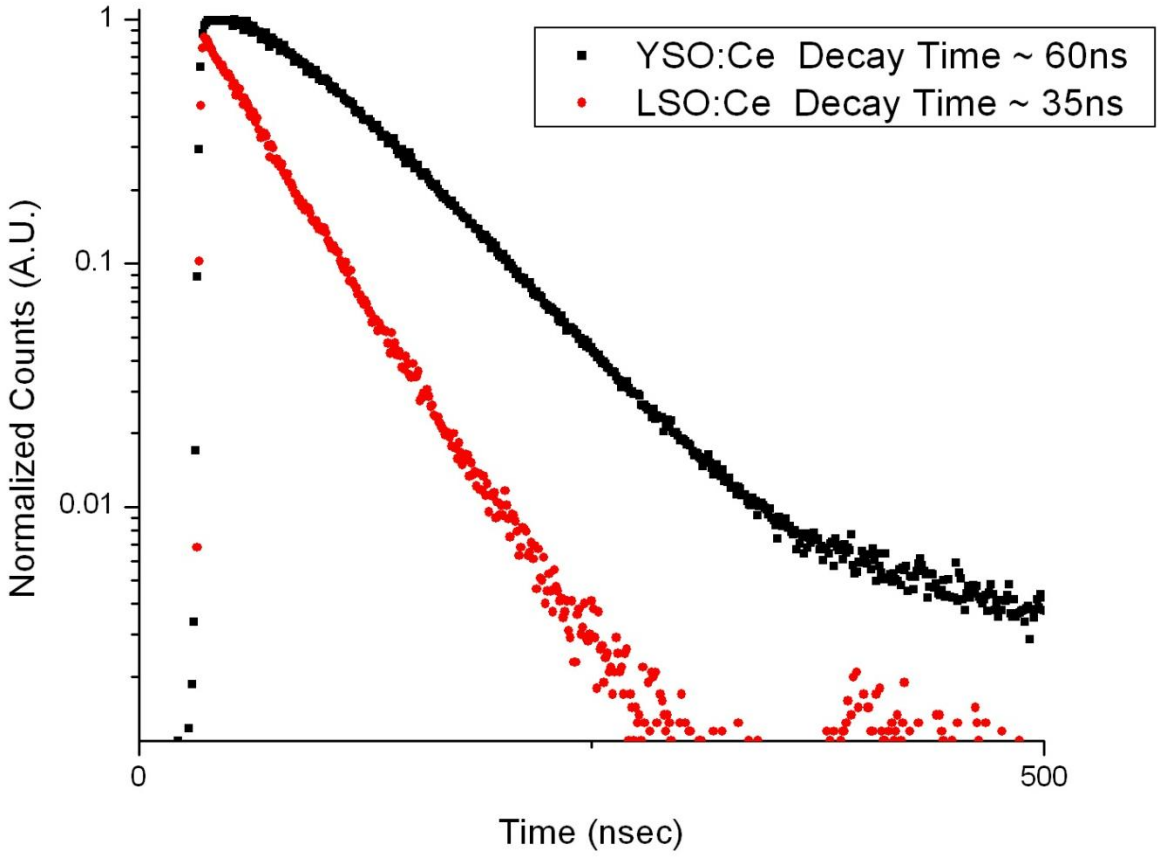

Figure 3.2. Scintillation decay time of YSO:Ce and LSO:Ce.

The low temperature decay time measurement also resulted in a faster decay time with the same sample. The time that was calculated from the one component exponential decay function was 27 ns. This is a decrease from the 60 ns decay time that was measured with the 300 K decay time setup

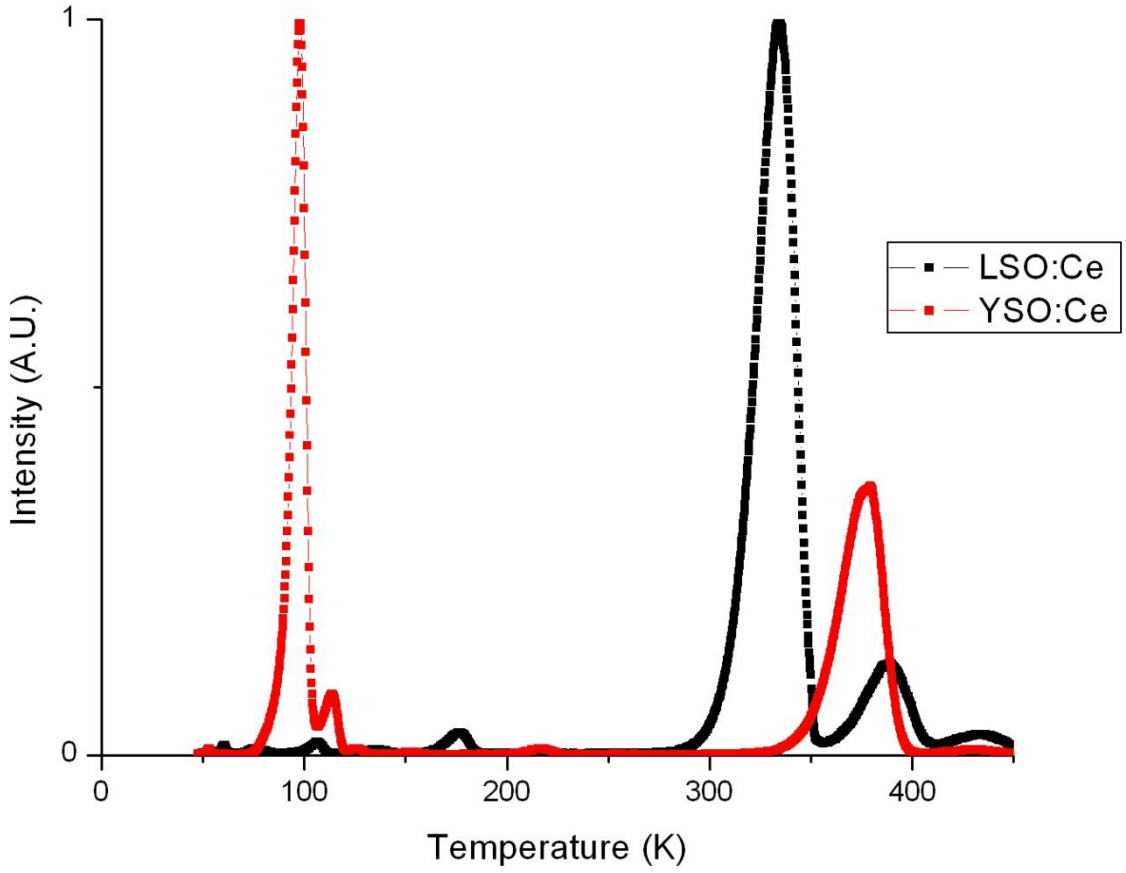

Figure 3.3. Glow Curves of LSO:Ce and YSO:Ce obtained with Thermoluminescence Techniques.

Discussion

The experiments that looked into the scintillation decay time mechanism as a function of energy gave little insight into the kinetics of the YSO. It did give direction to explore the crystal in further detail. The largest drive to understand the mechanism further was not the response to the excitation but the odd shape

of the decay of the YSO when making a direct comparison to LSO. The YSO decay spectrum made it difficult to fit the curve with any confidence. This difficulty in fitting the curve came from the extra component that made the function behave like a nonstandard exponential decay. This shape of the curve resulted in further study of the crystal in order to understand where this additional component of the decay came from.

The thermoluminescence experiment gave some insight into a fundamental difference between the LSO and YSO. One very large difference is the present of high intensity, low temperature traps. These low temperature traps correspond to shallow energy traps within the crystal. From the TL data, one can extract the trap lifetimes from the glow curve. This gives us the information that all of the shallow traps have lifetimes in the order of years at 40 K. It also shows that the shallow traps at room temperature have life times in a range of the order of a few nanoseconds to a few microseconds. Using the knowledge of the long lifetimes of the shallow traps at 40 K a prediction was made that at 40 K, once the traps were saturated, the long lifetime of the trap would make the trap irrelevant in the decay scheme. This would result in a decay time that would be close to the cerium transition time from the 5d to 4f level of 32 nanoseconds (Rothfuss, Melcher et al. 2009).

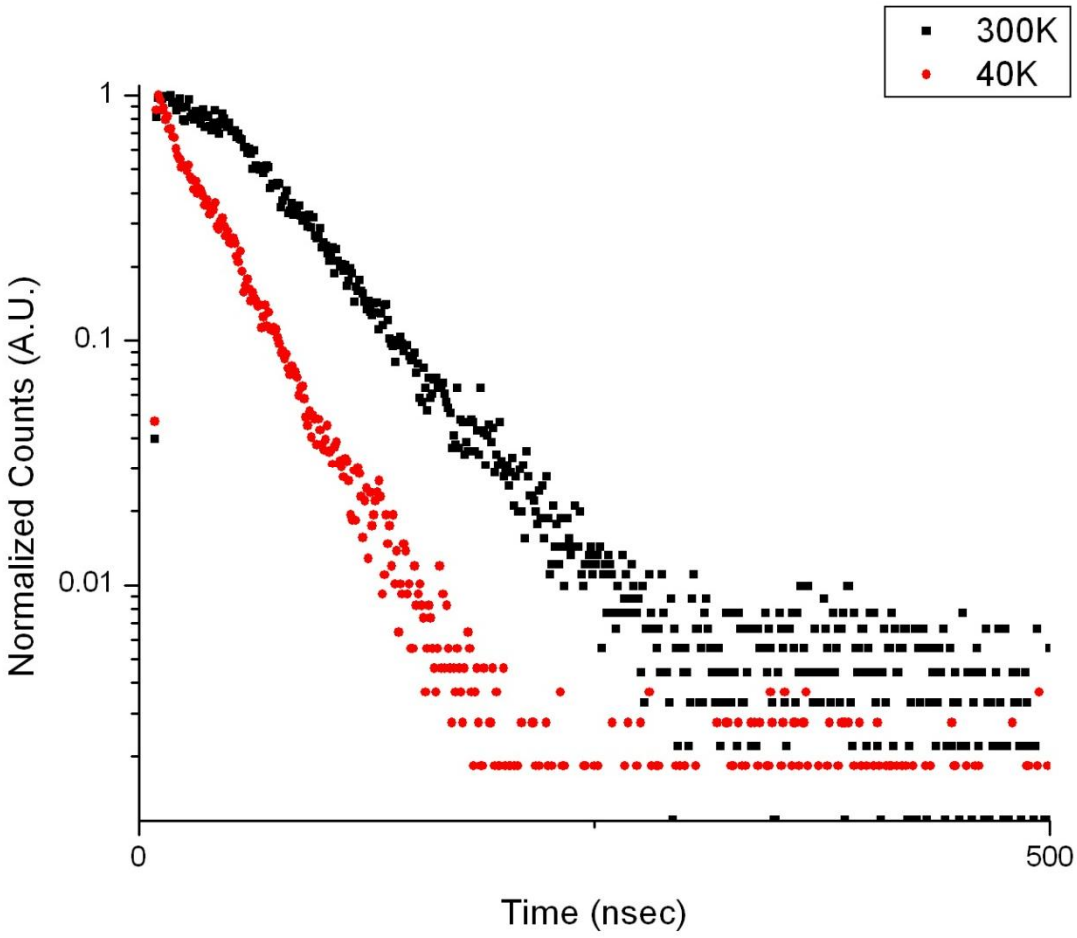

Figure 3.4. Scintillation decay spectrum of YSO:Ce at 40K and 300K.

Table 3.1. Trap Temperature and calculated trap lifetimes at different temperatures.

Temperature (K)	τ_{300}	τ_{40}
215	1.23 nsec	~ years
152	1.75 nsec	~ years
123	2.04 usec	~ years
109	231 nsec	~ years
98	37.9 nsec	~ years

Conclusions

It was seen that there is no dependence on gamma-ray excitation energy in the decay scheme of YSO:Ce. It was observed that the decay time does change with different particles that are incident on the crystal. It was also shown that two similar members of the earth oxyorthosilicates can differ in scintillation kinetics due to the role of electron traps. This is shown by comparing the data acquired from the decay time measurements and the thermoluminescence. The demonstration of the temperature dependence of YSO:Ce decay time was also shown. This strong temperature dependence and the presence of high intensity low temperature traps lead to the conclusion that the YSO:Ce decay scheme at room temperature is affected by the presence shallow electron traps.

References for Chapter 3

Bollinger, L. and G. E. Thomas (1961). "Measurement of the Time Dependence of Scintillation Intensity by a Delayed-Coincidence Method." Review of Scientific Instruments 32(9): 1044-1050.

Melcher, C. and J. Schweitzer (1991). Cerium-doped lutetium oxyorthosilicate: a fast, efficient new scintillator. Nuclear Science Symposium and Medical Imaging Conference, 1991., Conference Record of the 1991 IEEE, IEEE.

Suzuki, H., T. Tombrello, et al. (1993). "Light emission mechanism of $Lu_2(SiO_4)O$: Ce." Nuclear Science, IEEE Transactions on 40(4): 380-383.

Wojtowicz, A. J., P. Szupryczynski, et al. (2001). "Electron traps and scintillation mechanism in LuAlO3: Ce." Journal of Physics: Condensed Matter 13(42): 9599.

CHAPTER 4 THE EFFECT OF CA^{2+} CODOPING ON SHALLOW TRAPS IN YSO:CE SCINTILLATORS

A version of this chapter was submitted and accepted by H. Rothfuss as, *The Effects of Ca^{2+} Codoping on Shallow Traps in YSO:Ce Scintillators, IEEE Transactions on Nuclear Science 56, (958-961)*

This chapter is the reformatted version of the original work submitted to the referenced journal. No additional changes to the content of the original article were done other than formatting to conform to the thesis format and placement of figures to retain the flow of information that aids the reader.

Abstract

Low temperature (~35K) measurements of the scintillation kinetics of Y_2SiO_5:Ce (YSO:Ce) have previously illustrated that shallow electron traps can play an important role in the scintillation mechanism. In addition, divalent calcium co-doping of isostructural Lu_2SiO_5:Ce (LSO:Ce) has been shown to eliminate shallow electron traps and decrease scintillation decay time while maintaining high light output. Here we investigate the effect of Ca^{2+} codoping on the trap populations and scintillation kinetics of YSO:Ce. Single crystals were grown with Ca^{2+} concentrations up to 0.5 at% relative to Y. Thermoluminescence measurements indicate a significant reduction in shallow traps, and a marked change in the scintillation kinetics can be seen in the scintillation time profiles as a result of Ca^{2+} codoping.

Introduction

An indication of the role of shallow electron traps in the scintillation mechanism of Y_2SiO_5:Ce (YSO:Ce) was previously observed by comparing the scintillation kinetics at room temperature and 35K (Rothfuss, Melcher et al. 2007). At low temperature, the probability of electrons escaping from these traps is insignificant, and they have no effect on energy transfer to Ce^{3+} luminescence centers. At room temperature, however, the lifetime of the trapped electrons may be on the order of nanoseconds and the effect of trapping and subsequent thermal escape is observed as a lengthening of the scintillation rise time and decay time. In addition, previous studies have demonstrated that codoping of isostructural Lu_2SiO_5:Ce (LSO:Ce) with Ca^{2+} reduces the population of electrons in shallow traps and shortens the scintillation decay time from ~43 ns to ~30 ns (Yang, Melcher et al. 2009), (Spurrier et al. 2008). In the current study we use thermoluminescence to investigate the effect of Ca^{2+} codoping of YSO:Ce on electron trap populations and on the scintillation decay time. YSO:Ce provides a particularly good opportunity to study the effect of shallow traps on energy transfer due to the relatively large difference between the scintillation decay time (~60-80 ns) and the intrinsic luminescence decay time of Ce^{3+} (~40 ns) (Rothfuss, Melcher et al. 2007), (Rothfuss, Melcher et al. 2009).

Experimental Procedure

Four boules of YSO:Ce with varying calcium concentrations were grown using the Czochralski method in the system described in (Spurrier et al. 2008). The boules were all grown with a cerium concentration of 0.1 atomic percent; in all cases, the stated dopant concentrations refer to the initial concentration in the melt. The dopant concentration in the single-crystal boules will differ from that of the melt due to solid-liquid segregation and the fraction of the melt that has been solidified (Brandle 1980). A control boule without calcium was grown as a baseline to make comparisons of the effects of the calcium in the crystal matrix. The other three boules were grown with increasing amounts of calcium (0.1, 0.3, and 0.5 atomic %). All measurements were done on 4mm x 4mm x 4mm unpolished cubes.

A photoluminescence measurement was performed in order to obtain the emission and excitation information for the varying samples. This measurement was performed on a Hitachi fluorescence spectrophotometer F-4500 at room temperature. The sample cubes were arranged in a reflective geometry. In order to acquire the emission spectra, the sample was measured with a wavelength scan with excitation wavelength of 355 nanometers. The excitation scan was measured with a wavelength scan with a selected emission wavelength of 420 nanometers. The scan speed was 60 nanometers per minute, and the data were uncorrected for the spectral response of the instrument.

Charge carrier trap characteristics were investigated via thermoluminescence measurements. The study was performed by gluing 4×4×4 mm samples to the cold finger of a cryostat (CTI Model Cryogenic 22(He)) with a silver epoxy. The sample was then cooled to ~ 40K with a helium refrigerator. After a period of time to allow for thermal stabilization, the sample was irradiated with X-rays from an X-ray tube (Source 1 X-ray Model CMX003) operated at 35 keV and 1 microampere for 20 minutes. The thermoluminescence glow curve was acquired by measuring the luminescence as charge traps were evacuated by heating the sample from 40K to 400K at a rate of 9K per hour with a LakeShore Model 331 temperature controller. The photons emitted were captured with a Hamamatsu H3177 PMT operating at -1800V through a quartz window on the cryostat sleeve.

The time-correlated single photon technique of Bollinger and Thomas (Moses and Thompson 2006) was used to measure the sample decay times. Photonis XP2020Q photomultiplier tubes (PMT) were arranged in a perpendicular geometry with a variable shutter in front of the stop PMT. The shutter was reduced to an opening that would produce no more than 5% total count rate in the stop PMT with respect to the start PMTs count rate. A 10 µCi Cs-137 source was used as an excitation source; samples were continuously excited until there were at least 10,000 counts in the peak channel.

A low temperature decay time measurement was also performed to investigate the effects of the calcium codopant on the scintillation mechanism. The start and stop chain were the same as for the room temperature setup but were configured to measure a sample cooled within a cryostat chamber. The low temperature measurement was performed at approximately 35 K. In order to make sure that the measurement was consistent with the room temperature decay time measurement, a correlated measurement was performed within the cryostat chamber at room temperature. As with the corresponding room temperature decay time measurement, the samples were measured until a minimum of 10,000 counts were acquired in the peak channel.

Results

Emission and Excitation

Figure 4.1 shows the emission and excitation spectra for varying calcium concentrations in YSO:Ce. It is observed that there is no shift in energy levels as there are no spectral shift in the measured spectra; however, a suppression of the higher energy levels was seen which could be attributed to the optical absorption of calcium. This is supported by the observation that the degree of this suppression increases with higher calcium concentrations.

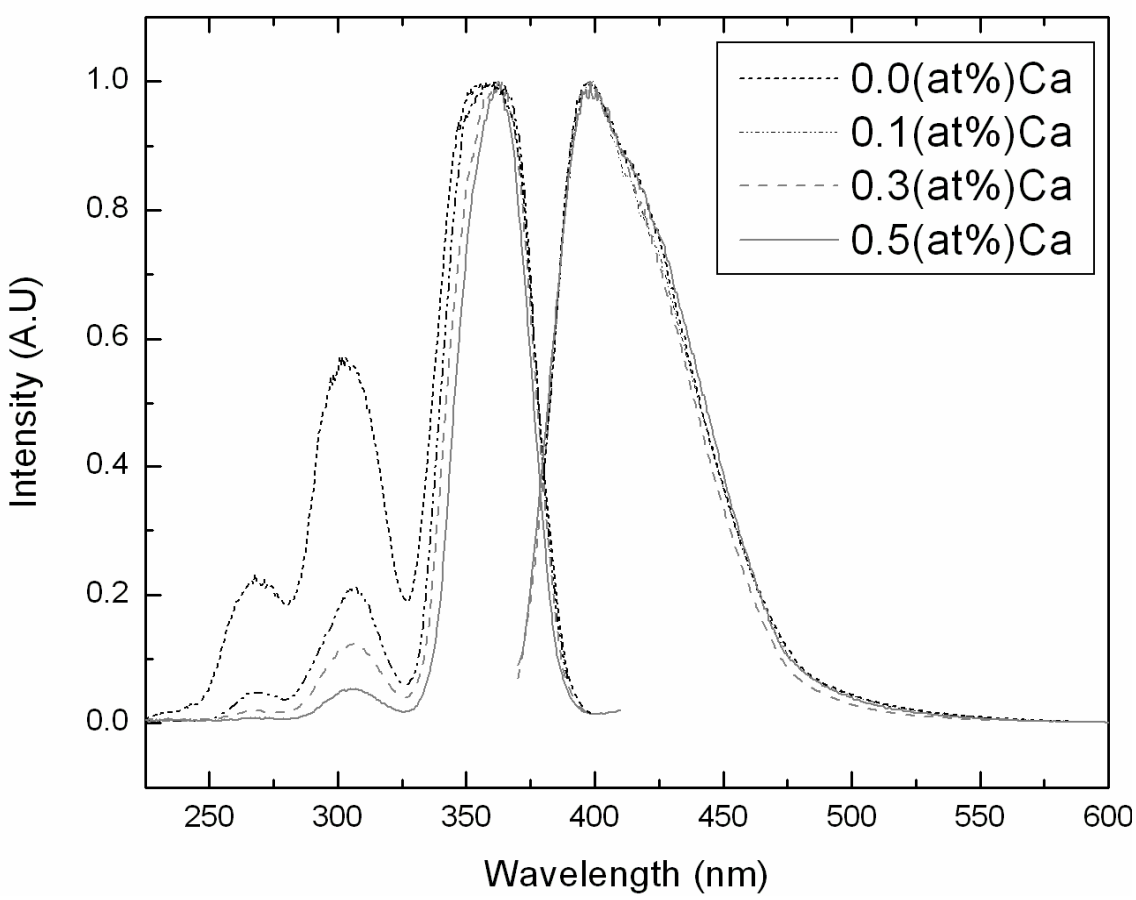

Figure 4.1. Emission and excitation spectra of YSO:Ce samples with varying in calcium concentrations of YSO:Ce.

Thermoluminescence

Figure 4.2 shows the thermoluminescence glow curves of YSO:Ce and YSO:Ce:Ca with 0.5 at% calcium over a temperature range of 40 to 400K. The spectra were normalized to the background rather than to a peak in order to show any change in magnitude of intensity of peaks in the glow curve. There is

an observed decrease in charge trap intensity in the sample with calcium in comparison to the samples without calcium. It was also seen that the initially low intensity traps have been reduced to background levels in the calcium codoped sample.

Decay Time Measurements

Based on the thermoluminescence results, it was predicted that the decay time would decrease as a function of increasing calcium concentration (Rothfuss, Melcher et al. 2007). As seen in Figure 4.3, the decay time did indeed decrease as the concentration of calcium was increased. The decay mechanism also changes as a function of the calcium concentration. The sample with no calcium is not easily modeled with a multiple component exponential function. In order to describe the decay time of the non-codoped sample, a range of the exponential decay must be selected to fit (~125-350 ns). This range isolates the main decay component by removing the non-exponential portion of the plot before ~125 ns and not fitting the longer decay time components past ~350 ns. The samples with higher concentration of calcium are well described with a single exponential function. This description could be a result of the scintillation mechanism becoming simpler as there are fewer traps contributing to the decay mechanism. The optimal concentration of calcium in the YSO:Ce matrix appears to be around 0.3 at% calcium, as shown in Figure 4.3, which reveals that there is no further decrease in decay time past this concentration. This is also a concentration for

which the single component exponential model fits the data well.

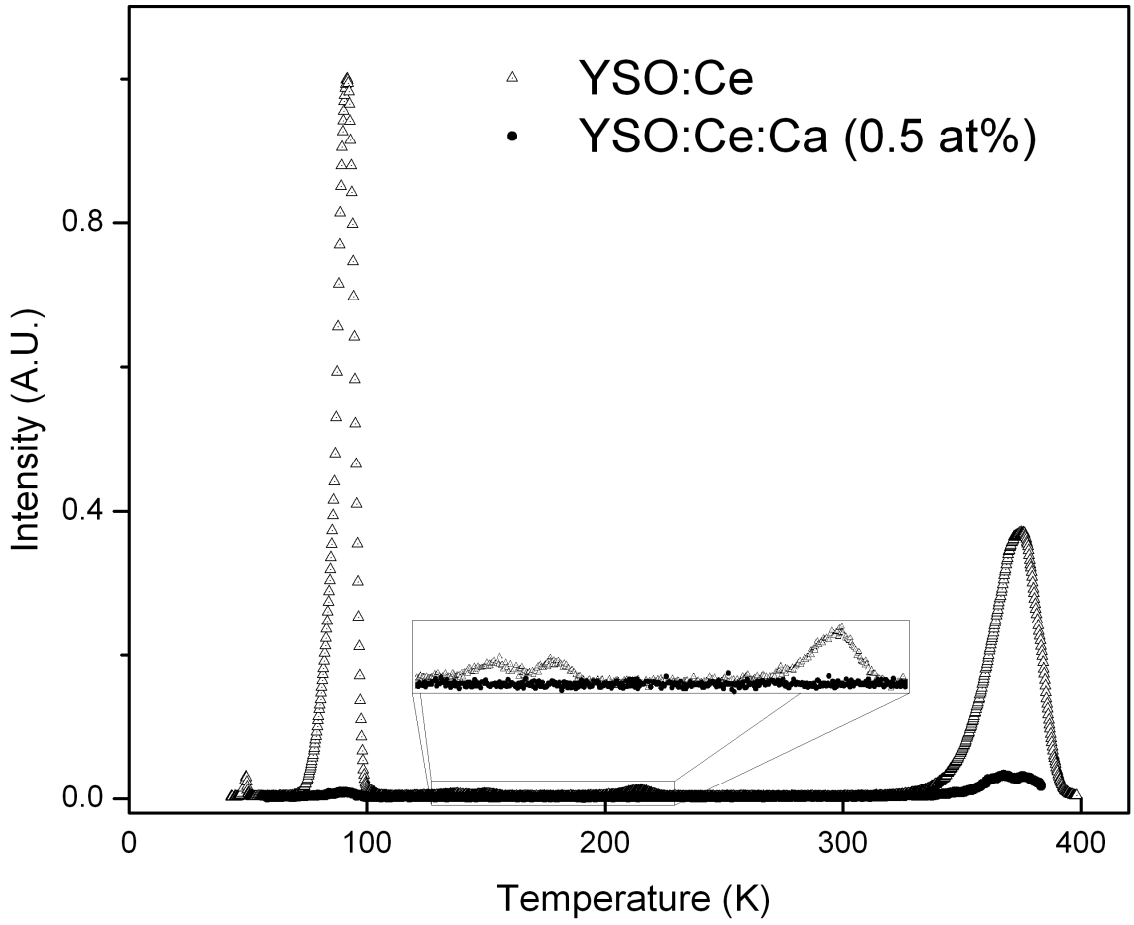

Figure 4.2. Thermoluminescence glow curve of YSO:Ce and YSO:CeCa

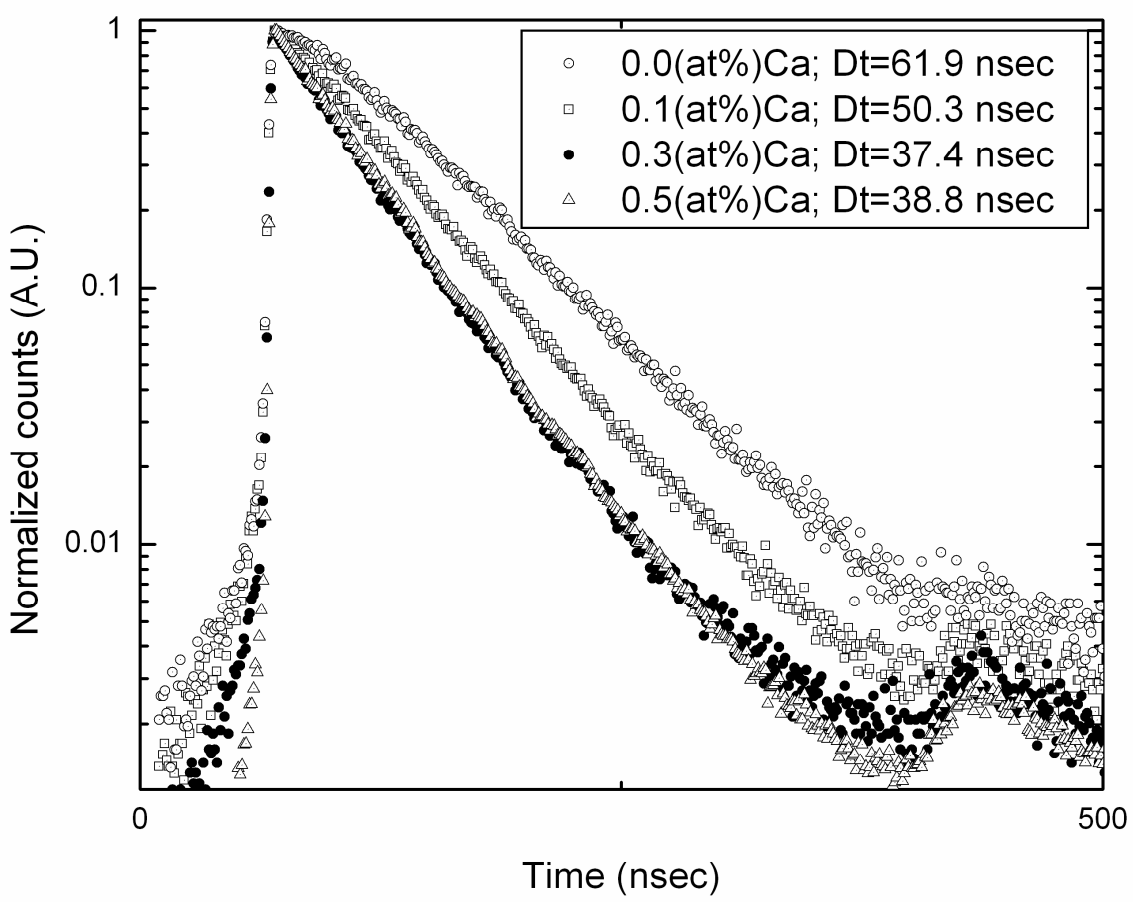

Figure 4.3. Room temperature decay time spectra of samples with varying calcium concentrations. Plots are normalized to the max counts.

Low Temperature Decay Time Measurements

To ensure that the decay time was reduced due to the suppression of charge traps, a low temperature measurement was performed. From previous experiments (Rothfuss, Melcher et al. 2007), it was shown that at low temperatures, charge traps are not an integral part of the decay kinetics and the

mechanism becomes primarily a function of the cerium transition. Figure 4.4

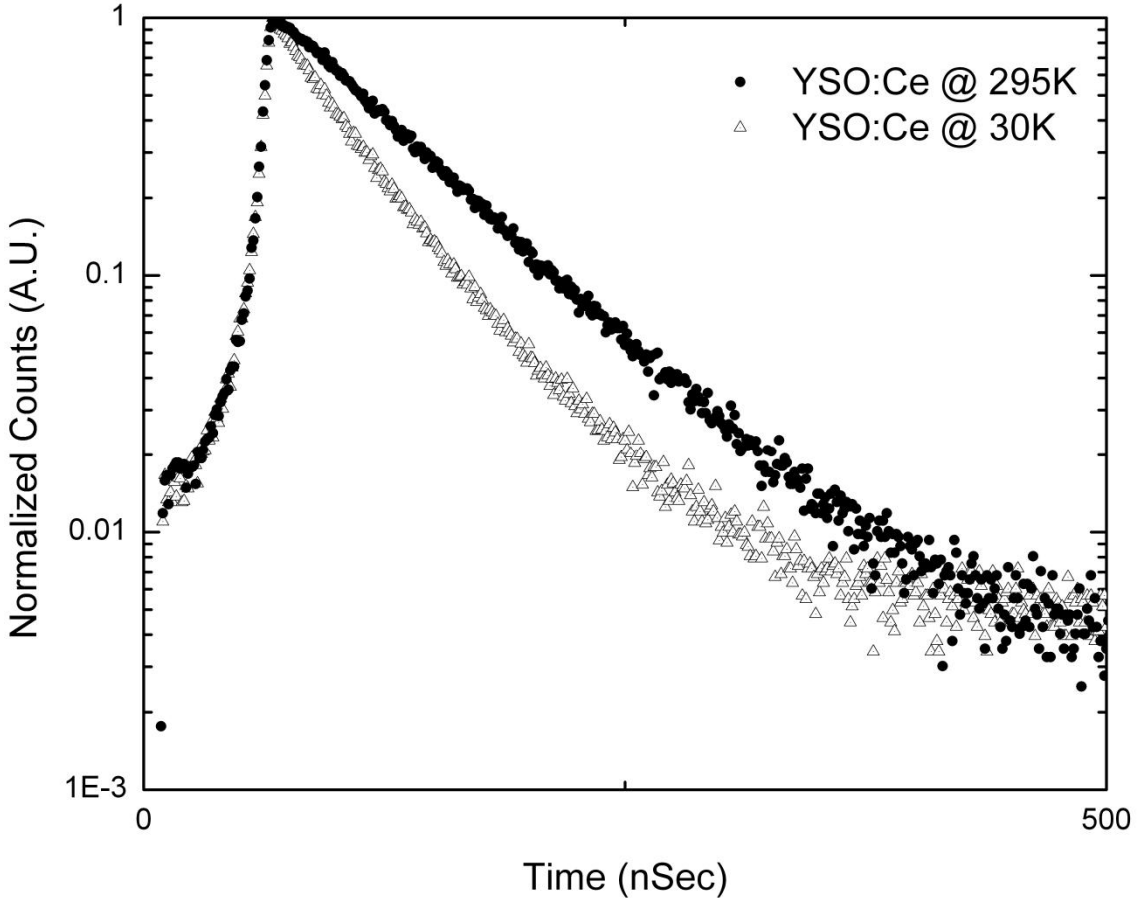

Figure 4.4. Decay scheme of YSO:Ce at 30 and 295 K

show the decay plot of both the low temperature and room temperature measurement of the YSO:Ce sample performed under the same condition. It is observed that this sample has a change in the decay scheme as the temperature is lowered to a region where the charge traps are not an integral part of the

decay mechanism. It is seen in Figure 4.4 that the decay mechanism simplifies to a decay scheme similar to that of the higher concentration calcium codoped samples. The decay time of the low temperature decay time measurement in Figure 4.4 is also around 38 nanoseconds.

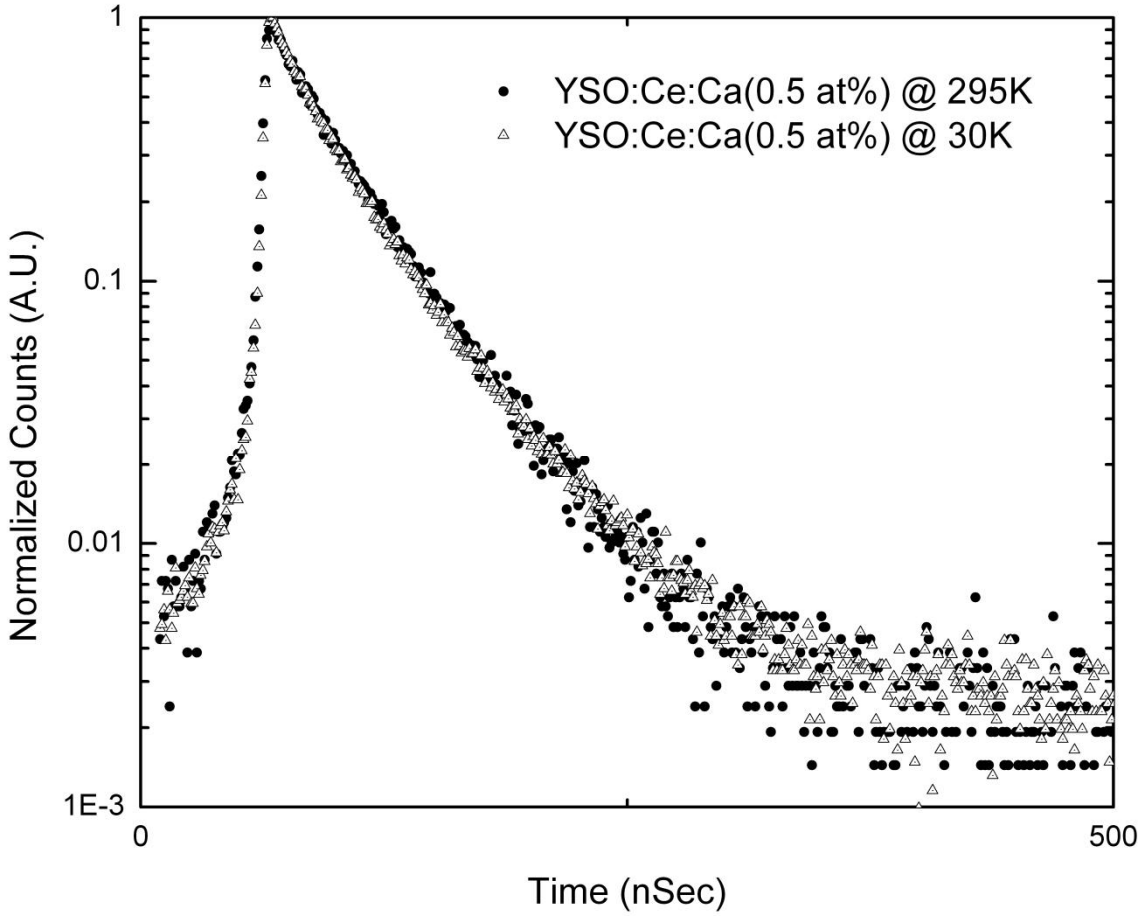

Figure 4.5 Decay scheme of YSO:CeCa (0.5 at%Ca) at 30 and 295 K.

The decay mechanism of the sample with 0.5 at% of calcium (Figure 4.5) is not dependent on the temperature. The decay time of this sample is also around 38 nanoseconds at both measured temperatures. This shows that the addition of calcium in the material has resulted in a suppression of charges traps to the extent that they do not contribute to the decay kinetics.

Discussion

As seen in the emission and excitation data there was no change in the energy levels of the cerium luminescence centers due to the presence of calcium. The suppression of the higher energy excitation levels could be caused by the optical absorption of the calcium. The calcium optical absorption was earlier reported as a probable source for the suppression of the higher energy excitation levels in LSO:Ce (Yang, Melcher et al. 2009). The suppression of these sites could also be due to a physical effect other than optical absorption of the calcium; further studies should be conducted to investigate this phenomenon.

The greatest effect observed in this study was the significant decrease in decay time and suppression of charge traps as a function of calcium codoping. From the thermoluminescence data, it was seen that calcium codoping played a role in suppressing the charge traps at all depths. This allows the decay mechanism to be primarily a statistical function of the cerium transition, and eliminates the additional statistical process of the trap lifetimes. It was observed that the gamma ray excited scintillation decay time of the higher concentrations of

calcium (> 0.3 at% Ca) achieves the direct UV-excited decay time of cerium in YSO [5] of 39 nanoseconds. In order to further strengthen the theory that the trap suppression is the cause of the decreased decay time, the decay time of the control, non-codoped, samples was measured at low temperatures (~35K). At low temperatures, the trap life time changes in magnitude from nanoseconds to years. This change in lifetime creates a trap that, once saturated, is of no significance to the scintillation decay mechanism. This measurement should yield a result that is similar to the higher concentration (>0.3 at%) of calcium. Our measurements showed that this was indeed the case. The low temperature decay time was reduced to around 38 ns, from the room temperature 62 ns decay time. The decay scheme also simplified to a single exponential decay, indicating that decay time became primarily a function of the cerium transition statistics.

To verify whether this effect was an artifact of the low temperature measurement or the result of an additional mechanism not associated with charge traps, a further measurement was performed with the 0.5 at% calcium sample at both low and room temperature. These results showed no change in the decay scheme as a function of temperature. This measurement indicates that the calcium suppresses the traps to a point at which they are of no significance in the decay mechanism. This also shows that the addition of the calcium takes the YSO:Ce close to the cerium transition times (Rothfuss,

Melcher et al. 2009).

Conclusions

Previous work showed that the scintillation decay of YSO:Ce can be reduced to a fast single exponential by cooling the crystal to ~35K and thereby eliminating the energy transfer role of shallow traps in the scintillation process. We have now observed that the same effect may be achieved at room temperature by codoping the crystal with divalent Ca^{2+}. Thermoluminescence measurements indicate that calcium reduces or eliminates the populations of various traps, thus enabling faster energy transfer to the Ce^{3+} luminescence centers. At a calcium codopant concentration of approximately 0.3 at% relative to Y, a scintillation decay time of ~38 ns is achieved which agrees well with the intrinsic Ce^{3+} decay reported by Suzuki et al. (Rothfuss, Melcher et al. 2009).

References for Chapter 4

Bollinger, L. and G. E. Thomas (1961). "Measurement of the Time Dependence of Scintillation Intensity by a Delayed-Coincidence Method." Review of Scientific Instruments 32(9): 1044-1050.

Brandle, C. (1980). "Crystal pulling." Cryst. Growth: 275-300.

Rothfuss, H., C. Melcher, et al. (2007). “Scintillation kinetics of YSO:Ce”. Nuclear Science Symposium Conference Record, 2007. NSS'07. IEEE, IEEE.

Spurrier, M. A., P. Szupryczynski, et al. (2008). "Effects of Ca^{2+} Co-Doping on the Scintillation properties of LSO:Ce”. Nuclear Science, IEEE Transactions on 55(3): 1178-1182.

Spurrier, M., P. Szupryczynski, et al. (2008). "The effect of co-doping on the growth stability and scintillation properties of lutetium oxyorthosilicate." Journal of Crystal Growth 310(7): 2110-2114

Suzuki, H., T. Tombrello, et al. (1993). "Light emission mechanism of Lu< sub> 2</sub>(SiO< sub> 4</sub>) O: Ce." Nuclear Science, IEEE Transactions on 40(4): 380-383.

Yang, K., C. L. Melcher, et al. (2009). "Effects of calcium codoping on charge traps in LSO: Ce crystals." Nuclear Science, IEEE Transactions on 56(5): 2960-2965.

CHAPTER 5 MEASURING THE NON-PROPORTIONAL RESPONSE OF SCINTILLATORS USING A POSITRON EMISSION TOMOGRAPHY SCANNER

A version of this paper is being submitted to IEEE Transactions on Nuclear Science for publication.

This chapter is the reformatted version of the original work submitted to the referenced journal. No additional changes to the content of the original article were done other than formatting to conform to the thesis format and placement of figures to retain the flow of information that aids the reader.

Abstract

A novel way of measuring the non-proportional response of scintillation materials, using a Positron Emission Tomography (PET) scanner, has been developed and tested. Using a Siemens Biograph mCT, a modified Compton coincidence technique is performed where the Compton scatter angular information data is collected by taking advantage of the fine angular sampling that is inherent to the PET scanner. Using the scatter angle information, the energy deposited in the sampled scintillator can be calculated. Comparing the calculated energy deposited versus the measured scintillator response yields the Compton electron non-proportional response.

Introduction

The non-proportional response of scintillators can be measured by

different techniques. One common technique is to measure the gamma ray response of the scintillator by using a radioisotope library and observing the relative positions of the photo-peaks of the known incident gamma or x-rays. This gives a non-proportional response of the measured scintillator at discreet points located at the energies of the incident gamma or x-rays. Another widely used method is known as the Compton coincidence technique (Rooney and Valentine 1996). This method measures the response of the scintillators to a Compton electron scattered within and measuring the Compton scattered gamma in another coincident detector. In order to estimate the energy deposited into the scintillator, either the Compton scattered gamma's energy or its scattering angle must be precisely measured. By measuring the scattered gamma energy directly or calculating its energy from the scattering angle, and ignoring the relatively small electron binding energy, the scattered electron energy deposited in the scintillator is simply the difference of the initial energy and the energy of the Compton scattered gamma. Comparing the measured scintillator response versus the energy deposited within the scintillator yields the non-proportional response of the scintillators of interest. Using a scintillator in coincidence with a PET scanner in a Compton-coincidence method produces angular data that can be used to compute the energy of the Compton scatted gamma. The advantage of using a PET scanner in coincidence with the scintillator under study is that it provides over 20,000 detectors in accurate

spatial location with excellent timing capabilities. This creates a more sensitive measurement of the scattered events, thus lowering the acquisition time needed to characterize the non-proportional response of a scintillator.

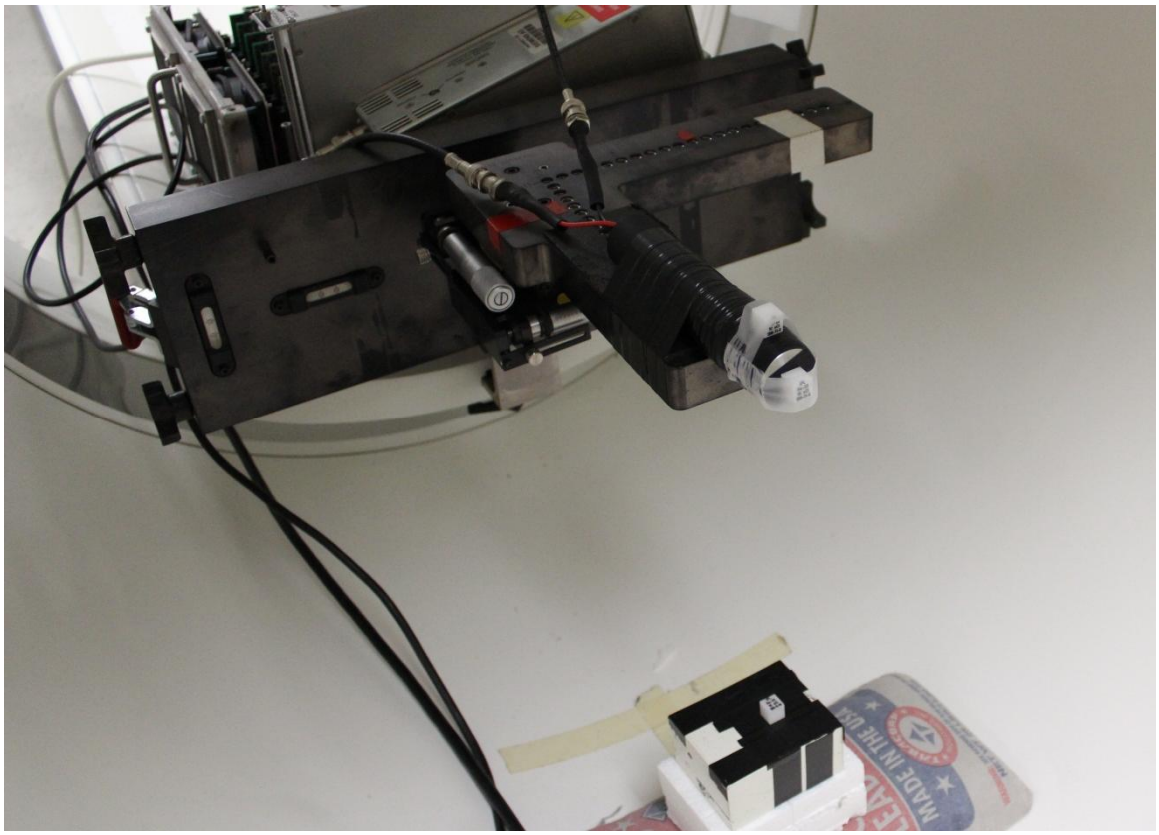

Figure 5.1. Photo of the scintillator (sample) mounted on the PMT and placed in the center of the PET scanner's field-of-view. Also seen is the collimator that directs the Cs-137 gamma beam to the scintillator and three Na-22 markers used for positional information.

Experimental Setup

The PET scanner used in the experiment was a Siemens Biograph mCT with four block detector rings. A single photomultiplier tube (PMT) (Hamamatsu H3177) was placed in coincidence with the PET scanner with a few modifications to the PET scanner. The scintillator to be characterized (referred to as sample from here out) was coupled to the PMT with optical grease. The sample was then wrapped in several layers of Teflon sheets and made light tight with several layers of black electrical tape. The non-proportional responses of two different scintillators were measured to validate the PET Compton coincidence method. An LSO:Ce sample was selected because it is the material in the PET scanner and the electronics are optimized for use with LSO:Ce. The LSO:Ce sample measured had dimensions of $1cm^3$ cube. The second sample selected was a 25.4 mm right cylinder NaI:Tl crystal. NaI:Tl was selected as its non-proportional response has been thoroughly studied with different methods and there are several references for comparison (Rooney and Valentine 1996), (Ugorowski, Harrison et al. 2010), (Hull, Woon-Seng et al. 2009), (Murray and Meyer 1961).

Modifications necessary to place the single tube in coincidence with the PET scanner ring involve modification to the input analog card that usually processes two block detectors. A block detector in the Siemens Biograph mCT is comprised of a 13x13 array of LSO:Ce pixels with dimensions of $4x4x20\ mm^3$. This array is coupled to a light guide and the generated photons are detected by

4 PMTs, which are coupled to the light guide. These 4 PMT signals are inputted into the analog card. In order to replace the block detectors signals with a single PMT, the single signal is split between the 4 inputs of the analog card. The signal from the single PMT is also placed in series with a resistor to ensure that the impedance of the single PMT is matched to the four channels of the analog card. The analog card is a subset of a detector electronics array (DEA) which processes the information of 16 block detectors. The PET scanner has a total of 12 DEAs that process the events of 192 block detectors (4 ring scanner). When the scintillators and the PMT being measured are placed in coincidence with the PET scanner, DEA 6 (Figure 5.2) is replaced with a modified DEA and the original PET scanner's DEA 6 is disabled.

The single PMT was powered by an external NIM high voltage power supply (Canberra Model 3002D) and the voltage was adjusted to maximize the usage of the dynamic range of the analog to digital converters (ADCs) on the analog card. The PMT and sample were mounted to a 2-dimensional translation stage that was mounted to the end of the patient bed of the PET scanner. The external NIM high voltage power supply and the modified DEA were set on the patient bed behind the experimental setup and were not in the PET field of view (FOV).

For positioning of the sample in the center of the FOV and the positioning of the opening of the collimator, Na-22 point sources were used. These sources

had an activity of around 10uCi each and had an active diameter of less than 1

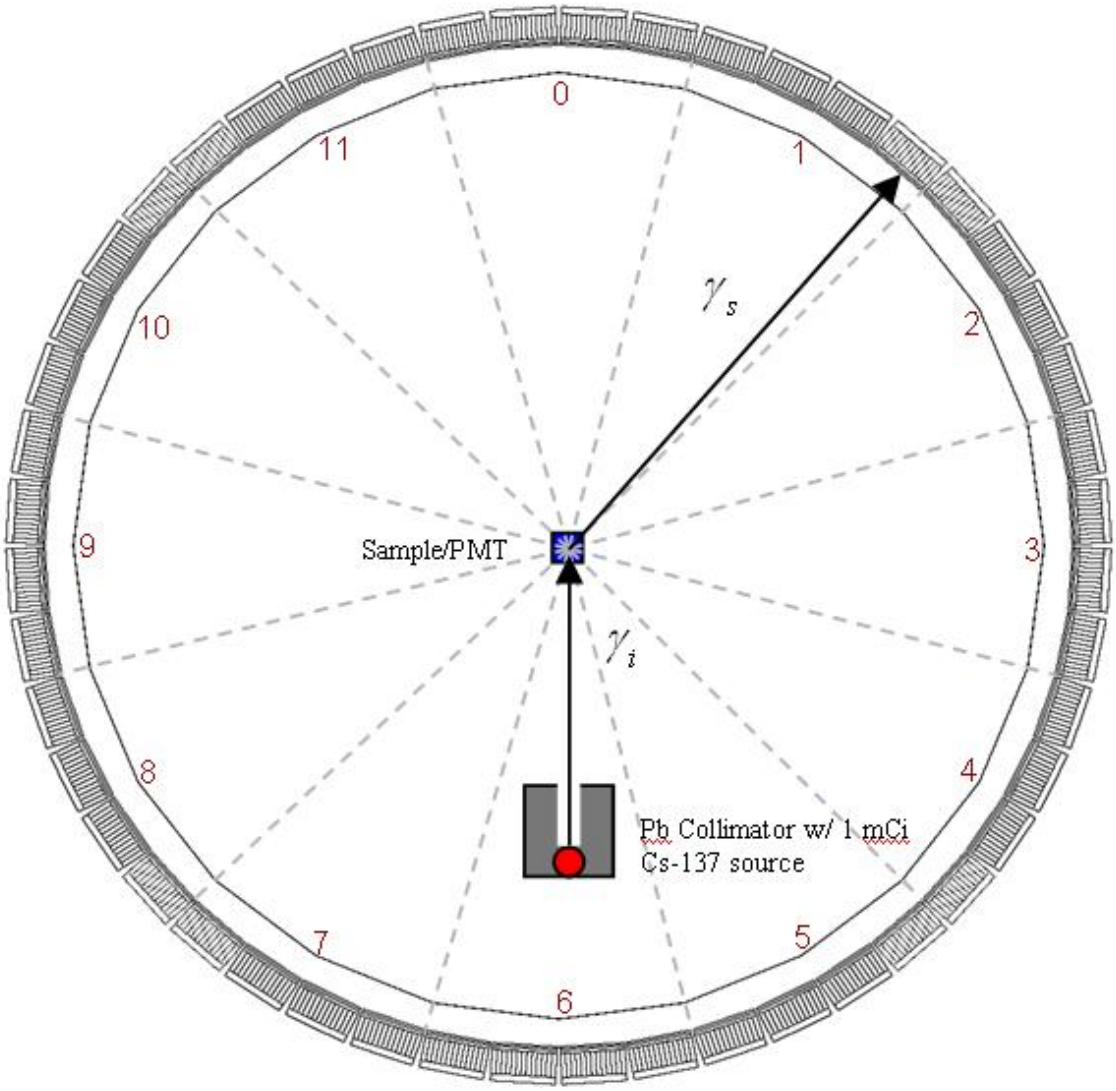

Figure 5.2. 2-dimensional diagram of the PET scanner in a Compton-coincidence mode with a sample mounted on single PMT. Sectors shown are coverage of the blocks that are processed by a corresponding DEA (numbered in red). Also shown are the incident gamma (γ_i) and the scattered gamma (γ_s).

mm. The mono-energetic source of gamma rays came from a 1 mCi Cs-137 point source that was collimated in a lead collimator with a cylindrical opening of 3mm diameter with ~25mm of lead shielding. During the Compton coincidence measurement, a copper shield is placed over the collimator opening to suppress the 32 keV X-ray from interacting with the sample. Initial alignment was performed with a plumb-bob to position the opening close to the center of the sample and the center of the bore of the collimator opening with gravity.

Methods

To measure the non-proportional response of the sample, the energy of the Compton electron deposited must be solved. As stated earlier, using the PET scanner, one can measure the Compton scattering angle preciously to a resolution of around half a degree. Using the relationship between the Compton scattering angle and the initial energy, the Compton scattered photons energy can be calculated using equation 5.1.

$$h\nu' = \frac{h\nu}{1+\left(\frac{h\nu}{m_o c^2}\right)(1-\cos\theta)} \qquad (5.1)$$

After solving for the Compton scattered photon energy, the Compton scattered electron energy deposited in the sample is simply found by

$$E_{Compton\_e^-} = E_{incidentPhoton} - h\nu' \qquad (5.2)$$

To precisely measure the scattering angle between the incident gamma and the scattered gamma, the location of the gamma source and the sample must be precisely known. The Na-22 point sources were positioned physically on the trans-axial and axial center of the sample and a third point source was positioned on the opening of the collimator. An acquisition was taken in the traditional mode of the PET scanner, and sinograms of the point sources were collected. After the acquisition, the Na-22 point sources are removed from the PET scanner. By reconstructing the sinograms, the locations of the point sources are mapped back to physical space with respect to the scanner. Issues such as the arc of the scanner and depth of interaction are corrected for in the reconstruction. Using the measured positions of the point sources, vectors can be created to represent the photon from the source to the sample and a second vector from the sample to the PET ring pixel that interacts with the scatted Compton photon. By taking the inner product of these 2 vectors, the angle between the incident photon and the Compton scatted photon are calculated. This angle gives us the energy deposited by the Compton electron in the sample as described by equations 1 and 2.

In order to see the non-proportional response of a sample, the measured

scintillation response must be compared to the determined energy deposited by the coincidental Compton events. The firmware was modified to output the deposited energy instead of the crystal identification traditionally used in the PET scanner. For slower scintillators, the integration time was extended to approximately 3 times the decay time. When running in the Compton coincidence mode, the lower level discriminator is set to the minimum value of 1 keV and the upper level discriminator is set to the maximum value of 1000 keV. The constant fraction discriminator threshold is adjusted to have a value that is just above the level of electronic noise and for the materials that were measured in this study, the delay was left at 1 ns.

Results

After the data is collected, it is processed into a list that has 1 keV bins that correspond to the calculated energy deposited into the sample from the Compton scattered electron. Each bin contains the measured energy from the sample (Figure 3) as it's processed and outputted from the modified analog card. This data can be displayed in a 2 dimensional histogram in order to see the non-proportional shape and any other anomalies with the data (Figure 4a). Upon analysis of the histogram, structured noise was observed in the 2-d non-proportional response plot. Taking a separate scan of the sample without the Cs-137 source yielded a background that originates from Lu-176 isotope that is present in the LSO:Ce in the scanner (Figure 5.4b). This background structure is

located in the histogram at locations that also correspond to the actual proportionality signal. It is also assumed that since the threshold of the CFD of the PET scanner triggers above 1keV of the measured sample, the 0 keV bin would be a system noise measurement moreso then the non-proportional response at that energy.

The first sample measured with this technique was the LSO:Ce 1cubic centimeter sample. This sample was measured for a total scan time of 2 hours. Only the coincidences between DEA 0-4 and 8-11 (Figure 5.2) were accepted. This results in the maximum energy of around 450 keV.

In order to obtain the non-proportionality curve of the material, first the data is conditioned by subtracting the 0 keV bin from the data to eliminate the Lu-176 background measured by the sample, and to eliminate any systematic noise that is added to the data from the PET electronics. The data of each of the 1 keV bins are then processed individually by finding the centroid of a fitted Gaussian of the measured data for the corresponding energy measured from the Compton coincidence angle (Figure 5.3). The non-proportional value at the energy bin that corresponds to the energy deposited by the Compton electron is equal to the measured response of the sample divided by a linear energy value. The linear energy value is obtained by taking an arbitrary Compton electron value and normalizing the non-proportional response to this value. Some non-proportional methods choose the 662 keV energy as the normalization energy. For this

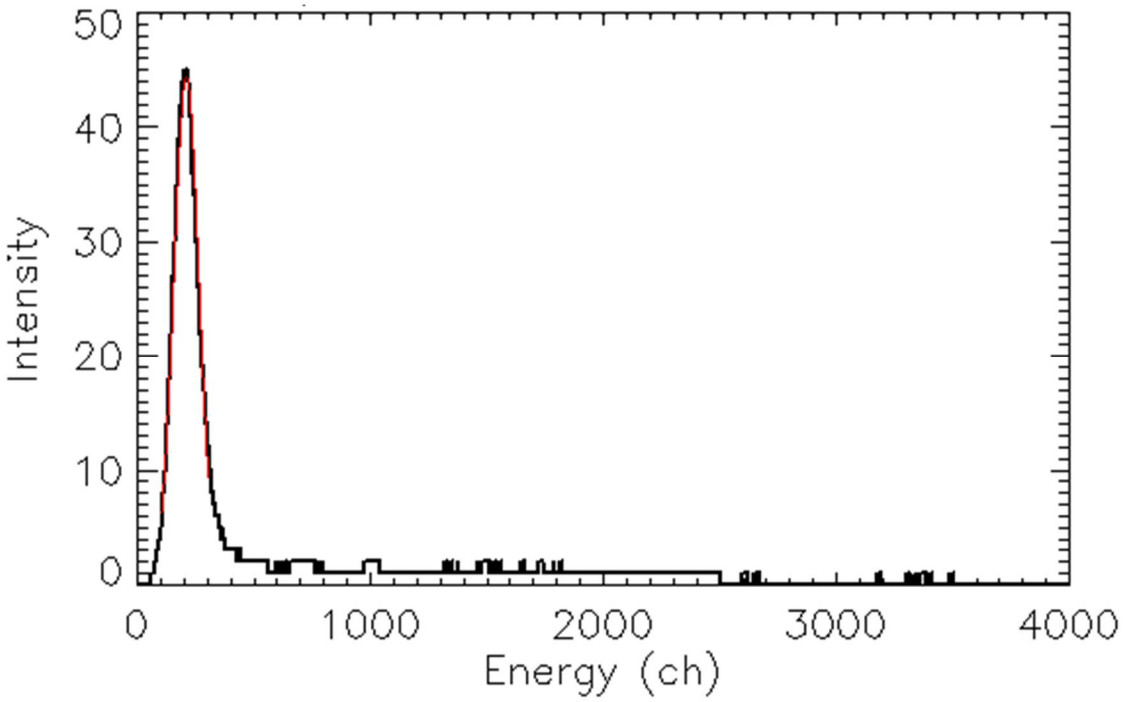

Figure 5.3. Plot of the 40 keV bin from a 2 hour measurement of LSO:Ce. Shown in red is the over plot of the Gaussian fit used to determine the centroid position of the measured response of the sample.

method, a value of 400 keV was selected. This number was chosen because of the 450 keV maximum energy that was obtainable from the scattering angles in the PET scanner. This value is also chosen because as the Compton electron energy deposited in the sample become higher then 400 keV, the corresponding Compton angles per 1 keV bin approach the angular resolution of around 0.5 degrees of the PET scanners pixels.

The resulting non-proportional plot of the measured LSO:Ce sample is

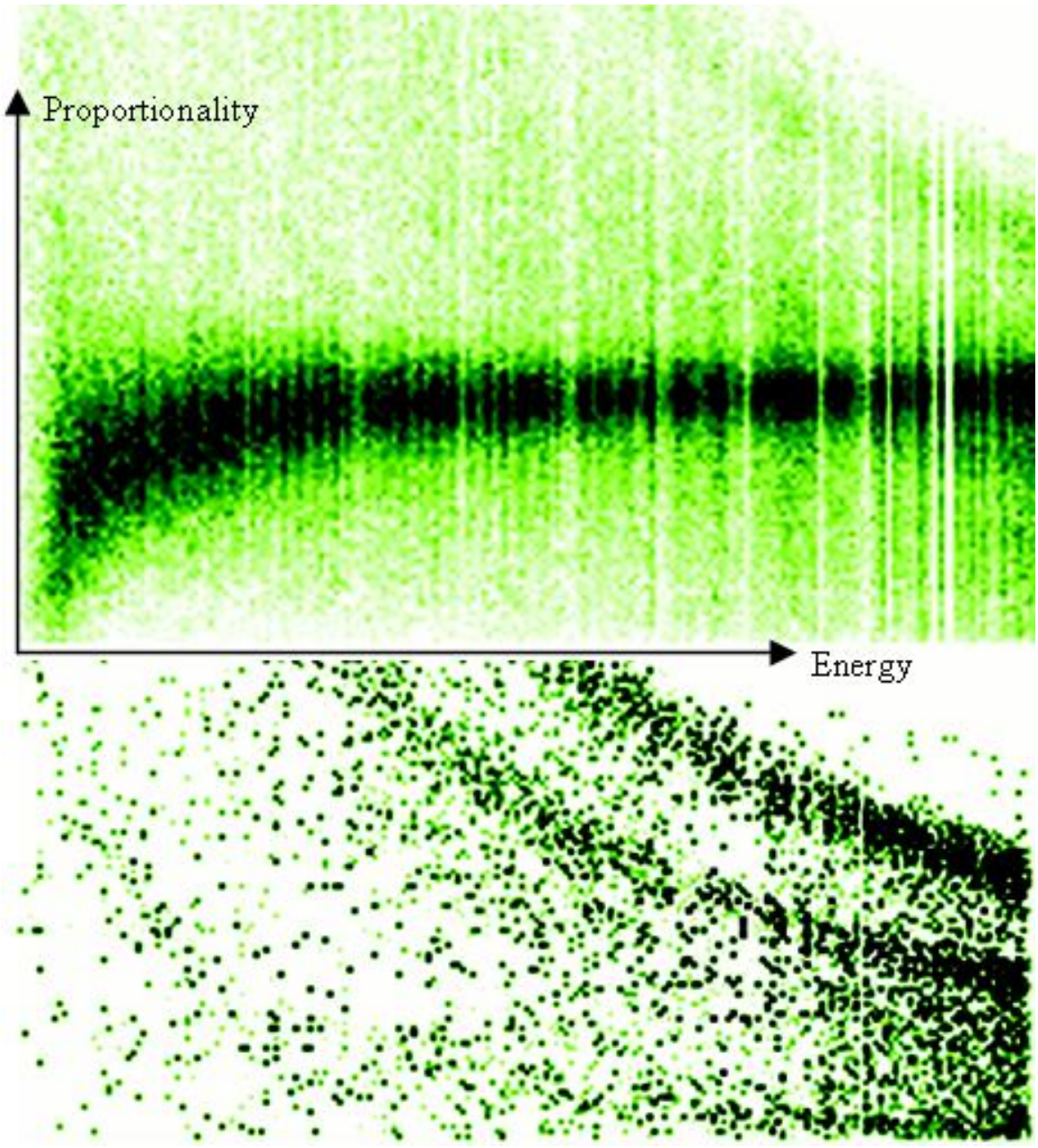

Figure 5.4a. 2 dimensional histogram of the non-proportional response of LSO:Ce measured for 1 hour in the PET Compton coincidence method with activation with Cs-137 source. 5.4b. 2 dimensional histogram of the background spectra acquired in 10 minutes with no source in the PET scanner.

plotted in Figure 5.5. The resulting data agrees with other non-proportional measurements performed on LSO:Ce samples (Balcerzyk, Moszynski et al. 2000), (Moszyński 2010). There is a noticeable sparseness in the data at the higher measured Compton electron energies. This is from the lower probability of scattering at these angles from the Klein-Nishina cross section and the fitting routines constraint of a minimum number of integral counts in the region used for fitting to determine the centroid of the distribution as discussed and shown in Figure 5.3.

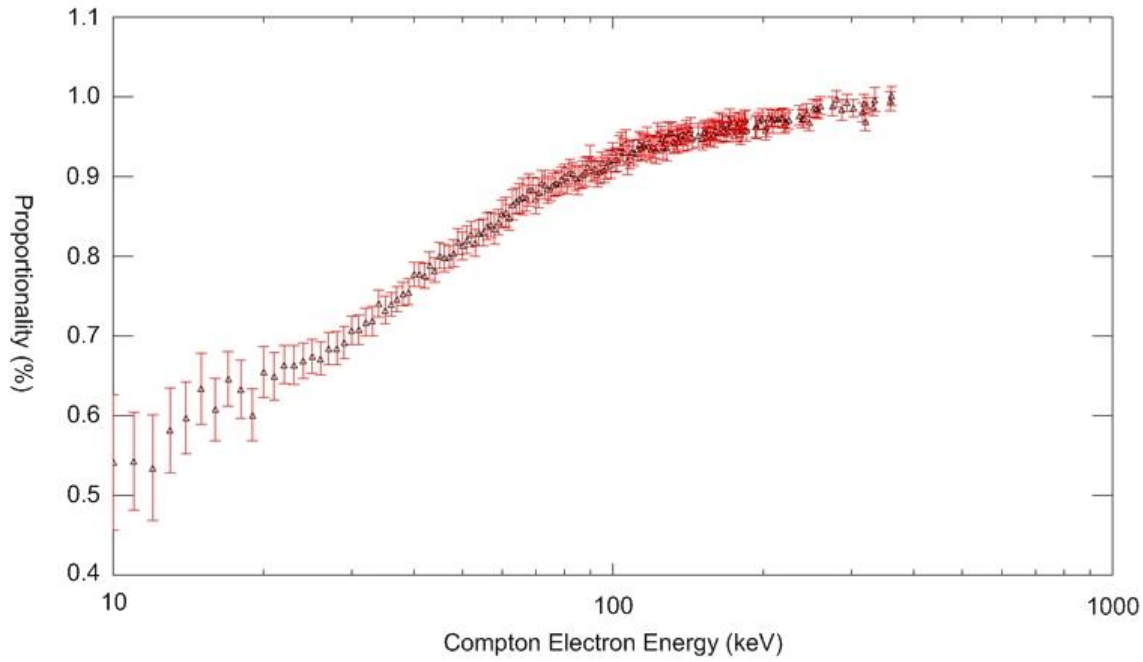

Figure 5.5. The electron non-proportional response for a 1cmx1cmx1cm cube of LSO:Ce. Acquisition time was 2 hours.

The second sample that was measured to validate the technique was a NaI:Tl sample. The sample was enclosed in an aluminum can with a transparent window to transmit the scintillation photons. The integration time in the PET electronics for the NaI:Tl sample was increased to 800 ns and the measurement time was lengthened to 6 hours in order to obtain more statistics for this material as this is one of the most reported scintillator for the response with several methods to characterize its non-proportional response. The resulting plot of this sample is plotted in Figure 5.6. The data obtained from this sample agrees well with selected published results of electron response non-proportionality studies (Ugorowski, Harrison et al. 2010), (Hull, Woon-Seng et al. 2009).

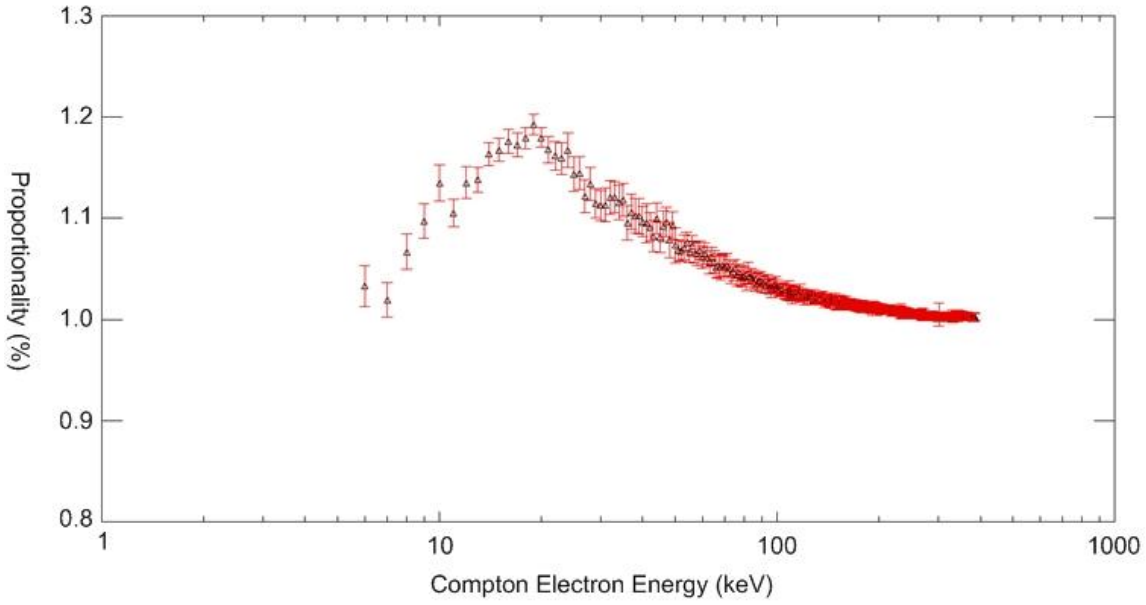

Figure 5.6. The electron non-proportional response for a 1 inch x 1 inch diameter NaI:Tl sample. Acquisition time was 6 hours.

Conclusions

A new technique to measure the non-proportional response was tested and validated against other methods. The method gives some advantages over other methods as it presents the data in 1 keV bins. This gives a finer sampling of the non-proportional curve over the isotope library method and some other presented Compton coincidence methods. Another advantage to the method is that the speed of the acquisition is faster than other Compton coincidence methods. From the measurements performed, it can be extracted that acquisition times are on the order of a few hours depending on the desired level of acquired statistics. An issue found in this technique is the increase of noise with the increase of integration time. The solution of conditioning the data by subtracting the 0 keV bin is a partial solution to this issue, but is not an exact answer. By working to reduce this noise the data will improve especially at the lower Compton electron deposition energy. Increasing the acquisition time is one way to extent the non-proportional response curve to lower energies, but noise at longer integration times, system noise and low number of photoelectrons generated at low electron energies within the sample are the largest contributor to the lower energy limit of this method. Work to improve these aspects of the measurement system is far more important to obtain even lower energy responses then increasing the acquisition times.

References for Chapter 5

Balcerzyk, M., M. Moszynski, et al. (2000). "YSO, LSO, GSO and LGSO. A Study of Energy Resolution and Nonproportionality." IEEE Transactions on Nuclear Science 47(4): 1319-1323.

Hull, G., C. Woon-Seng, et al. (2009). "Measurements of NaI(Tl) Electron Response: Comparison of Different Samples." Nuclear Science, IEEE Transactions on 56(1): 331-336.

Moszyński, M. (2010). "Energy resolution and non-proportionality of scintillation detectors – new observations." Radiation Measurements 45(3-6): 372-376.

Murray, R. and A. Meyer (1961). "Scintillation Response of Activated Inorganic Crystals to Various Charged Particles." Physical Review 122(3): 815-826.

Rooney, B. D. and J. D. Valentine (1996). "Benchmarking the Compton coincidence technique for measuring electron response nonproportionality in inorganic scintillators." Nuclear Science, IEEE Transactions on 43(3): 1271-1276.

Ugorowski, P. B., M. J. Harrison, et al. (2010). "Design and performance of a Compton-coincidence system for measuring non-proportionality of new scintillators." Nuclear Instruments and Methods in Physics Research Section A: Accelerators, Spectrometers, Detectors and Associated Equipment 615(2): 182-187.

CHAPTER 6 SUMMARY AND CONCLUSIONS

This collection of work demonstrated the effect that non-proportionality has on the energy resolution of scintillators. It also looked at a possible solution to the non-proportional response by studying the scintillation kinetics of YSO:Ce and creating permanent solutions to issues that affected the energy migration. The work ended with the creation of a new technique to measure the electron non-proportional response of scintillators.

The Monte Carlo simulation developed showed that the amount of energy resolution broadening could be modeled and applied to the measured LSO:Ce scintillator system once parameters such as optical properties and the non-proportional response are known. In this particular study, the non-proportional response used for the LSO:Ce scintillator was extracted from the literature and obtained from a radioisotope method. Future work in simulations can include the new measured electron non-proportional response, as this response would be a more realistic response compared with discrete energy points obtained from a radioisotope library. The electron response is also a more accurate representation of the physics after a Compton electron is ejected as is modeled in the simulations. Another interesting result not initially observed from the Monte Carlo study of the non-proportional response is that the full energy peak should not be symmetric if it is not proportional. There is an observed skewness to the lower energy side of the full energy peak of both the experimental data and

the simulated data. This is due to the non-proportional response of LSO:Ce scintillators. From its normalized value at 662 keV, the response decreases in proportionality as the energy deposited in the scintillator decreases. Because of this continuous decrease in proportionality toward the lower energies, the full energy peak is skewed to the lower energy side due to a partial deposition from a first interaction being a Compton scatter. There may be a way to characterize the non-proportionality of a scintillator material by deconvolving its non-proportional response from the full energy, if one can assume all other processes are symmetrically distributed within the full energy peak.

The study of the scintillation kinetics of YSO:Ce demonstrated that the scintillation kinetics are a function of charge traps and could be modified to improve the energy migration that results in luminescence. From thermoluminescence measurements, it was seen that the trap structure resulted in many charge traps with lifetimes on the order of nanoseconds at room temperature. This allowed these particular charge traps to participate in the scintillation kinetics for YSO:Ce at room temperature. This was observed by the difference of the decay time spectrum for YSO:Ce in comparison to another silicate material LSO:Ce. Also observed was large difference between scintillation decay time and photo-excited decay time, pointing to impeding of charge carriers after ionization and prior to emission by the luminescence center. By changing the temperature of the YSO:Ce sample, it was shown that the

charge trap lifetimes could be controlled. At cryogenic temperatures, these charge trap lifetimes are calculated to be on the order of years. After saturation of the shallow traps, they no longer influence the scintillation process. When measuring the scintillation decay time at cryogenic temperatures, the decay time is reduced to a value similar to the photo-excited decay times. The additional decay time from charge trapping within the energy migration step is significantly reduced.

From the results of the scintillation kinetics of YSO:Ce it was shown that reduction of charge traps in the material results in improved energy migration. This prompted a study to find a way to permanently reduce the charge traps in YSO:Ce in order to improve the overall scintillation characteristics. Those results lead to a co-doping study with calcium with varying concentrations to observe it's effect in YSO:Ce. From previous work (Yang, Melcher et al. 2009), calcium co-doping had been performed during Czochralski growth of single crystal silicate scintillators. These co-doped scintillators yielded good results in measured scintillation properties regardless of the co-doping concentrations of added calcium to the crystal matrix. The calcium co-doping of YSO:Ce also resulted in improved measured scintillation properties, particularly the scintillation decay time. The thermoluminescence glow curve of YSO:Ce:Ca also reveals that most of the charge traps are significantly reduced if not eliminated from the curve. This is reflected in the scintillation decay times with higher concentrations of

calcium co-dopants, the scintillation decay time approaches the photo-excitation decay time and is described by single exponential decay. In the sample grown that included a co-dopant concentration of 0.5% atomic with respect to yttrium, the light output was not significantly increased but the energy resolution did make an improvement from 12.4% to 9.4%.with a ~4% increase in scintillation light output in the calcium co-doped sample (Figure 6.1). This shows in this particular system, the broadening comes from the intrinsic energy resolution term discussed in chapter 1.

In order to compare any change in the non-proportional response of the YSO:Ce and YSO:Ce:Ca samples, a new method to measure the electron non-proportional response was developed and benchmarked. The method uses angular information by measuring Compton coincidence events with a PET scanner. This method was validated using LSO:Ce and NaI:Tl as both of these samples are well reported materials using several techniques to measure their non-proportional response. The results agreed well with other published results of electron non-proportional response for these materials. The results also showed that these materials could be characterized in a few hours, which is faster than any other electron response method reported.

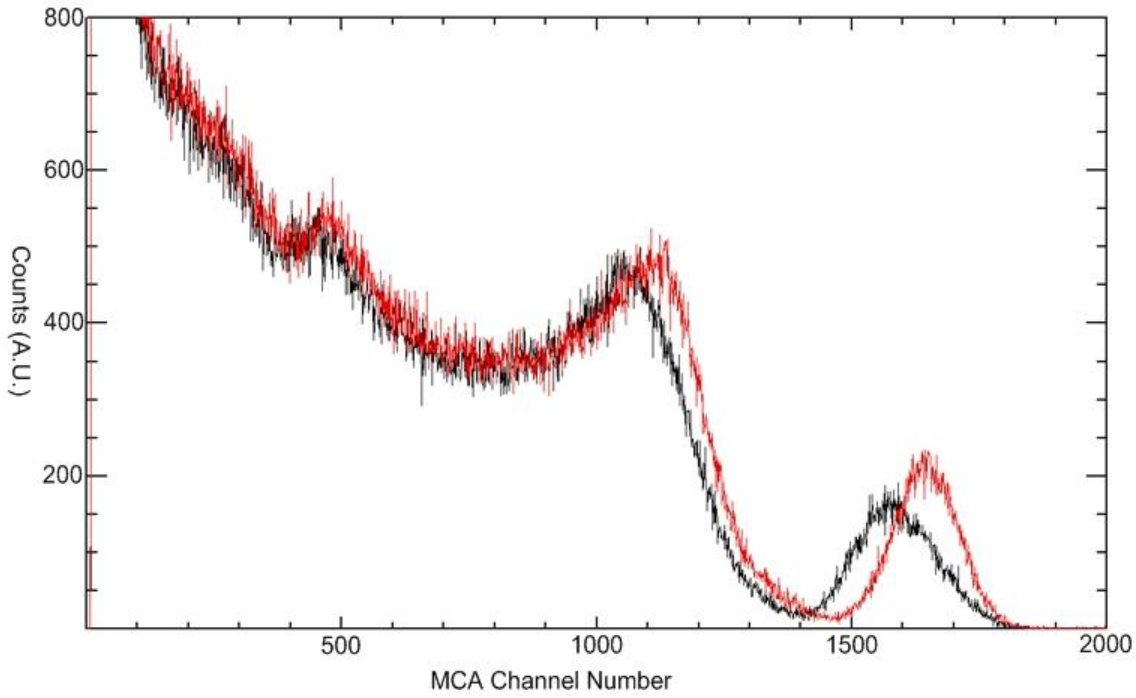

Figure 6.1. Pulse height spectra of a 1 cubic cm sample of YSO:Ce (black plot) and a 1 cubic cm sample of YSO:Ce:Ca (red plot). Both samples were measured under exact conditions and show relative difference between the light outputs and energy resolutions of the samples.

Using this new technique, a study of YSO:Ce and YSO:Ce:Ca was performed, as it was hypothesized that through an observed improvement in the energy migration, an improvement in the non-proportional response could occur. The electron non-proportional response has been measured for the case of LSO:Ce and LSO:Ce:Ca with no appreciable difference between the two samples (Payne, Moses et al. 2011). From co-doping studies of LSO scintillators

(Spurrier, Szupryczynski et al. 2008) and YSO scintillators, it was observed that the change observed from co-doping had a larger effect on YSO systems in particular, the change in the scintillation kinetics at room temperature as seen from the change in scintillation decay time. Figure 6.2 shows the comparison of the YSO:Ce and YSO:Ce:Ca samples with a measurement time of 2 hours per sample. From the figure, it is seen that the non-proportional response between

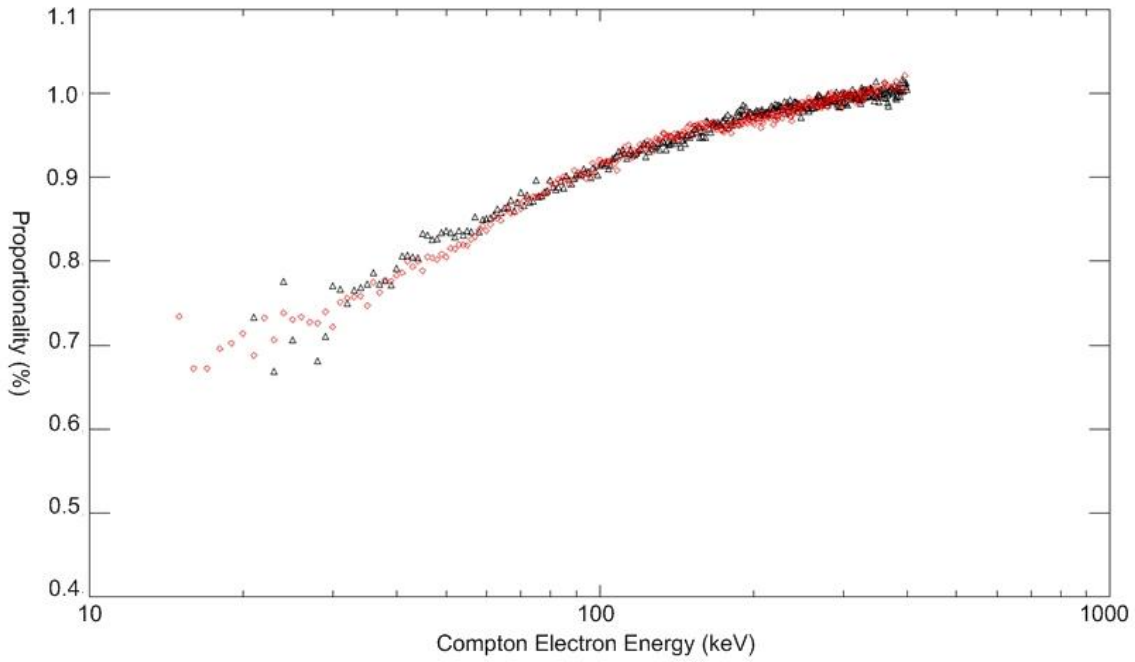

Figure 6.2. Plot of the non-proportional response of YSO:Ce (Δ) and YSO:Ce:Ca (O) measured for 2 hours per sample. Both samples measured were 1x1x1 cm cubes.

the 2 samples follows the same trend with no large measurable difference. This concludes that even with the marked improvement of the energy migration of YSO:Ce scintillators, the non-proportional response is not improved. From Figure 6.1, however, there was a measurable and visible improvement in the energy resolution of these scintillators without a large improvement in light output. Recalling equation 1.3, the energy resolution is a quadrature sum of several effects for a scintillator system. Since the differences in counting statistics between the two measured samples are approximately 4% different, an assumption is made that the significant contributor to the energy resolution is still within the intrinsic resolution part of the equation. The intrinsic resolution contribution to the energy resolution was separated into 2 parts as shown in equation 1.4 where the two contributing mechanisms for the intrinsic resolution broadening are the non-proportional response of the scintillator and in-homogeneity within a sample. This leads to a conclusion that the improvement of the energy resolution of the calcium co-doped sample is due to a more homogeneous material. This effect creates an energy resolution broadening by having regions within the sample that respond to the incident ionizing radiation differently enough to shift the full energy peak. The result of this shifting of response leads to a convolved full energy peak with contributors from these different response regions. This result can be further confirmed from work done by Cutler (Cutler, Melcher et al. 2009), where the results of the non-proportional

response of several samples were measured, and the results showed less sample-to-sample variation in the calcium co-doped samples when compared to the samples without the co-doping.

Conclusions

It was demonstrated that the energy resolution of a scintillator is a factor of many contributors. It was earlier shown that the non-proportional response of scintillators was a significant contributor to the energy resolution of a scintillator. Through the work, an improvement to the energy resolution was obtained from our studies and co-doping with calcium. Even though it was found that the energy migration improvement did not improve the non-proportional light yield response, the energy resolution was improved within the intrinsic contributions by an improvement in the homogeneity of the scintillator. The current quest to improve the energy resolution of scintillators by means of improving the non-proportional response should also consider other factors that contribute to the energy resolution. This collection of work concluded that in YSO scintillators, the energy resolution also suffers from material in-homogeneity even though the growth technique and controls for this particular scintillator are quite mature. This additional contribution to the energy resolution from in-homogeneity may affect the energy resolution of many other scintillators. Another observation is that perhaps the increase of homogeneity could be the cause for the decrease of

charge traps and the reason for the increase in energy migration. Such claims do require more work to substantiate them.

References for Chapter 6

Cutler, P. A., C. L. Melcher, et al. (2009). "Scintillation Non-Proportionality of Lutetium-and Yttrium-Based Silicates and Aluminates." IEEE Transactions on Nuclear Science 56(3): 915-919.

Payne, S. A., W. W. Moses, et al. (2011). "Nonproportionality of Scintillator Detectors: Theory and Experiment. II." Nuclear Science, IEEE Transactions on 58(6): 3392-3402.

Spurrier, M. A., P. Szupryczynski, et al. (2008). "Effects of Ca^{2+} Co-Doping on the Scintillation Properties of LSO:Ce" Nuclear Science, IEEE Transactions on 55(3): 1178-1182.

Yang, K., C. L. Melcher, et al. (2009). "Effects of calcium codoping on charge traps in LSO: Ce crystals." Nuclear Science, IEEE Transactions on 56(5): 2960-2965.

APPENDICES

Appendix A

Electromagnetic Radiation

Electromagnetic radiation is defined as energy with no mass and an electrical and magnetic component. It follows the wave-particle duality and travels at the speed of light (as light is a form of electromagnetic radiation). To classify a quantum of electromagnetic radiation, its energy or wavelength must be known. If one of these parameters is known, the other can be related with a simple equation (equation A.1).

$$E = \frac{hc}{\lambda} \qquad \text{(A.1)}$$

Though the electromagnetic spectrum is wide and has many applications, the x-ray and gamma ray regions are the portions of the spectrum that are of interest in scintillators and their applications.

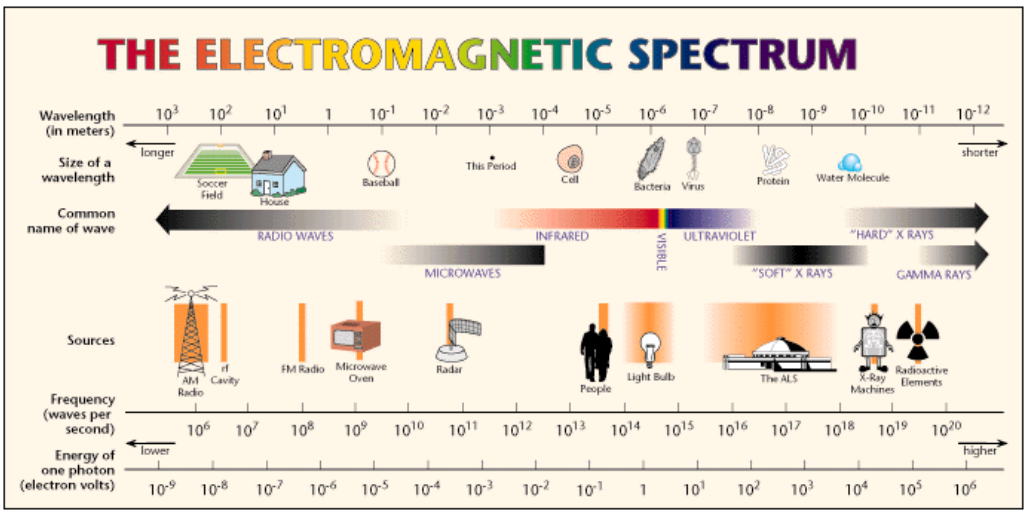

Figure A.1. Diagram of the Electromagnetic spectrum across the range of wavelengths, frequencies and energies with the common names associated with the range. (http://www.lbl.gov/MicroWorlds/ALSTool/EMSpec/EMSpec2.html)

X-Ray and Gamma Radiation

X-ray and gamma radiation are ionizing electromagnetic radiation. This differentiates it from other electromagnetic radiation in the way it interacts with matter. It also differs from other forms of ionizing radiation that one might think could be used in the same way for some other scintillator applications. Some of the other types of ionizing radiation include alpha, beta, protons and neutrons. Gamma and x-ray radiation give an advantage as they have some probability to pass through matter as a function of the electron density and material density of

a particular material. This particular characteristic gives rise to many applications such as the ones discussed in the introduction.

Interaction of Gamma Radiation with Matter

Gamma radiation interacts with matter differently than other forms of radiation such as charged particles. The interactions of gammas with matter are discrete processes. The results of any of these discrete processes are partial or full absorption of the incident gamma. The energy that is lost from the incident photon is transferred to electron energy. There are several different possible types of gamma interactions with matter (Table A.1). The major physical processes that govern the mechanisms of the applications presented here will be further discussed is the following sections (highlighted in table A.1). The other processes presented in table 1 are much less frequent and not major contributors to the physical mechanisms of the applications discussed here.

Table A.1. Table of processes of gamma interactions with matter.

	Absorption	Coherent Scattering	Incoherent Scattering
Atomic Electrons	Photoelectric Effect	Rayleigh Scattering	Compton Scatter
Nucleons	Photodisingration of Nuclei	Thomson Scattering	Nuclear Resonance Scattering
Electric Field	Pair Production	Delbruck Scattering	Unobserved

Because these processes are unique to gamma radiation, gammas are more penetrating in materials than charged particles. Another unique property to gammas over charged particles is that the energy is not reduced as it passes through a material; instead the intensity of an incident beam of gammas is reduced in intensity as a function of material thickness. Assuming that the dominating processes of gammas in materials are the photoelectric effect, Compton scatter and pair production, any interaction of a gamma with a material removes the interacted photon from the beam. This reduction of intensity to an incident gamma beam can be shown in equation A.2.

$$I(x) = I_o \exp(-\mu x) \qquad \text{(A.2)}$$

Where I_o is the incident gamma intensity, μ is the linear attenuation coefficient, and x is the thickness of the material the gamma beam is incident upon. The linear attenuation coefficient is simply the sum of the probabilities of any of the processes will happen in a particular material (equation A.3).

$$\mu = \mu_{Photoelectric} + \mu_{Compton} + \mu_{Pair\ Production} \qquad \text{(A.3)}$$

When searching for these probabilities, databases are available for construction of tables that present the probabilities for the individual processes and can construct these tables for a variety of compositions, compounds and elements. These tables report the probabilities as mass attenuation coefficients instead of linear attenuations coefficients (Figure A.2).

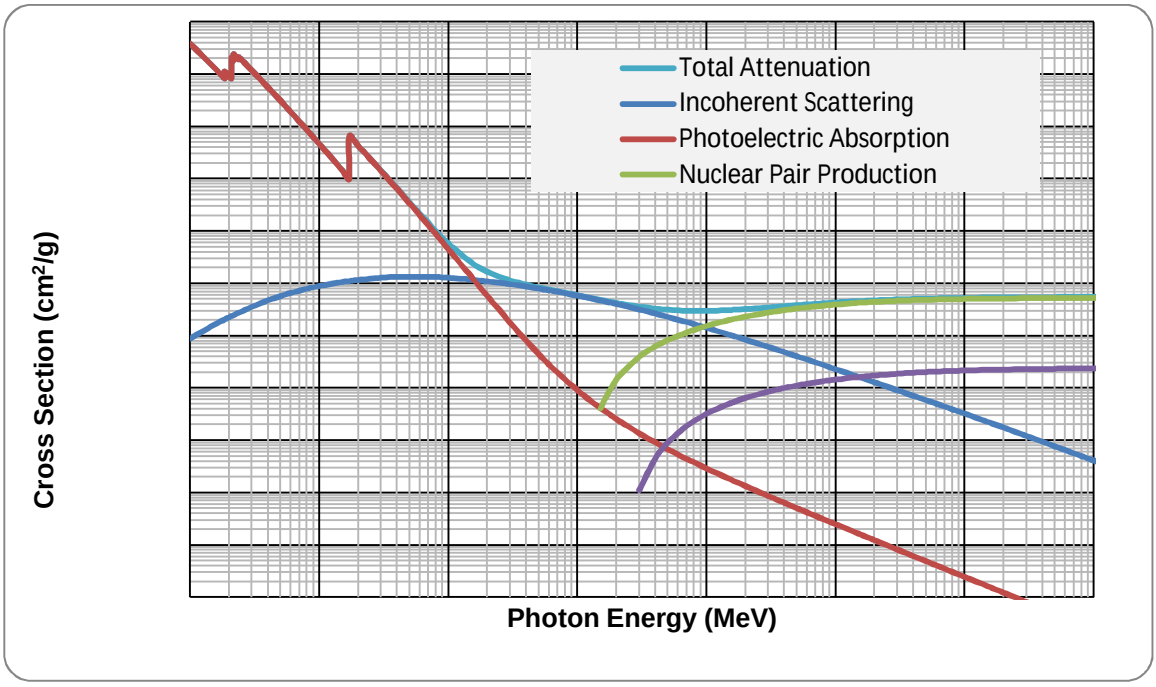

Figure A.2. Plot showing Mass attenuation coefficiants for YSO. Cross section data was obtained from NIST XCOM. (http://physics.nist.gov/cgi-bin/Xcom).

This is because compounds and compositions have varying densities depending on the state of the material. The density of the material that is interacting with the gamma beam is an important property of the material because where the

density of the material increases, so does the probability of interaction. The mass attenuation coefficient plot shown in Figure A.2 demonstrates the breakdown of some of the dominating processes as a function as energy and is commonly displayed in units of cm^2g^{-1}. The mass attenuation coefficient of a compound or composition is constructed using the following equation (equation A.4).

$$\left(\frac{\mu}{\rho}\right) = \sum_i w_i \left(\frac{\mu}{\rho}\right)_i \qquad \text{(A.4)}$$

Therefore, the intensity of a beam of gammas incident on a known material with a known density can be calculated as (equation A.5).

$$I = I_o \exp(-\left(\frac{\mu}{\rho}\right)\rho x) \qquad \text{(A.5)}$$

Knowing the nature of attenuation of gamma radiation within matter gives us insight into how some of the medical imaging modalities such as the planar x-ray and CT work on the principle of intensity of radiation that is attenuated in the body when the matter that is scanned varies in probabilities of interactions and density. It also can demonstrate the effectiveness of a particular detector material's efficiency to detect a gamma event of a particular energy. This

knowledge can also be used in selecting how much detector material is necessary in all detection applications to detect a certain percentage of incident gamma radiation of a specific energy or energy range by varying the x (detector thickness) to maximize detection efficiency.

Compton Scatter

The Compton scatter is an interaction between an incident gamma ray and an electron of the material it is interacting with. The interaction can be seen as a collision event, in which the gamma ray hits the electron and ejects it from its bound state. The energy is transferred to the electron and the gamma is scattered from its initial track at an angle that is related to the energy transferred to the electron (Figure A.3).

The relationship between the energy of the scattered gamma ray and the scattering angle can be derived from conservation of momentum and energy and relating them with relativistic relationship between energy and momentum.

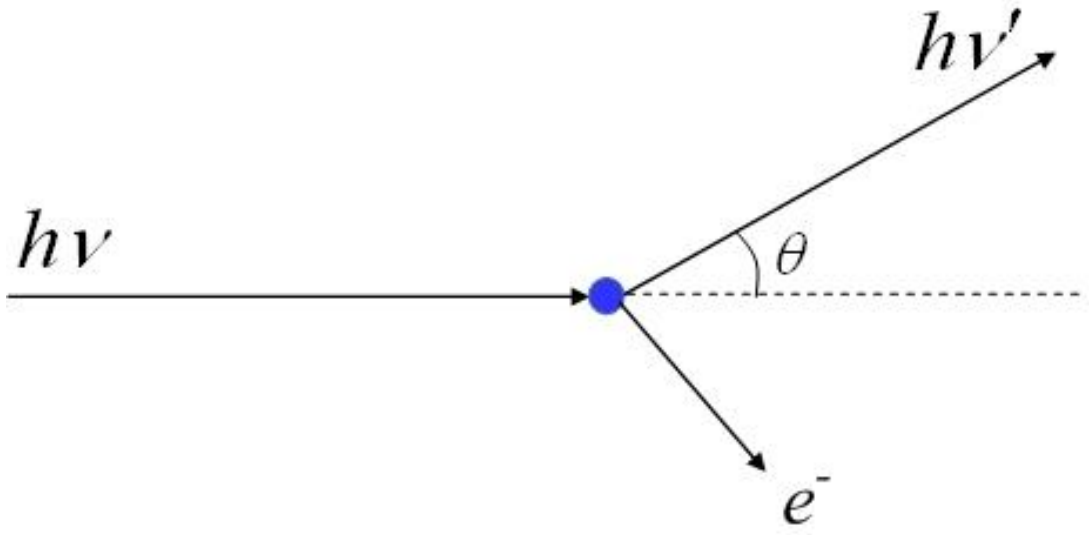

Figure A.3. Simple diagram showing the Compton scatter of an incident gamma ray (hv), the scattered gamma ray (hv') and the ejected electron resulting from the collision.

The energy of the scattered gamma can be related to the scatted angle with the following equation.

$$h\nu' = \frac{h\nu}{1+\left(\frac{h\nu}{m_o c^2}\right)(1-\cos\theta)} \quad \text{(A.6)}$$

Also using simple conservation of energy, the energy that is transferred to the ejected electron is simply,

$$E_{ejected\_e^-} = h\nu - h\nu' \text{ (A.7)}$$

From these relationships it can be seen that the Compton scatter has an energy limit of the energy that can be transferred to the struck electron. As the angular limits of scatter are from 0 degrees to 180 degrees, the max energy transfer occurs at a scattering angle of 180 degrees. Figure A.4 shows the energy of the scattered gamma ray (black plots) and the energy transferred to the ejected electron (red plots) of 4 different incident photon energies as a function of gamma ray Compton scatter angle. From these plots it is also easily observed that the higher the energy of the incident gamma ray, the higher the energy that can be transferred to the interacted electron.

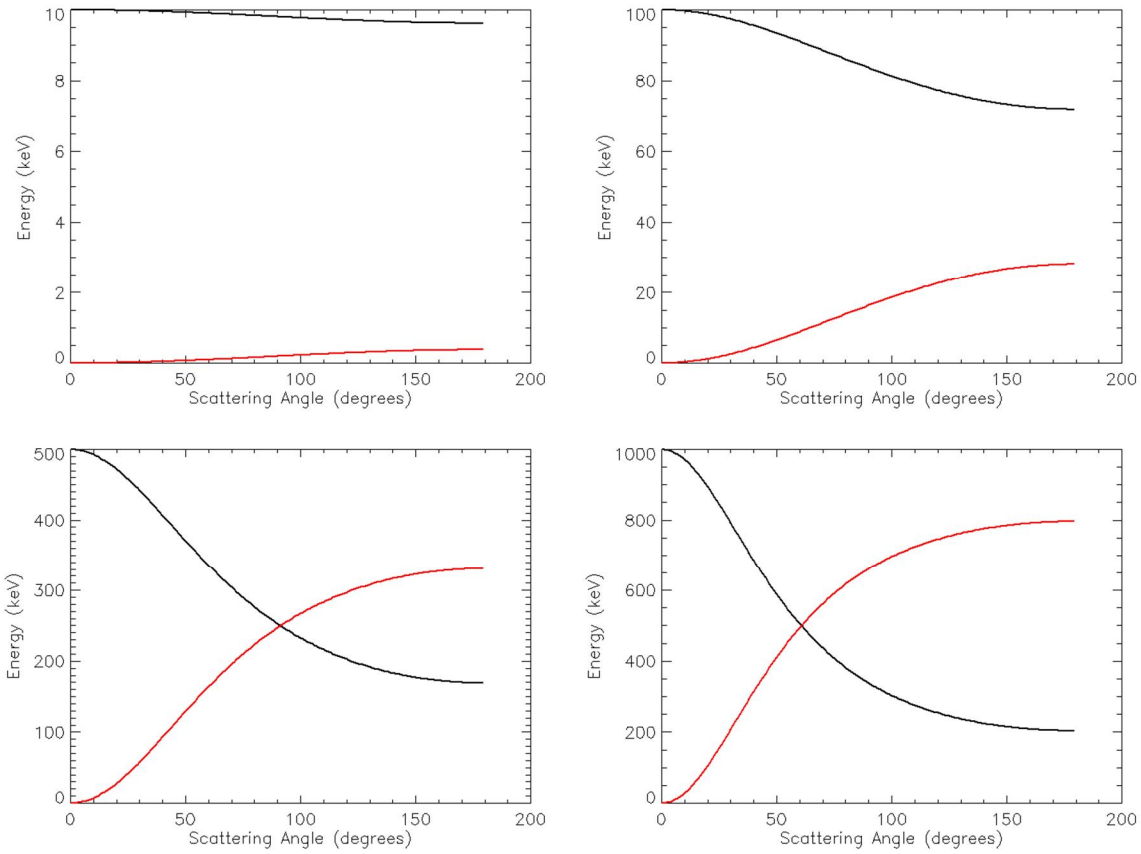

Figure A.4. Plots of the energy deposited (red plot) and the energy of the Compton scattered photon after an initial Compton scatter event. The plots are for an incident photon of 10,100, 500 and 1000 keV.

Klein-Nishina formula

The scattering angle of the gamma ray resulting from a Compton scatter event is not entirely random. There is a probabilistic bias to certain scattering angles depending on the incident gamma ray energy. This is predicted by the

Klein-Nishina formula that predicts the differential scattering cross section (equation A.8).

$$\frac{d\sigma}{d\Omega} = r_o^2\left(\frac{1}{1+\alpha(1-\cos\theta)}\right)^3\left(\frac{1+\cos^2\theta}{2}\right)\left(1+\frac{\alpha^2(1-\cos\theta)^2}{(1+\cos^2\theta)[1+\alpha(1-\cos\theta)]}\right) \qquad \text{(A.8)}$$

Where r_o is the classical radius of an electron, α is $\frac{h\nu}{m_o c^2}$ and θ is the scattering angle of the gamma ray with an electron (as shown in Figure A.3). It is seen that at higher incident gamma energies, the scattering angle favors forward scattering by the Klein-Nishina formula as seen in Figure A.5.

This specific property is important as the Compton scatter is the dominating interaction of gamma rays in many materials with the energies that originate from isotopic sources. Therefore all of the applications mentioned prior are affected by the Compton scatter mechanism. The Klein-Nishina probability distribution gives insight to the behavior of the Compton scattered gamma rays probable scattering angle which allows for modeling of the mechanism and corrections where the Compton scatter is an undesirable mechanism such as in medical imaging and x-ray/gamma ray imaging.

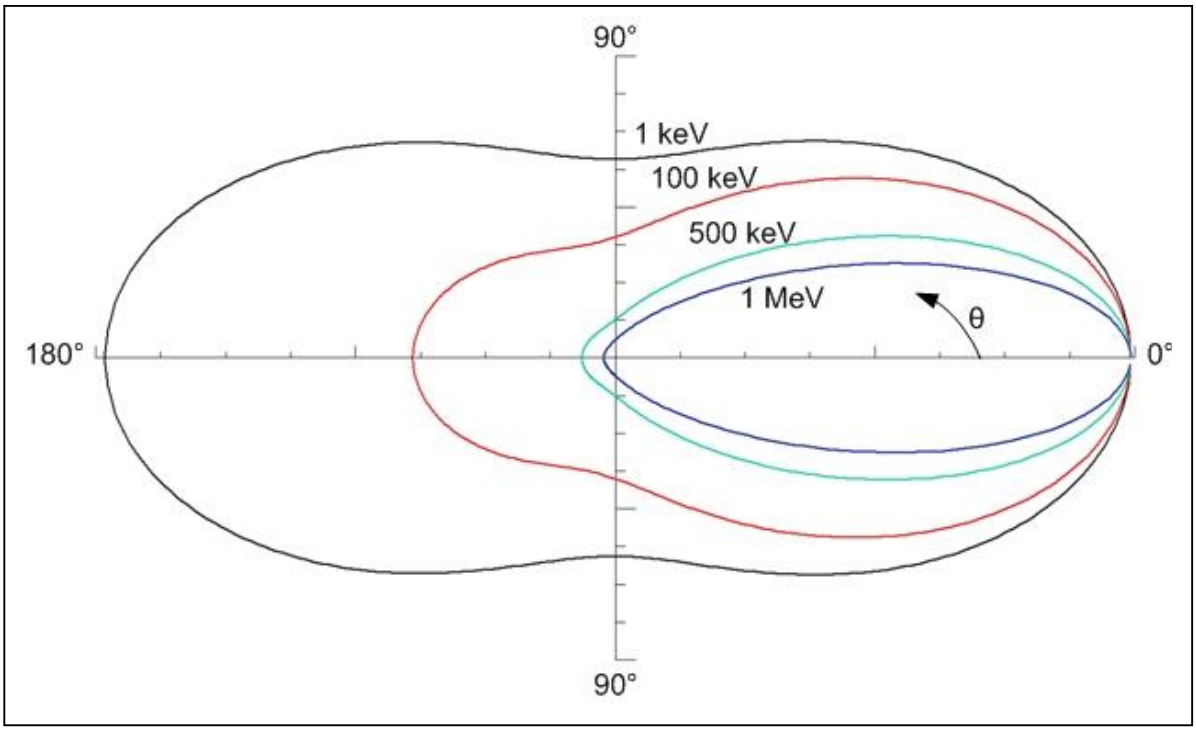

Figure A.5. Polar plot of the scattering angle probability with separate plots to demonstrate the difference of probabilities as a function of incident gamma ray energy.

Photoelectric Effect

The photoelectric effect is the interaction that results in absorption of an incident gamma ray by an atomic electron. The photoelectric effect is the dominating effect for lower energy gamma ray (less than ~100 keV) for most materials. Upon absorption of the incident gamma ray, a photoelectron is created and ejected from an atomic shell (Figure A.6).

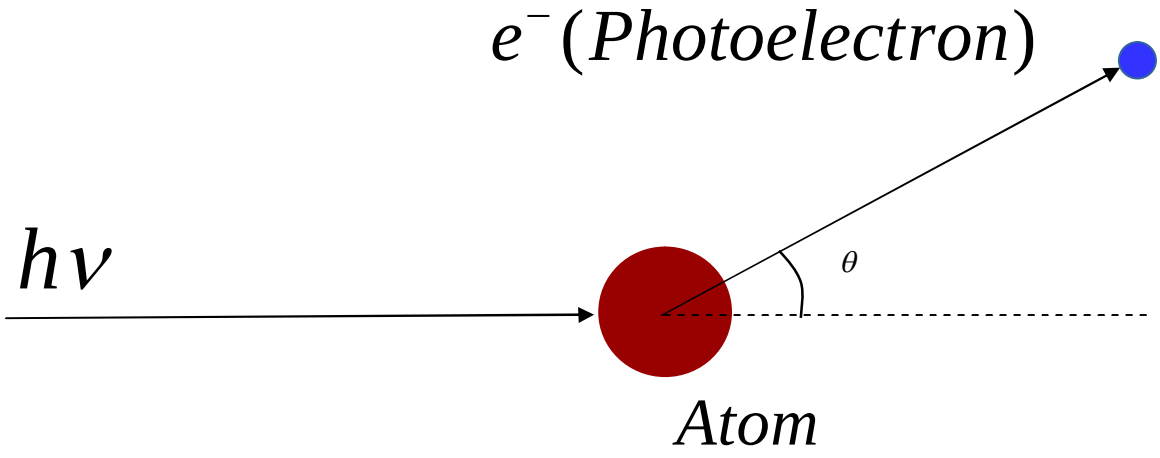

Figure A.6. Simple diagram showing the photoelectric absorbtion of an incident gamma ray (hv), the resulting photoelectron ejected from the interaction.

It is found that most of the photoelectric absorptions occur within the K and L shells of atoms. The K shell of atoms is the innermost shell in an atom which results in the highest binding energy of the K shell's electrons. Therefore for the photoelectric effect to occur, the incident photon must have more energy than the binding energy of the electron bound to an atom. The resulting ejected photoelectron leaves the atom with energy T (equation A.9).

$$T = h\nu - B_{energy} \qquad \text{(A.9)}$$

Where *hv* is the incident gamma ray energy and B_{energy} is the binding energy of the electron. Once the photoelectron is liberated from its atomic shell, the electron vacancy is filled resulting in a characteristic x-ray or an Auger electron.

Pair Production

At gamma energies higher then $2m_oc^2$ (1.02 MeV), there is a probability for another interaction with matter called pair production. This interaction is where the incident gamma is absorbed and results in emission of an electron and a positron with total energy equal to the incident gamma (equation A.10).

$$h\nu = (T(electron) + m_o c^2) + (T(positron) + m_o c^2) \qquad \text{(A.10)}$$

Where *hv* is the incident gamma ray energy and T is the kinetic energy of the electron or the positron. As seen in the cross section plot in Figure A.2, the process becomes energetically favorable at energies above $2m_oc^2$ and becomes the primary interaction in higher energies (>10MeV).

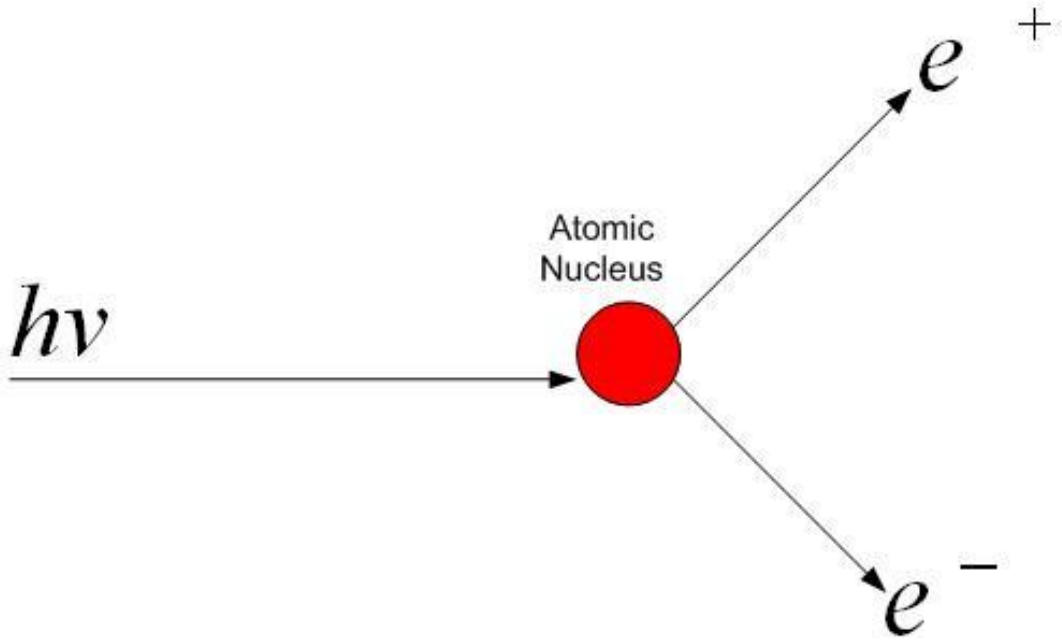

Figure A.7. Simple diagram showing the pair production interaction of an incident gamma ray (hv) with the atomic nuclear field. The result of the reaction yields a positron and electron also shown in the figure.

From table A.1., it is seen that this is an absorption interaction when the gamma interacts with the electrical field of atom. The interaction is dominated with the interaction between the gamma and the nuclear field, but has some probability to interact with the field of an electron to a less extent.

References for Appendix A

Evans, R. D. and A. Noyau (1955). The Atomic Nucleus, McGraw-Hill New York.

Knoll, G. F. (1989). Radiation Detection and Measurements, Wiley.

Appendix B

Common Characterization Techniques for Scintillation Materials

In order to quantify the scintillation properties that are necessary for determining the properties of a scintillator material, there is some fairly standard measurement techniques used to characterize a particular scintillator. Although there are more than discussed in this section, the ones that are relevant to this work will be discussed.

Pulse Height Spectrum

The pulse height spectrum measurement is an important measurement where many scintillation properties can be extracted. This measurement is essentially a response measurement for a scintillator to a particular ionizing radiation. The resulting spectrum acquired from this technique is known as the pulse height spectrum, but also known as the energy spectrum as was shown in Figure 1.2. A basic block diagram showing the NIM electronics chain used to measure samples from this work is shown is Figure B.1.

From the pulse height spectrum, many scintillation material properties can be determined. As discussed in chapter one, the energy resolution of the scintillator system can be extracted from the spectrum. Another property of a

scintillator that can be measured from this technique is the non-proportional response with isotope library technique also discussed in chapter one. By using the pulse height spectrum of several radioisotopes with varying gamma energies, the resulting pulse height spectra can yield the non-proportional response of a particular scintillator.

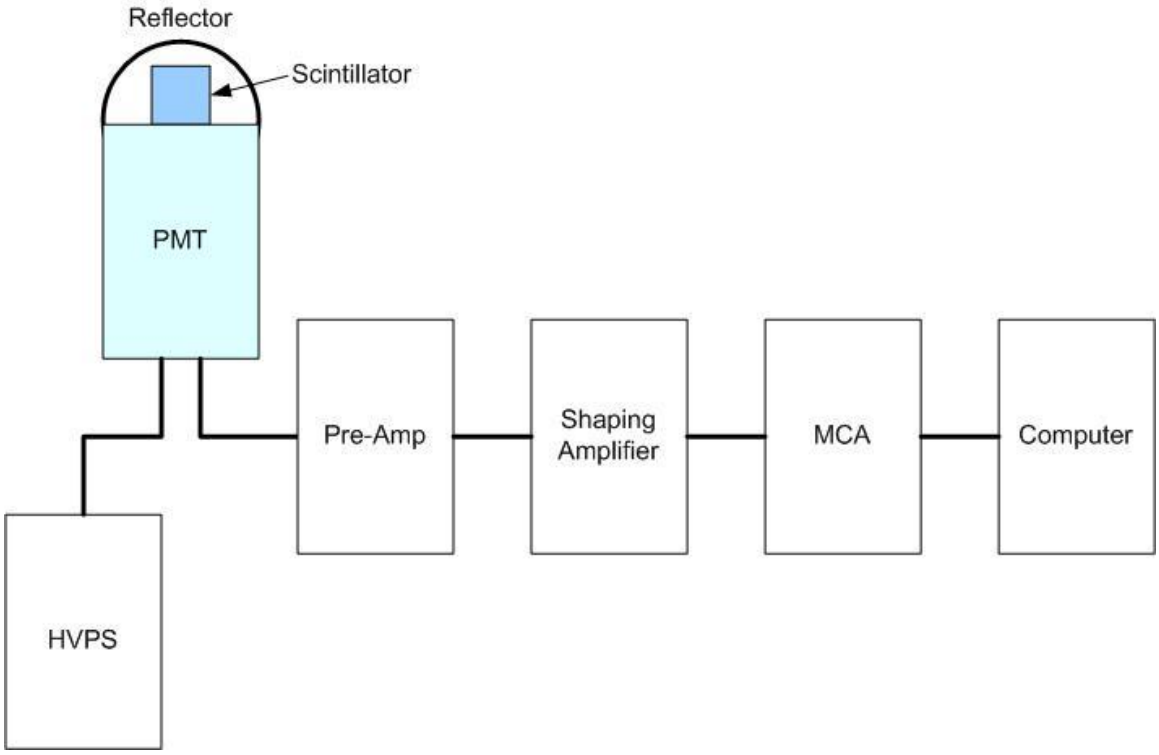

Figure B.1. Diagram of a pulse height measurement setup used to obtain spectra in this work

A scintillation property that is commonly reported is the absolute light output (or yield). This property can be determined from pulse height spectra analysis and some system information such as spectral quantum efficiency of the

photosensor and the linearity of electronic amplifiers. By observing the response with no light source, a single photoelectron spectrum can be acquired. When measuring a scintillator, the measurement can be thought of as measuring some amount of photoelectrons. By making some assumptions to the efficiency of the total number of photons emitting from a scintillation event to the number of photoelectrons created in the photosensor, the absolute light output can be measured.

Excitation and Emission Spectrum

The excitation and emission spectrum measurement is a technique used to obtain information of the electronic transfer of the excited and ground states of the luminescence centers within a specific host material. Although there can be different luminescence centers in inorganic scintillators, this work focuses on cerium as the activator. The result of these measurements is the excitation and emission spectra of the measured sample and gives insight to the optical behaviors of the luminescence centers in a particular matrix. The measurements performed in this work were done on a spectrofluorometer (Hitachi F-4500 fluorescence spectrophotometer) with a 90 degree beam to photo detector geometry. The operation is a scanning operation with either the excitation or emission being held fixed. For an emission scan, the excitation wavelength of the incoming beam is held constant and the emission wavelength is selected using a monochrometer to determine the intensity of the emission while scanning

across a range of emission wavelengths. Inversely, the excitation scan is performed by holding a constant emission wavelength by adjusting the monochrometer for a specific wavelength and scanning across a range of excitation wavelengths and recording the intensity as a function of the excitation wavelength. The information obtained can give information such as changes in stokes shifts, preferential activator locations in a host material, excitation and ground state level splitting information and other information.

Decay Time Measurements

Decay time measurement using the Bollinger and Thomas method produces the statistical scintillation decay time spectrum of a scintillator. This decay time convolves all effects including the initial ionization, the energy migration to a luminescence center and the statistical decay time of the luminescence center. This measurement can be performed at varying temperatures and differing activation methods using electromagnetic radiation or charged particles, but always operate on a principle of the start signal originating from many scintillation photons and a stop signal from a single photon originating from the same scintillation event. The setup used in this collection of work is shown in Figure B.2. The setup used is derived from the original setup for time correlated single photon measurements presented in (Bollinger and Thomas, 1961).

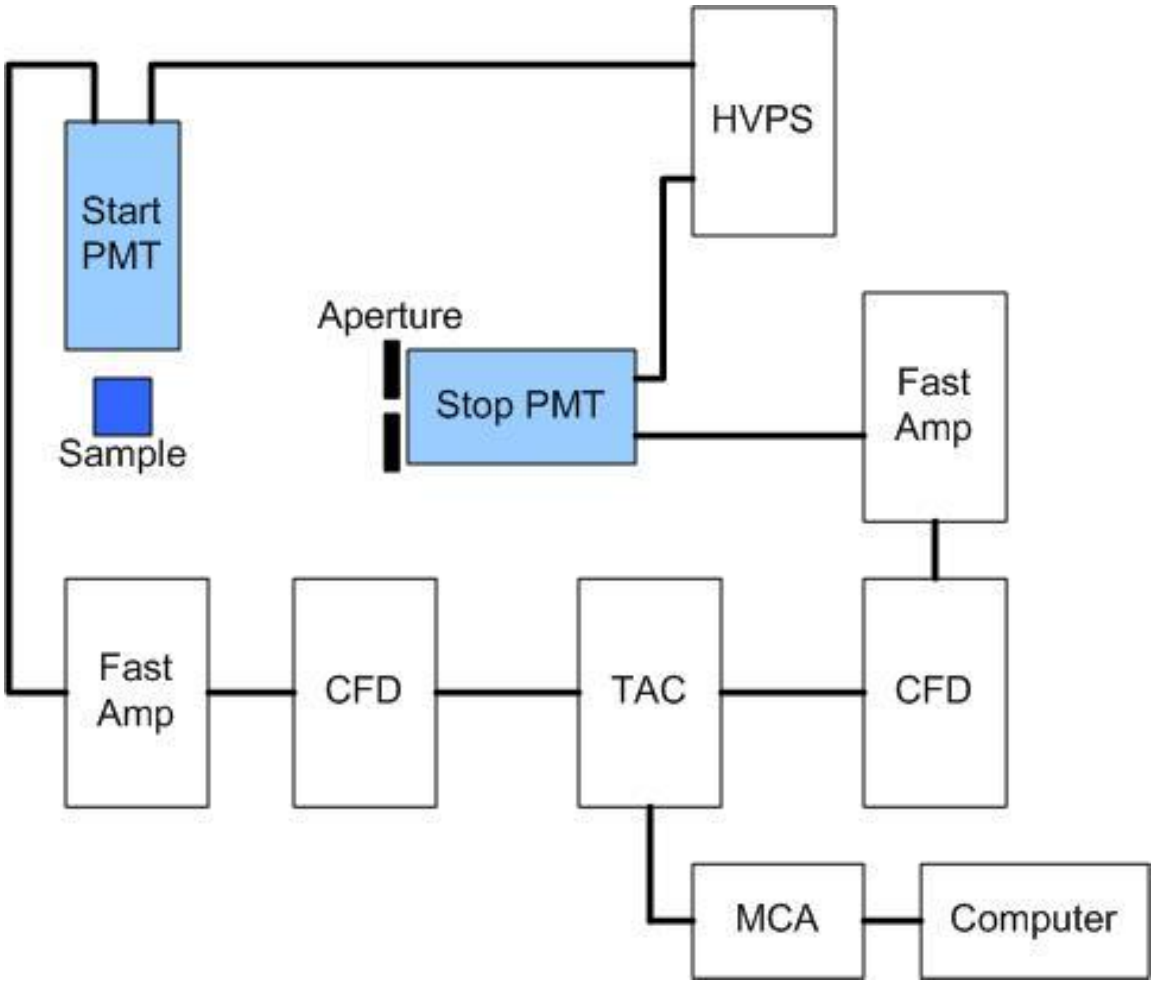

Figure B.2. Block diagram of setup used for time correlated single photon measurements performed for this work.

The data obtained is a pulse height spectra, where the pulse heights recorded are proportional to the time difference of the start and stop pulses. This time scale is set by the time to amplitude converter (TAC) and can be scaled to match the scintillation decay time of the scintillator sample being measured. Once the spectrum is acquired it is post processed with software capable of data fitting.

Since the decay process is generally easily modeled with an exponential decay, the data is modeled with an exponential decay model with an appropriate number of decay components.

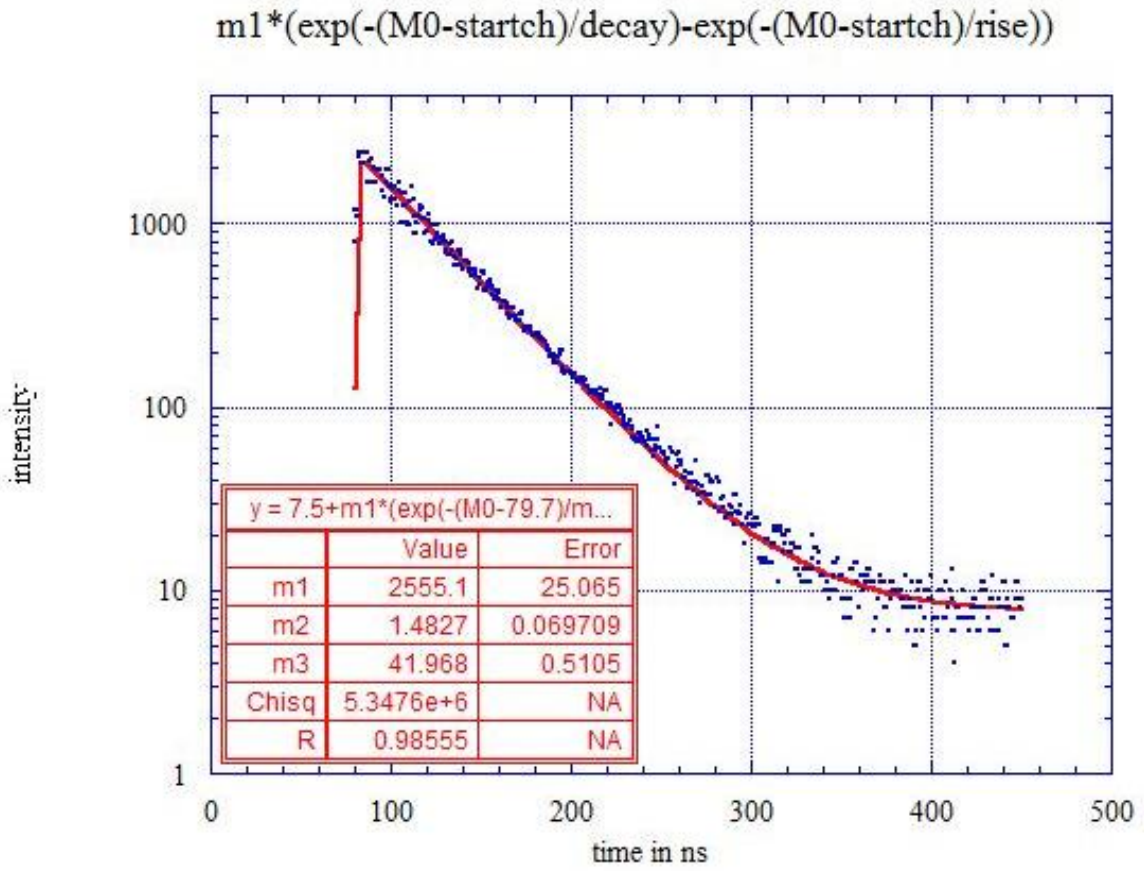

Figure B.3. A scintillation decay time spectrum for LSO:Ce. Plot demonstrates the one component exponential fit for the rise and decay time of the sample.

Thermoluminescence

Thermoluminescence measurements are a technique that reveals the measureable charge trap structure for luminescence materials. The technique is performed by mounting a sample onto a cryostat cold finger which is sealed in a vacuum chamber. The setup used in this collection of work (Figure B.4) had stainless steel shroud with quartz window to allow the optical signal of the sample to be measured. The shroud is also equipped with a beryllium window in order to allow passage of radiation from outside the shroud to the sample inside of the shroud. The radiation source used in this work was an x-ray generator generally operated at 35kV and 0.1mA. To perform the measurement, the cold finger is brought down to cryogenic temperatures (<40K). Once the material is stable at low temperature, the sample is irradiated with x-ray radiation. The sample is then heated at a fixed rate and the signal from the de-trapping resulting from thermal excitation is recorded as intensity versus temperature. This result is the glow curve of the sample. The glow curve can be further analyzed to characterize traps that are observed with this method. The model applied to the glow curve is based on the work by (Randall and Wilkins,1945) where the model gives information on charge traps depth, frequency of the trapped electron or hole and trap lifetime as a function of the scintillator temperature. The equation used to model the traps in the glow curve is shown in eq B.1.

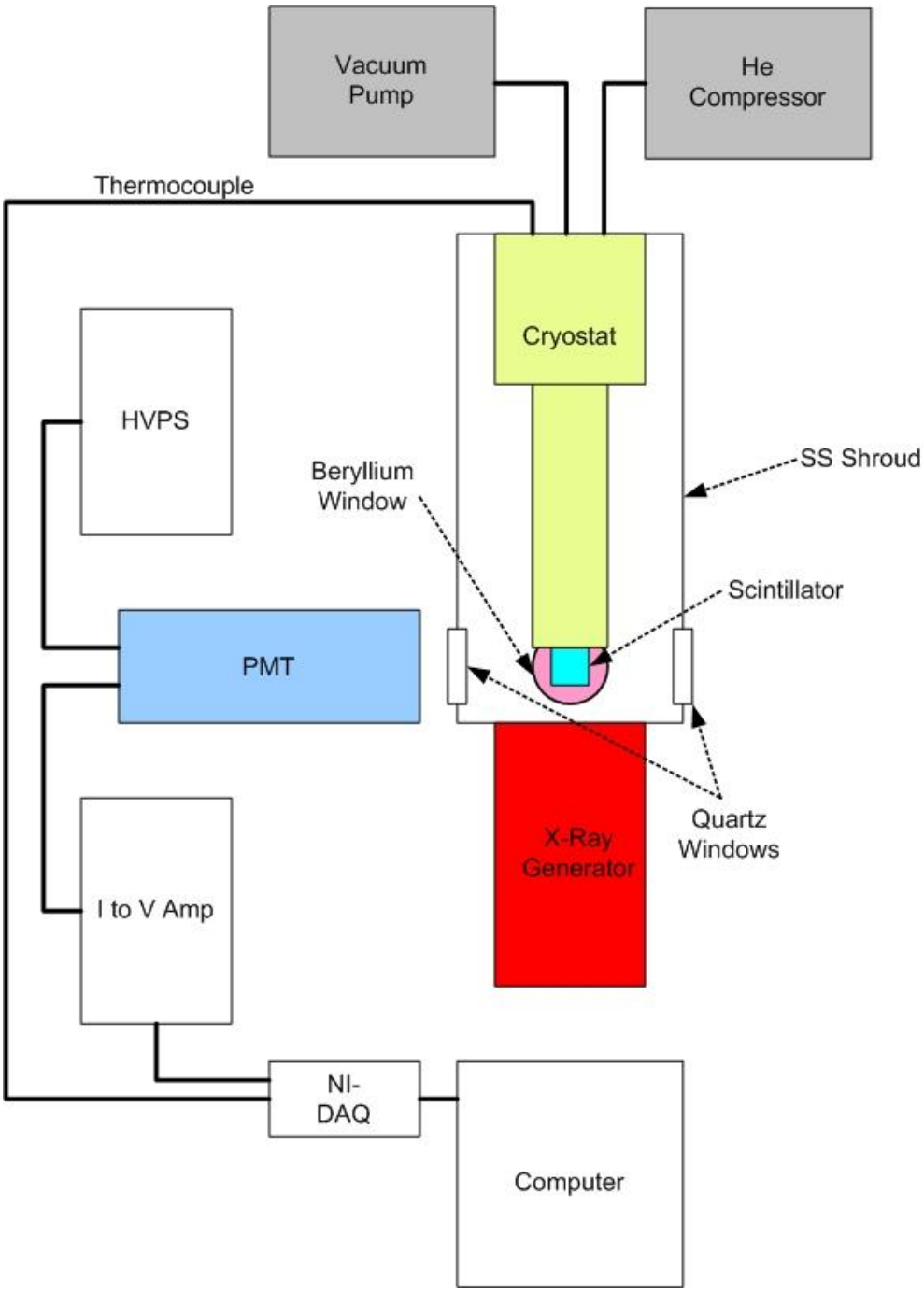

Figure B.4. Block diagram of the thermoluminescence setup used in this work.

$$I(T-\Delta T) = n_o s e^{-\left(\frac{E}{kT}\right)} e^{-\left(\frac{s}{\beta}\right)\int_{T1}^{T2} e^{-\left(\frac{E}{kT}\right)} dT} \qquad \text{B.1.}$$

Where I is a traps intensity, s is the frequency factor, β is the heating rate, and E is the activation energy. K is the Boltzmann's constant and T is the temperature. An example of a glow curve with fits for observed traps is shown in Figure B.5. The plot also shows the software program (Glodo, 2001) used in this collection of work.

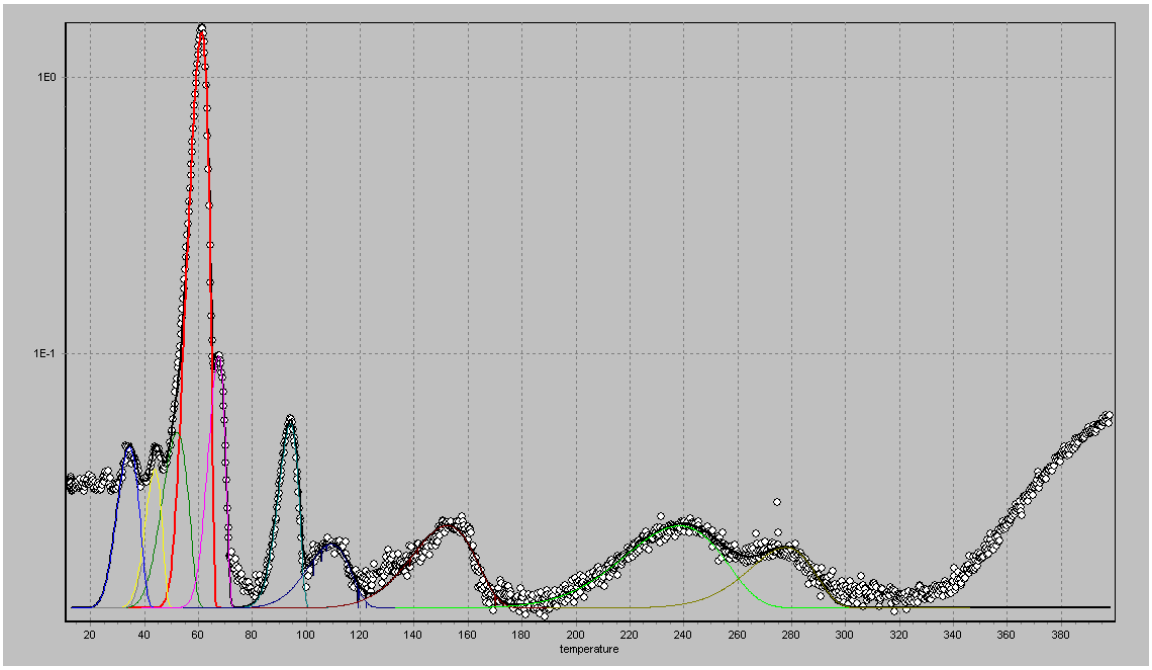

Figure B.5. Plot of the measured glow curve for a SrI_2 scintillator grown at the SMRC. Measurement temperature range was from ~15K to 400K.

References for Appendix B

Bollinger, L. and G. E. Thomas (1961). "Measurement of the Time Dependence of Scintillation Intensity by a Delayed-Coincidence Method." Review of Scientific Instruments 32(9): 1044-1050.

Glodo, J. (2001) TLSimFit (Version 0.99a) [computer software], Originally obtained from J. Glodo.

Randall, J. and M. Wilkins (1945). "Phosphorescence and electron traps. I. The study of trap distributions." Proceedings of the Royal Society of London. Series A. Mathematical and Physical Sciences 184(999): 365-389.

VITA

Harold E. Rothfuss Jr was born to Harold E Rothfuss and Kim Young Rothfuss on the 16th of November 1979 in Seoul Korea. Being in a military family, he was raised in several places that included the states of Illinois, New York, Texas Germany and Tennessee. After completing high school he enlisted in the Army as an infantryman. After a short stint, he started his academic career at the University of Tennessee in 1999. He completed his bachelor's degree in nuclear engineering in 2003 at the same time being employed by CPS Innovations (later acquired by Siements) in the physics group. Harold then started graduate school in the physics department and after an interruption including a deployment in support of Operation Iraqi freedom for a total time period of 20 months, returned to work for Siemens. At this time under persuasion from his PhD advisor Dr. Chuck Melcher, he re-enrolled in graduate school for a degree in Material Science and Engineering. In May 2013, he completed his PhD and graduated some 14 years after starting his academic career. He is married to his wife of 14 years Aehee Rothfuss and has 2 beautiful girls, Helen and Abigail. He is still employed by Siemens and still in the physics group under direction of Dr. Mike Casey.